AGU PUBLICATIONS

JGR

Journal of Geophysical Research: Solid Earth

RESEARCH ARTICLE
10.1002/2013JB010762

Key Points:
- We provide an up-to-date active fault map for Myanmar and its surroundings
- We summarize historical seismic activity and its plausible sources
- We discuss the earthquake potential of the region

Supporting Information:
- Readme
- Figure S1
- Figure S2
- Figure S3
- Figure S4
- Figure S5
- Figure S6
- Figure S7
- Figure S8
- Figure S9
- Figure S10
- Figure S11
- Figure S12
- Figure S13
- Figure S14
- Figure S15
- Figure S16
- Figure S17
- Figure S18
- Figure S19
- Figure S20
- Figure S21
- Figure S22
- Figure S23
- Figure S24
- Figure S25
- Figure S26
- Figure S27
- Figure S28
- Figure S29
- Figure S30
- Table S1

Correspondence to:
Y. Wang,
y.Wang@ntu.edu.sg

Citation:
Wang, Y., K. Sieh, S. T. Tun, K.-Y. Lai, and T. Myint (2014), Active tectonics and earthquake potential of the Myanmar region, *J. Geophys. Res. Solid Earth*, *119*, 3767–3822, doi:10.1002/2013JB010762.

Received 9 OCT 2013
Accepted 9 MAR 2014
Accepted article online 15 MAR 2014
Published online 25 APR 2014

Active tectonics and earthquake potential of the Myanmar region

Yu Wang[1,2], Kerry Sieh[2], Soe Thura Tun[3], Kuang-Yin Lai[4,5], and Than Myint[3]

[1]Division of Geological and Planetary Sciences, California Institute of Technology, Pasadena, California, USA, [2]Earth Observatory of Singapore, Nanyang Technological University, Singapore, [3]Myanmar Earthquake Committee, Myanmar Engineering Society, Yangon, Myanmar, [4]Department of Geosciences, National Taiwan University, Taipei, Taiwan, [5]Institute of Earth Sciences, Academia Sinica, Taipei, Taiwan

Abstract This paper describes geomorphologic evidence for the principal neotectonic features of Myanmar and its immediate surroundings. We combine this evidence with published structural, geodetic, and seismic data to present an overview of the active tectonic architecture of the region and its seismic potential. Three tectonic systems accommodate oblique collision of the Indian plate with Southeast Asia and extrusion of Asian territory around the eastern syntaxis of the Himalayan mountain range. Subduction and collision associated with the Sunda megathrust beneath and within the Indoburman range and Naga Hills accommodate most of the shortening across the transpressional plate boundary. The Sagaing fault system is the predominant locus of dextral motion associated with the northward translation of India. Left-lateral faults of the northern Shan Plateau, northern Laos, Thailand, and southern China facilitate extrusion of rocks around the eastern syntaxis of the Himalaya. All of these systems have produced major earthquakes within recorded history and continue to present major seismic hazards in the region.

1. Introduction

In the context of plate tectonics, the eastern margin of the Indian Ocean is a right-lateral convergent plate boundary (Figure 1a). Along the entire plate boundary, the Sunda megathrust accommodates eastward subduction of oceanic under predominantly continental lithosphere. Right-lateral strike-slip faults traverse the entire margin, from Sumatra in the south to Myanmar in the north. The Sumatran fault accommodates most of the right-lateral component of oblique convergence along the 2000 km length of Sumatra [e.g., *Fitch*, 1972; *Sieh and Natawidjaja*, 2000; *Chlieh et al*., 2008; *McCaffrey*, 2009]. An en echelon spreading center carries a large component of the dextral component of deformation beneath the Andaman Sea [*Curray*, 2005]. Farther north, the Sagaing fault plays a significant dextral-slip role along a 1400 km span centered on Myanmar [e.g., *Win Swe*, 1970; *Vigny et al*., 2003; *Curray*, 2005]. Both the Sunda megathrust and Sagaing fault systems terminate northward into the eastern Himalayan syntaxis.

The 1000 to 1300 km wide terrane bisected by the Sagaing fault is tectonically complex. On the west is the subducting oceanic Indian plate, and on the east are the predominantly continental Yangtze and Sunda blocks (Figure 1a). Between the Indian plate and the Sagaing fault is an elongate tectonic block that is commonly called the Burma plate or the Burma sliver [*Curray et al*., 1979]. Between the Sagaing fault and the Yangtze and Sunda blocks is a terrane that includes the Shan Plateau, characterized by a plexus of dextral and sinistral strike-slip faults (Figure 1b) [*Lacassin et al*., 1998].

Geodetic measurements show that the motion of the Indian plate relative to the Sunda block ranges from about 3 to 4 cm/yr at the latitude of Myanmar [*Sella et al*., 2002; *Kreemer et al*., 2003b; *Prawirodirdjo and Bock*, 2004; *Socquet et al*., 2006; *DeMets et al*., 2010]. The Sagaing fault accommodates only about 2 cm/yr of the north component of this relative motion [*Bertrand et al*., 1998; *Vigny et al*., 2003; *Socquet et al*., 2006; *Maurin et al*., 2010; *Wang et al*., 2011]. The megathrust and related upper plate structures also absorb some of the India-Sunda plate motion [e.g., *Nielsen et al*., 2004; *Socquet et al*., 2006]; the rest of the oblique strike-slip motion may be partitioned into the interior of the Burma plate [e.g., *Socquet et al*., 2006]. Except under southernmost Myanmar, the geometry of the subducting slab is well established from hypocenters of an east-dipping Wadati-Benioff zone [e.g., *Ni et al*., 1989; *Richards et al*., 2007]. The 60 km isobath runs approximately beneath the eastern flank of the Indoburman range.

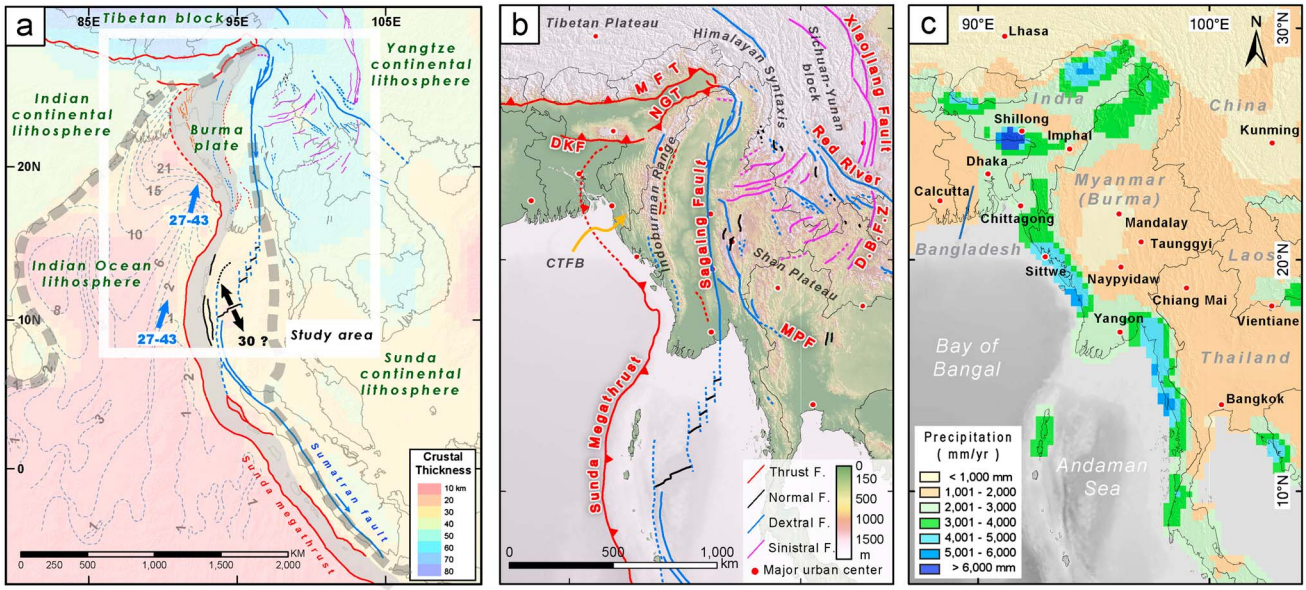

Figure 1. Major tectonic elements of the Myanmar region and the extreme variation in rainfall that influence the preservation of tectonic landforms. (a) Crustal thickness associated with the major plates and tectonic blocks of the region. The blue arrow shows the direction of Indian plate motion relative to Sunda plate [e.g., *Socquet et al*., 2006]. The black arrow shows the opening direction of the Central Andaman spreading center. The velocity is in mm/yr. (b) Two major fault systems accommodate the northward translation of the Indian plate into Eurasia. These are the northern extension of the Sunda megathrust and the Sagaing fault system, which form the western and eastern margin of the Burma Plate. Conjugate right- and left-lateral faults of the Shan plateau and southern China accommodate southwestward extrusion of the Sichuan-Yunnan block around the eastern Himalayan syntaxis. (c) Extreme variations in annual rainfall across the region result in extreme variations in preservation of tectonic landforms. The precipitation data are from GPCC global data [*Rudolf and Schneider*, 2005].

Historical records demonstrate that great and destructive earthquakes have occurred throughout much of the region (Figure 2). These reports are sparse but informative [*Halsted*, 1841; *Oldham*, 1883; *Coggin Brown*, 1914; *Coggin Brown et al*., 1931; *Coggin Brown and Leicester*, 1933; *Chhibber and Ramamirtham*, 1934; *Win Swe*, 2006; *Martin and Szeliga*, 2010]. Although they provide important information about the general locations and approximate sizes of the earthquakes, they reveal little or nothing about the character of the causative faults. In fact, until 2011, no postearthquake investigations had involved mapping the surface trace of an active fault in the country of Myanmar. For example, only the pattern of seismic intensities [*Oldham*, 1883] supports the contention that the 1839 Ava earthquake, which killed more than 500 people in central Myanmar, resulted from rupture of a section of the Sagaing fault west of Mandalay [*Le Dain et al*., 1984; *Win Swe*, 2006]. A far more mysterious example is the earthquake of 1927, which was felt most strongly north of Yangon [*Coggin Brown*, 1929; *Chhibber and Ramamirtham*, 1934]. Potential seismic sources in this region remain speculative, even though the earthquake was close to the region's largest city, which is home to more than four million people and continues to grow rapidly.

2. Methodology

The aforementioned geological, seismological, and geodetic investigations do not constitute a systematic assessment of the neotectonic architecture of the Myanmar region and its seismic potential. Here we present a new synthesis of regional kinematics that relies principally on a modern geomorphologic analysis of tectonic landforms. The last such geomorphological study appeared three decades ago [*Le Dain et al*., 1984]. That study relied upon Landsat satellite imagery, whereas our principal data are from shaded-relief digital-elevation imagery. In recent years, modern geomorphologic analyses founded upon the use of digital elevation models and high-quality imagery have substantially improved understanding of the kinematics and seismic potential of many other regions. A few examples include work in Sumatra [*Sieh and Natawidjaja*, 2000], Taiwan [*Shyu et al*., 2005], and the eastern Tibetan plateau [*Densmore et al*., 2007].

In this paper, we describe the geomorphologic expression of active faults and folds within and around Myanmar. We then discuss the implications of this analysis for understanding the active tectonics of the

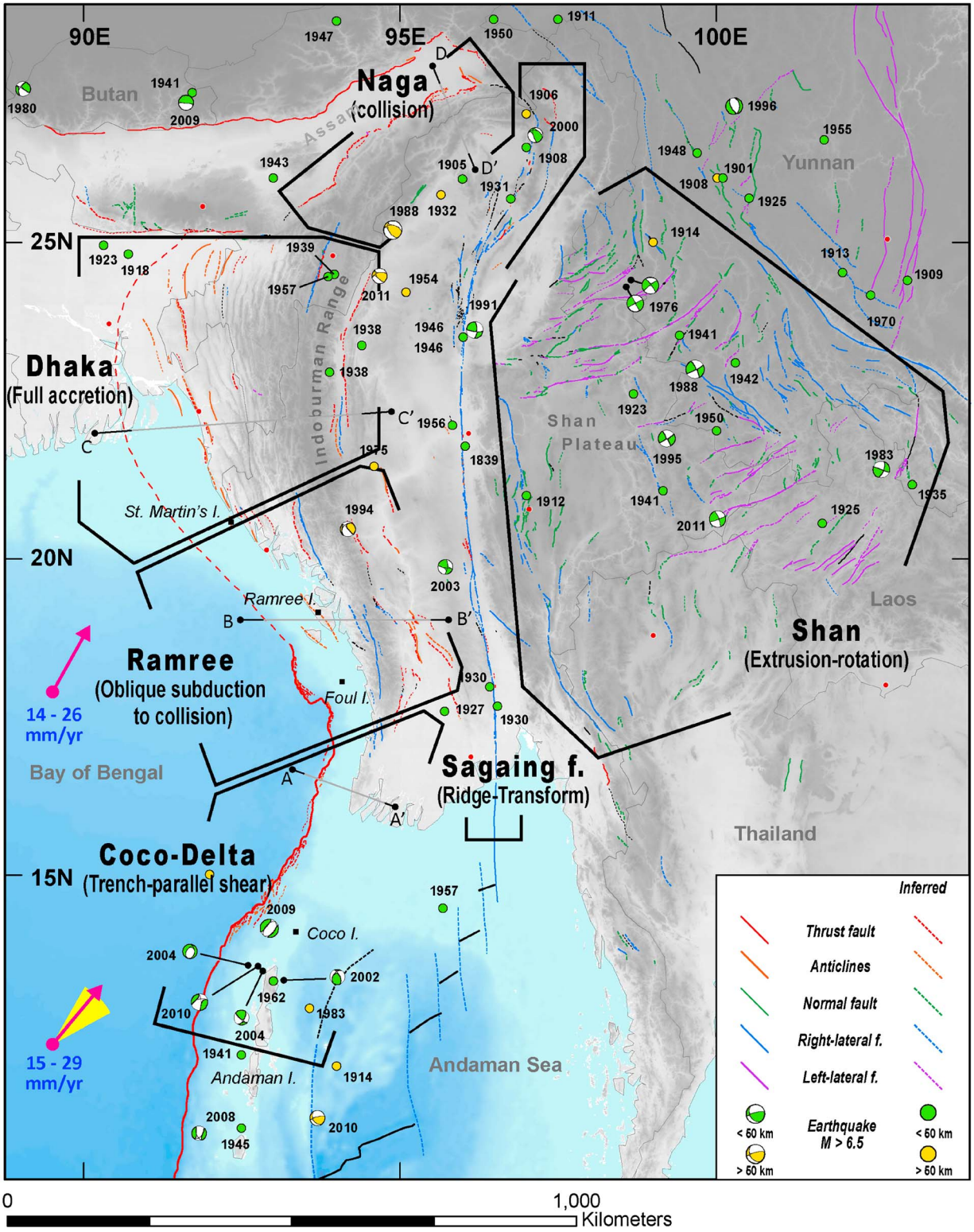

Figure 2. Simplified neotectonic map of the Myanmar region. Black lines encompass the six neotectonic domains that we have defined. Green and Yellow dots show epicenters of the major twentieth century earthquakes (source: *Engdahl and Villasenor* [2002]). Green and yellow beach balls are focal mechanisms of significant modern earthquakes (source: GCMT database since 1976). Pink arrows show the relative plate motion between the Indian and Burma plates modified from several plate motion models [*Kreemer et al*., 2003a; *Socquet et al*., 2006; *DeMets et al*., 2010]. The major faults west of the eastern Himalayan syntax are adapted from *Leloup et al*. [1995] and *Tapponnier et al*. [2001]. Yellow triangle shows the uncertainty of Indian-Burma plate-motion direction. A more detailed, high-resolution map, from which is this figure was derived, appears in the supporting information Figures S2 and S4–S12.

area, drawing also on geodetic analyses, local structural studies, historical earthquake accounts, and other seismological data. Our goal is to construct a view of the neotectonic architecture of the region that provides a clear framework for understanding of the recent seismic activity and the potential for future large earthquakes.

Our geomorphologic analysis relies heavily on terrestrial shaded-relief maps constructed from the Shuttle Radar Topography Mission (SRTM version 2 to version 4 at 90 m resolution) [e.g., *Jarvis et al*., 2008] and offshore shaded-relief maps derived from ETOPO-1 [*Amante and Eakins*, 2009]. We also use stereoscopic imagery constructed from the Advanced Spaceborne Thermal Emission and Reflection Radiometer (ASTER VNIR L1B at 15 m resolution). An index of these data appears in the supporting information Figure S1. Together these data resolve topographic features far better than nonstereoscopic imagery and enable a broad but detailed survey of the region.

In places of particular interest, we also use aerial photographs at scales of about 1:50,000 and 1:25,000. Figure S1 in the supporting information shows the coverage we used. Where available, we integrate the high-resolution bathymetric data and structural geologic maps published by others to inform our interpretations.

Our reliance on geomorphic expression of tectonic landforms implies that our analysis is limited by their expression and preservation, which varies, of course, as a function of the type of deformation [*Yeats et al*., 1997; *Burbank and Anderson*, 2011]. Strike-slip faults have a vastly different geomorphic expression than thrust faults and normal faults, and fast-slipping faults show up in the landscape more clearly than slow-slipping faults.

Modulating these expressions of active structures in the landscape is the degree of interaction of the solid earth with the atmosphere and hydrosphere. In particular, variations in rainfall play a major role in the variable expression of tectonic landforms. Figure 1c shows that average annual rainfall across the region varies by at least a factor of 5. Rainfall in Bangladesh and along the western Myanmar coast is 2 to 3 times greater than in the central Burma basin and farther east [*Rudolf and Schneider*, 2005; *Rudolf et al*., 2010]. All else being equal then, erosion would reduce a young tectonic structure in the central or eastern regions less than if the same active feature were on the western flank of the Indoburman Range or in Bangladesh.

Another variable in the expression of tectonic landforms is the youthfulness of the landscape [*Yeats et al*., 1997]. For example, the expression of active faults and folds on the young prograding river deltas of southern Myanmar will be limited to very youthful features not buried by rapid sedimentation. Older and more prominent tectonic landforms would be evident only on older landscapes.

For these two reasons, we must expect that our analysis of active tectonic features will not be uniformly sensitive to rates of activity across the entire region. Active features along the western coasts and on the southern deltas are less likely to be clearly expressed than features elsewhere in the region.

3. Neotectonics of the Myanmar Region

Figure 2 is a simplified version of our neotectonic mapping of the Myanmar region, drafted at a scale of about 1:10,000,000. This scale is far smaller than the 1:50,000 to 200,000 scales at which we mapped structures using the SRTM and other topographic data. We provide a more detailed neotectonic map in the supporting information (Figures S2 and S4–S12).

Figure 2 shows the division of Myanmar's three principal tectonic regimes into six domains, each defined by its particular geomorphological and structural expressions of tectonic activity. In the Indoburman range, along-strike variations in expression of convergence vary appreciably, so we have divided this system into four distinct structural domains. In the next section, we discuss each of these four domains separately, beginning in the south and ending in the north.

3.1. The Indoburman Range

In its grand, arcuate northward sweep from southern Myanmar toward the Himalaya, the Indoburman range of western Myanmar evolves from narrow, low hills at 16°N to a very broad and high range near 24°N (Figure 2). Farther north, on the south side of India's Assam valley, the mountains swing toward the east-northeast and narrow considerably.

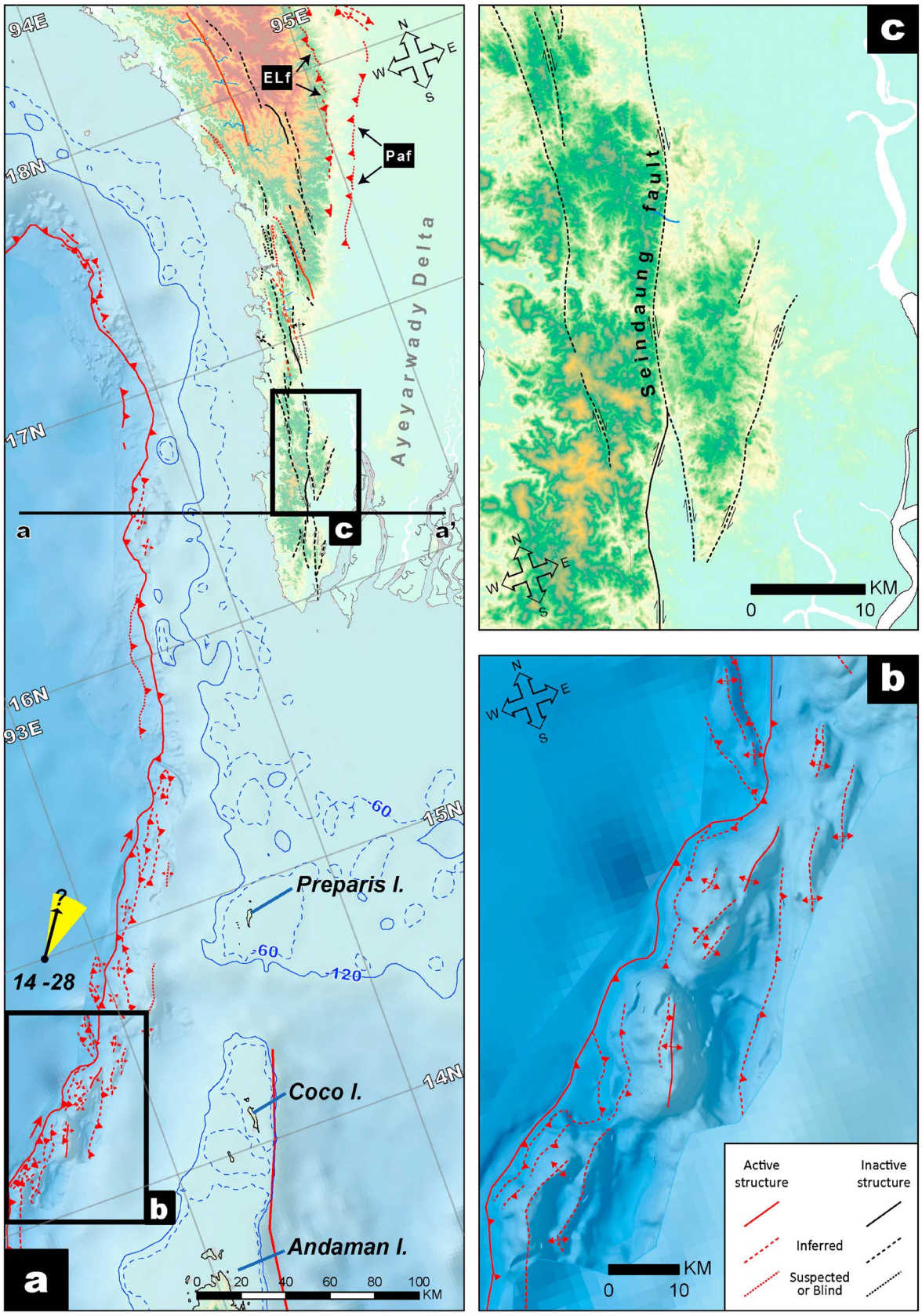

Figure 3

In the far south, highly oblique convergence dominates within what we term the Coco-Delta domain. Its northern neighbor, the Ramree domain, represents a transition from oblique subduction to nearly orthogonal subduction that involves a thick accretionary wedge of sediment. The broadest portion of the Indoburman range comprises the Dhaka domain, in which a very wide belt of folded and faulted sediment mantles a very low-angle subduction megathrust. East of the Shillong plateau is the Naga domain, where the northern edge of the Burma plate overrides India's Assam block.

3.1.1. Coco-Delta Domain

The 500 km span of the Sunda megathrust between the Andaman islands and the southern end of the Indoburman range trends decidedly more easterly than adjacent sections (Figures 1 and 2). In fact, the trend of the deformation front between about 14.2°N and 17°N is nearly parallel (within the uncertainties) to the direction of relative motion between the Indian plate and the Burma sliver plate (see Figure S3, last column of row 5, and Table S1). This implies that subduction and accretion should be very slow here and that relative motion across the boundary should be predominantly right lateral at a rate between about 14 and 28 mm/yr (Table S1). The lack of a Wadati-Benioff zone down dip of the deformation front between about 14°N and 17.8°N [*Ni et al*., 1989; *Richards et al*., 2007] lends further support to this concept. Other areas of highly oblique subduction are similar in this regard (for example, the Scotia arc and Queen Charlotte Islands) [e.g., *Pelayo and Wiens*, 1989; *Mazzotti et al*., 2003; *Bustin et al*., 2007]. Additional support for low rates of convergence across the Coco-Delta domain comes from seismic tomography, which shows only weak evidence of a slab extending downdip [*Li et al*., 2008].

The low relief of both the Indoburman range and the fore arc in this region and their narrow (70 to 90 km) width imply low rates of uplift and little total accretion. The small sizes of Coco and Preparis Islands relative to the Andaman islands farther south also likely reflect lower rates of uplift and accretion (Figures 2 and 3). Between Preparis Island and the southern tip of the Indoburman range, rates of uplift are so low that erosion and sedimentation on the Ayerawaddy (Irrawaddy) Delta have kept pace with any ground rising above wave base (Figure 3a). Additional support for low rates of uplift and scant accretion in the Coco-Delta domain is the fact that the Indoburman range is far narrower and lower in the Coco-Delta domain than in the next domain to the north. The precise coincidence of the southward diminishment of the Indoburman range with the northeastward extrapolation of the Coco-Delta section of the plate margin argues for an abrupt and sustained drop off of the uplift that has created the Indoburman ranges. This is clear evidence that the abrupt bend in the plate margin at the northeastern end of the Coco-Delta domain coincides with a sharp and major change in accretion and uplift rates.

Despite the abovementioned evidence for minimal vertical deformation, our bathymetric mapping along the steep escarpment of the plate margin shows clearly that there is a convergent component to deformation within the Coco-Delta domain. Swath bathymetry data from *Nielsen et al*. [2004] show that the 2 km high slope rising from the flat floor of the Indian Ocean is much steeper than is typical for accreting sedimentary prisms but very similar to the slopes of highly oblique convergent margins. We do not see clear boundaries between dextral fault segments and thrust fault segments. Instead, the right-stepping en echelon character of both the deformation front and of some anticlines just upslope prove that the sense of slip along the section from 14° to 15.5°N is dextral-reverse rather than purely dextral (Figure 3b).

Strike-slip faults within the thin southern tail of the Indoburman range conform to the dextral-reverse nature of the Coco-Delta domain. Breaking the low topography of its eastern portion are several linear features that strike roughly parallel to the range front and to the nearby plate margin (Figures 3a and 3c). One outlying block, partially surrounded by sediments of the Ayeyarwady River, appears to have shifted right laterally about 10 km from the main body of the range along the Seindaung fault. Unfortunately, the resolution of the SRTM imagery is too coarse to tell whether or not the faults laterally offset small channels and ridges there, so we do not venture an opinion as to whether or not these faults are currently active. Their sharp geomorphic expression does, however, suggest that they have been active within the Quaternary Period. Farther north,

Figure 3. (a) Major active faults within the Coco-Delta domain. Paf = Pathein fault; Elf = East-Limb fault. Black arrow shows the Indian-Burman plate motion direction. Yellow triangle marks the uncertainty of the direction. (b) Structures along the deformation front include a series of anticlinal structures very close to the trench. Detailed inset bathymetry is from *Nielsen et al*. [2004]. (c) Seindaung fault and other dextral-slip faults along the eastern flank of the southern Indoburman range. Although these faults are clearly expressed in the topography, we cannot identify any obvious young offset features.

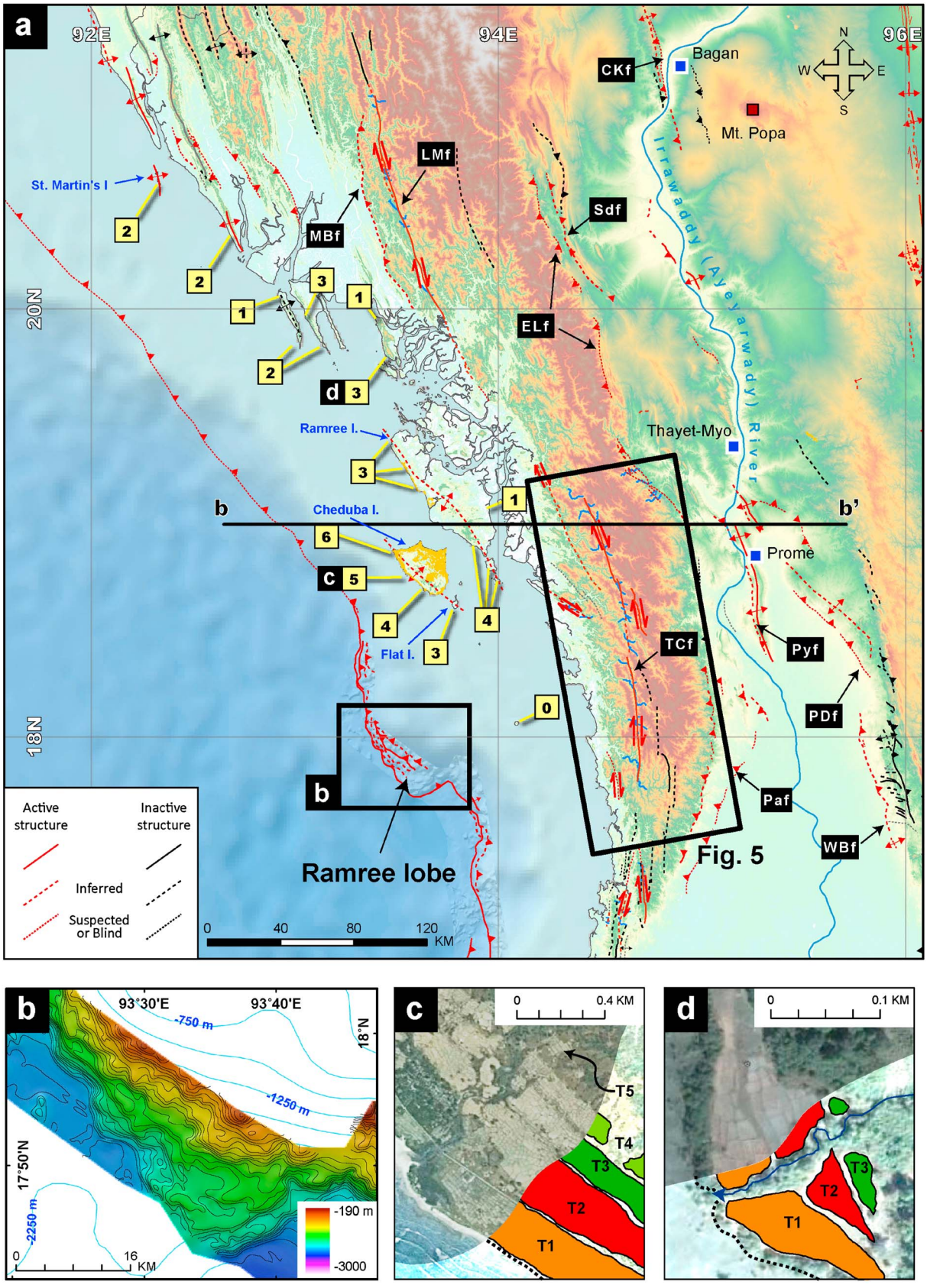

Figure 4

where the Indoburman range widens and transitions to the next domain, drainages are larger and more developed. Some of these display right-lateral offsets of about 10 km. We discuss these further in the next section.

Coseismic and postseismic displacements of the great 2004 Aceh-Andaman earthquake confirm and illuminate the dextral-reverse nature of slip across the Coco-Delta domain. *Meltzner et al*. [2006] show that several decimeters of uplift occurred on Coco Island and that Preparis may have risen 20 to 30 cm. Horizontal deformations were measured as far north as about 13.5° [*Chlieh et al*., 2007]. Whereas horizontal motions farther south along the arc were nearly perpendicular to the plate margin, the five stations on the Andaman Islands (between 12 and 13.5°N) experienced a marked dextral component as well. Their coseismic and postseismic motions are nearly parallel to the strike of the Coco-Delta domain plate margin and imply up to 5 m of purely dextral slip at the very southern end of the Coco-Delta domain and equal parts of dextral and thrust motion on the megathrust beneath the rest of the Andaman Islands.

3.1.2. Ramree Domain

The Ramree domain is the northern neighbor of the Coco-Delta domain (Figure 2). Sustained convergence and accretion along this 450 km section of the plate margin have produced a belt of deformation that increases in width from about 170 km in the south to about 250 km in the north (Figure 4a). Further evidence of northward-increasing convergence through the Ramree domain is the pronounced rise in height of the Indoburman range, from less than 1000 m in the south to more than 2000 m in the north. Seismicity of the subducting Indian plate also becomes more pronounced from south to north. In the south, the deepest hypocenters of the Wadati-Benioff zone are about 70 km deep and 140 km east of the deformation front, whereas in the north, hypocenters reach depths of about 120 km and extend to about 300 km from the deformation front (NEIC catalog, 1976 to 2010).

Plate-vector diagrams that relate motion of the Indian plate to the Sunda block and ascribe about 20 mm/yr of dextral slip to the Sagaing fault imply dextral-oblique convergence rates between 14 and 26 mm/yr across this domain (Figure S3, last row of columns 3 and 4). Taking the vector diagram at face value, one would expect the ratio of convergence to dextral slip to be about 3:2.

With these broad attributes of the Ramree domain in mind, we now discuss geomorphologic evidence of recent neotectonic activity, moving from west to east, from the offshore and coastal regions to the interior of the Indoburman range and then to the plains east of the mountains. We begin with bathymetric evidence for the nature of deformation at the deformation front offshore and then proceed to document bathymetric and topographic evidence for activity on thrust faults within the accretionary prism nearer the coast. We then present evidence for an important dextral strike-slip fault within the mountains and a backthrust along the eastern flank of the mountains. Finally, we describe thin-skinned folds and faults to the east.

3.1.3. Deformation Front and Active Structures in the Accretionary Prism

High-resolution bathymetry between 17° and 18.5°N displays clear evidence of tectonic shortening at and adjacent to the deformation front along the southern half of the domain [*Nielsen et al*., 2004]. Accretion of sediment is particularly clear along the salient that they call the Ramree lobe, between 17°40′ and 18°N (Figure 4b). In contrast to the Coco-Delta domain, features of dextral slip along the deformation front are far less clear than along the southern part of the Ramree domain.

East of the deformation front, along the coast, is abundant evidence for youthful folding. Flights of uplifted coastal terraces are clear even in nonstereographic, high-resolution satellite imagery, because vegetation differences differentiate flat terrace treads from steep terrace risers (Figures 4c and 4d). Figure 4a shows that the number of terraces visible in this imagery varies across the region.

Thus far, Cheduba and Ramree Islands, which appear to have the largest number of marine terraces, have yielded the most definitive data on uplift patterns and timing. *Shishikura* [2009] and *Than Tin Aung et al*.

Figure 4. (a) Major active faults within the Ramree domain (name abbreviations in black boxes). Numbers in yellow boxes indicate number of marine terraces visible in high-resolution satellite imagery. (b) Detailed bathymetry of the Ramree lobe shows clear geomorphic expression of imbricated faults and anticlines, which imply active shortening near the deformation front. (c) Marine terraces on the western side of Cheduba Island (colored patches) from satellite imagery. (d) Nested alluvial fan surfaces north of Ramree Island show episodic uplift during the seaward growth of the fan. WBf = West Bago-Yoma fault; PDF = Paungde fault; MBf = Minbya fault; LMf = Laymyo fault; TCf = Thahtay Chaung fault; Elf = East-Limb fault; Sdf = Sidoktaya fault; PTf = Pato fault; Pyf = Pyay fault; CKf = Chauk fault

[2008] showed that these two islands and coastlines up to 100 km farther northwest have been rising incrementally throughout the late Holocene, presumably in association with large earthquakes. They also report that the terraces on the islands northwest of Ramree Island tilt northeastward.

Wang et al. [2013b] added substantial detail to this story. They demonstrated that the islands are the subaerial expressions of two doubly plunging antiforms. The long axes of these antiforms run parallel to the deformation front for more than a hundred kilometer (Figure 4a) and their southwestern flanks are far steeper than their northeastern flanks. They also demonstrate from field measurements and radiometric dating of middle to late Holocene terraces that each of the islands is tilting progressively and independently toward the mainland coast, rising most rapidly along their southwestern coasts. The pattern of uplift implies that the two asymmetric antiforms are rising on the backs of two contemporaneously active northeast-dipping faults (splay faults) within the accretionary prism.

Eyewitness accounts collected by a British survey team 80 years after the great Arakan earthquake suggest that the lowest terrace on Cheduba and Flat Island rose out of the sea during the great 1762 Arakan earthquake [*Halsted*, 1841; *Mallet*, 1878; *Oldham*, 1883]. *Wang et al*. [2013b] demonstrate via U-Th disequilibrium dating of coral microatolls that the most recent large uplift of both Ramree and Cheduba Island did, indeed, occur during the great Arakan earthquake of 1762.

3.1.4. Dextral Strike-Slip Faulting in the Indoburman Range

Although evidence of dextral slip along the deformation front is obscure within the Ramree domain, clear evidence for a 160 km long right-lateral strike-slip fault exists within the Indoburman range, from about 17.75° to 19°N (Figure 4). This clearly suggests some partitioning of dip slip and strike slip between the megathrust and the structures in the accretionary prism. All major rivers flowing to the southwestern coast exhibit sharp dextral deflections of many kilometer along the trace of this structure, which we call the Thahtay Chaung fault (labeled TCf in Figure 4), after one of the large river channels that it offsets (Figure 5). Between 17.75°N and 18.5°N, the best fitting offsets for the major stream canyons are predominantly between 10.3 and 11.3 km. From 18.5°N to 19°N, the best fit offsets diminish from about 11 to about 5 km. The fault may splay northwestward into two or more obscure structures before dying out, but the geomorphological evidence for this is not at all compelling.

The acute angle between the nearly north-south strike of the Thahtay Chaung fault and the northwesterly trends of the large offset streams suggests substantial dextral warping associated with dextral slip on the fault. Such dextral warping is especially clear within several kilometers of the fault, where major channels flow northwestward toward the western flank of the Indoburman range.

We can speculate about the age of the cumulative ~10 km offsets and about the ratio of dextral slip to convergence across the Ramree domain. It is reasonable to assume that the Thahtay Chaung fault began to develop river-channel offsets once the turbidites of the regional bedrock rose above the sea and fluvial channels began to incise. The time of this emergence must substantially postdate the age of the beds, which are shown on the geological map of *Brunnschweiler* [1966] to be Miocene flysch. If the drainage system began to develop around 5 Ma in this part of Indoburman range, then the 10 km offsets of the Thahtay Chaung fault would have developed at an average slip rate about 2 mm/yr. This would be more than an order of magnitude less than the rate of convergence across the entire domain.

The Thahtay Chaung fault is the only active strike-slip fault that we could recognize from the SRTM topography (Figure 4). Even though the southwestern flank of the Indoburman range is remarkably straight between about 18.75° and 20° and between 20° and 21°N, a notably linear valley extends northwestward from the mountain front; these features do not appear to reflect active strike-slip faulting. Careful inspection of these and other, lesser lineations in the Ramree domain revealed very little evidence for young strike-slip faulting. We conclude that the Thahtay Chaung fault is the only clear manifestation of strike-slip faulting in the Ramree domain.

3.1.5. Active Faults and Folds East of the Indoburman Range

The eastern flank of the Indoburman range is an impressive escarpment along the entire length of the Ramree domain, averaging slopes of ~3° from the crest of the range to the mountain front. This is far steeper than the average ~1° slope of the southwestern flank of the range. The morphology of the mountain front suggests that it is rising along an active, west-dipping reverse fault. Along most of its length, however, there is scant evidence (at least at the resolution of the SRTM imagery) for fault scarps that would indicate a young fault breaking to the surface.

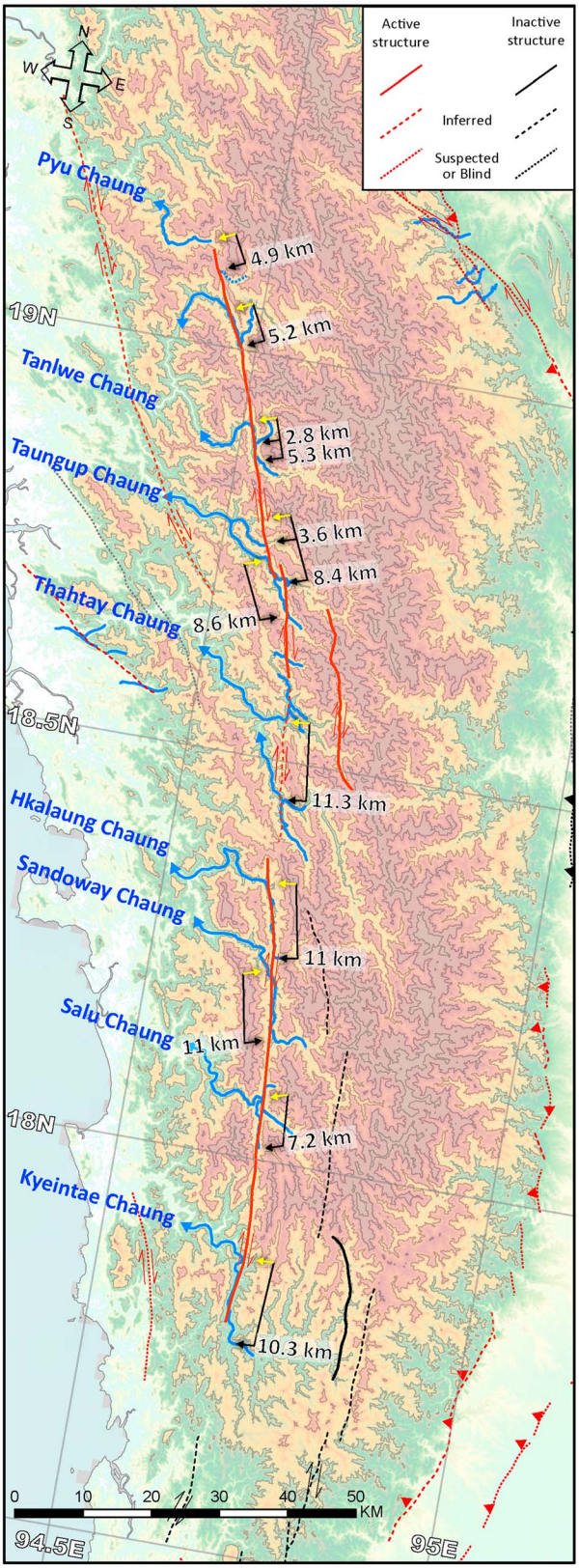

Figure 5. Right-lateral offset of river channels along the Thahtay Chaung fault, within the Indoburman Range. The maximum geomorphic offset is about 10.3 km, close to the southern limit of the fault.

A more plausible explanation is that the escarpment has been produced by flexure. Bedding orientations and dips along the mountain front would help us infer the underlying structure, but bedding is cryptic in the SRTM imagery, and few published works address this section of the range. Structural sections from *Brunnschweiler* [1966] and *Bender and Bannert* [1983] suggest steep eastward dips of the bedrock along the escarpment and that these beds have been overridden by the east-dipping thrust faults of the Central Basin. Our guess is that the mountain front is mainly a fold scarp due to slip on a ramp beneath the mountain range that ruptures to the surface only locally, if at all. If this is the case, then young folds 10 to 100 kilometer to the east, in Myanmar's Central Basin and the floodplain of the Ayeyarwady River (Figure 4), may result from a décollement that emanates from the top of this blind structure and traverses eastward at shallow depth to a position beneath them.

Several short scarps and folds in the central valley are topographically obvious, and we propose that they are active. For example, near 18°N we observe a series of highly dissected lateritic terraces 10 to 20 km east of the mountain front that are 20 to 30 m higher than the active floodplain of the Ayerawaddy. Many of these have fan shapes that suggest they represent alluvium originating from the Indoburman range. The linearity of the eastern edge of these terraces suggests that these are fault scarps rather than cuts into alluvial fans by a laterally migrating Ayeyarwady River. We do not see scarps on younger, unlaterized fluvial or alluvial deposits in the coarse SRTM imagery, so we have no clear evidence for latest Pleistocene or Holocene rupture.

Several other reverse faults east of the Indoburman range also have mild geomorphologic expressions that might indicate current activity at slow rates in the central Burma basin. All of these are in the hundred kilometer or so east of the Indoburman range, and most are associated with anticlinal folding. The West Bago-Yoma fault (WBf, Figure 4) and the

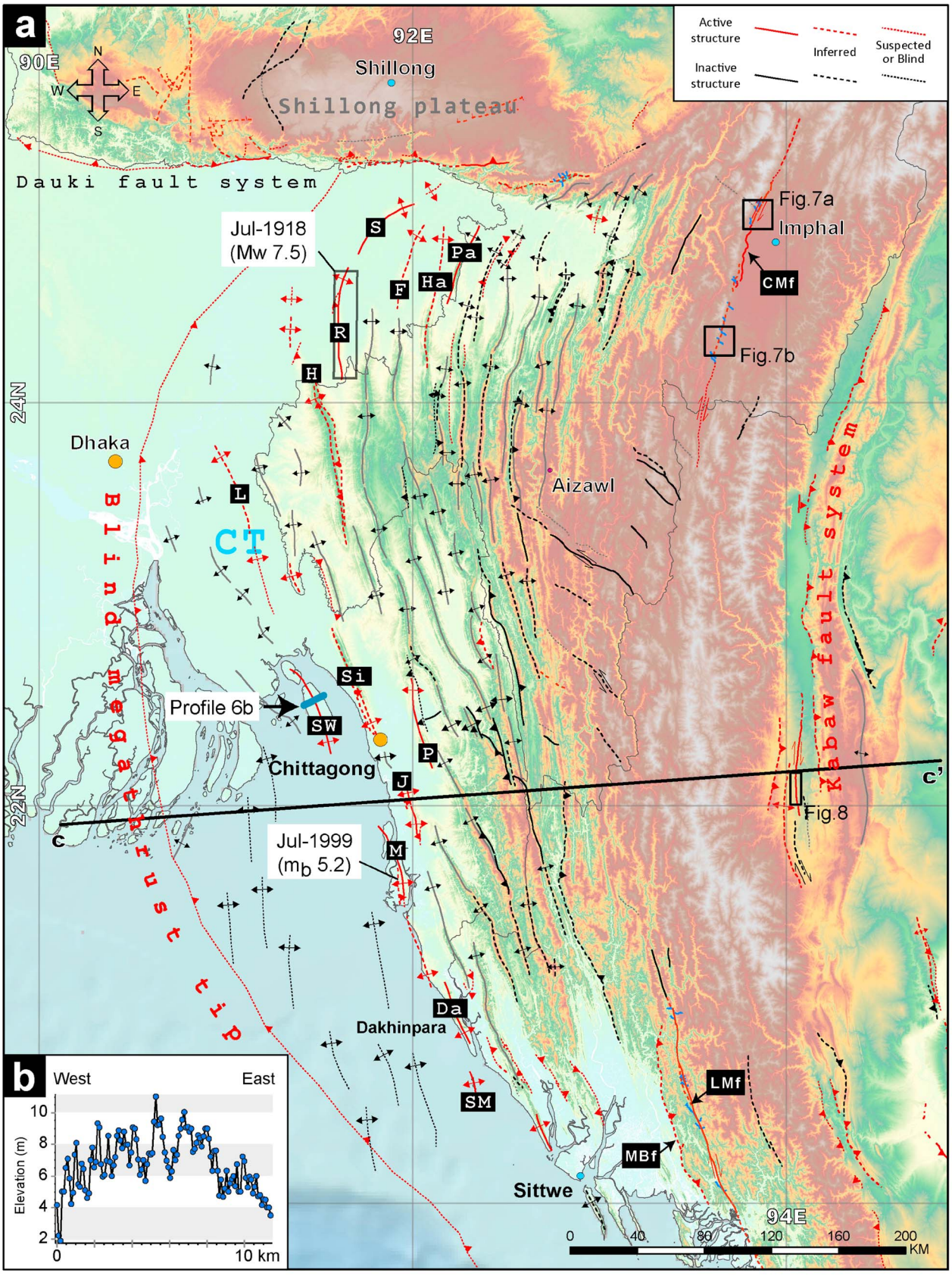

Figure 6

Paungde Fault (PDf, Figure 4) are two east-dipping reverse faults that show clear activity during the late Quaternary Period. Speculating that the 30 m high uplifted surfaces on the hanging wall formed about 120 ka above a 45° northeastward-dipping reverse fault, we calculate convergence rates of about 0.4 mm/yr. At least two of these folds and reverse faults cross the Ayerwaddy River, but the coarseness of the 90 m SRTM and 15 m ASTER imagery precludes recognition of small river terraces that would confirm young anticlinal deformation.

Eyewitness accounts of a phenomenon associated with the Prome earthquake of 1858 support the hypothesis that this field of folds and faults is seismically active. The strongest shaking of this widely felt large earthquake was reported from the reach of the Ayerwaddy valley that encompasses the cities of Prome and Thayet-Myo (Figure 4). Eyewitnesses report that in the several hours following the earthquake, the Ayerawaddy near Thayet-Myo flowed upstream [*Oldham*, 1883]. This could be explained by sudden uplift across the 30 km long, 10 km wide anticline that crosses the Ayerwaddy about 20 km downstream from the city. The river drops about 2 m between Thayet-Myo and the anticline, so if incremental uplift of a few meters occurred during the earthquake, the river gradient might have been impeded enough to cause the river surface to be instantaneously tilted upstream. A considerable amount of time would have been necessary for the river surface to reequilibrate to an appropriate gradient. This explanation is identical to that advanced for the retrograde flow of the Mississippi river in the hours following the New Madrid earthquake of February 1812. During that event, a 6 m uplift of the Tiptonville dome, an anticline astride the river, caused the river to flow upstream and overflow its banks [*Fuller*, 1912; *Penick*, 1981; *Mueller and Pujol*, 2001].

3.2. Dhaka Domain

North of the Ramree domain, the Burma sliver plate collides with the thickest part of the great Ganges-Brahmaputra delta. The effect of this collision with a 20 km thick pile of Eocene to Holocene sediment (Figure 1a) has been the formation and rapid westward propagation of a great fold and thrust belt within the sediments of the eastern side of the delta (Figure 6a). The total width of this Chittagong-Tripura fold belt (CTFB) and the higher part of the Indoburman range approaches 400 km at 23°N. The crest of the Indoburman range increases in height northward from the Ramree domain to nearly 3000 m at 21.3°N and retains a height of more than 2000 m for many hundreds of kilometer northward. We refer to this ~500 km long section as the Dhaka domain, after the largest city near the fold and thrust belt.

In marked contrast to domains to the south and north, a well-expressed Wadati-Benioff zone illuminates the subducting Indian oceanic lithosphere of the Dhaka domain [e.g., *Ni et al*., 1989; *Satyabala*, 1998; *Guzmán-Speziale and Ni*, 2000]. Hypocenters occur as deep as 200 km and up to 450 km from the deformation front. Few of the focal mechanisms are consistent with slip on the megathrust; most reveal steeply dipping strike-slip and normal faulting associated with internal deformation of the downgoing slab [e.g., *Satyabala*, 1998; *Rao and Kalpna*, 2005]. Beneath the Chittagong-Tripura fold belt, several moderate earthquakes show dextral or reverse faulting in the shallow part of the crust; however, their hypocenters are not well constrained by the global seismic network. The seismic silence of the megathrust raises an important question: Does the megathrust in the Dhaka domain slip only aseismically or is it capable of generating great megathrust earthquakes?

GPS-based vector diagrams suggest that modern relative motions between the Indian plate and the Burma plate at the latitudes of the Dhaka domain are similar to relative motions across the Ramree domain (Figure S3, rows 1 and 2). Relative motion between the Indian plate and Sunda plate, with 18–22 mm/yr of right-lateral slip on the Sagaing fault removed, yields oblique convergence between the Indian plate and Burma plate. At 21.25°N, estimated motions of 12 to 25 mm/yr are predominantly perpendicular to the deformation front, with a small component of dextral strike slip [e.g., *Socquet et al*., 2006]. Further north, at 23.5°N, the dextral strike-slip motion increases significantly due to the change of megathrust fault's

Figure 6. (a) Active faults and anticlines of the Dhaka domain superimposed on SRTM topography. Most of the active anticlines lie within 120 km of the deformation front. Red lines are structures that we interpret to be active. Black lines are structures that we consider to be inactive. CT = Comilla Tract. White boxes contain the dates and magnitudes of earthquakes mentioned in the text. CMf = Churachandpur-Mao fault; SM = St. Martin's island antilcline; Da = Dakshin Nila anticline; M = Maheshkhali anticline; J = Jaldi anticline; P = Patiya anticline; Si = Sitakund anticline; SW = Sandwip anticline; L = Lalmai anticline; H = Habiganj anticline; R = Rashidpur anticline; F = Fenchunganj anticline; Ha = Hararganj anticline; Pa = Patharia anticline. (b) Profile from SRTM topography of Sandwip Island. Cross-section CC′ appears in Figure 19.

orientation. Relative motion of a station within the fold belt (Aizawi, Figure 6a) is about 10 mm/yr eastward toward Dhaka [*Jade et al*., 2007; *Banerjee et al*., 2008]. Although GPS stations are too sparse to fully map strain accumulation across the Burma plate at this latitude, this measurement is consistent with a predominance of convergence and a minimal oblique component. Farther north and east, Imphal is converging southwestward toward Dhaka at between 11 and 20 mm/yr. This implies significant active right-lateral strike-slip faulting or clockwise rotations at this latitude.

With these broad attributes of the Dhaka domain in mind, we now discuss stratigraphic, geomorphologic, and seismic evidence of recent neotectonic activity, moving from west to east, as we did for the Ramree domain. We begin with a discussion of the history of deformation within the Chittagong-Tripura fold belt (CTFB) on the eastern flank of the Ganges-Brahmaputra delta. We then proceed to document topographic evidence for activity on faults within the higher parts of the Indoburman range. Finally, we discuss the significance of the steep eastern flank of the range and evidence for and against active faulting in the lowlands farther east.

3.2.1. Chittagong-Tripura Fold Belt

Relevant to our neotectonic analysis is a large body of work on the geological architecture and history of the Ganges-Brahmaputra delta and the CTFB. We begin with a summary of salient information.

The Ganges-Brahmaputra delta rests on lithosphere that is transitional between thick, buoyant Indian continental lithosphere on the west and north and dense Indian oceanic lithosphere on the east (Figure 1a) [e.g., *Alam*, 1989; *Curray*, 1991]. Sediment contributions to the delta began to arrive from the Himalaya and Indoburman range around the early Oligocene epoch (~35 Ma) and have been prograding southward to the present day [e.g., *Curiale et al*., 2002; *Curray et al*., 2002]. The arriving mass of these sediments loaded and depressed the underlying lithosphere, leading to the creation of additional accommodation space for deltaic sediment. Additional lithospheric depression and accommodation space has resulted from the southward thrusting of the Shillong Plateau over the delta through the past 5 million years and from the westward thrusting of the Indoburman ranges toward the delta [e.g., *Johnson and Alam*, 1991]. Altogether, current thicknesses of the deltaic sediment now range from about 12 to 21 km on the western flank of the Dhaka domain [*Curray*, 1991; *Brune et al*., 1992].

The Chittagong-Tripura fold belt has developed within the upper parts of this thick deltaic sequence. Many folds are clearly visible in the SRTM imagery as north-northwest-striking anticlinal and synclinal hills (Figure 6a). Through construction of a balanced cross section across the CTFB, *Maurin and Rangin* [2009] estimated a total east-west shortening of about 11 km in the past 2 million years, which implies a long-term shortening rate of about 5 mm/yr.

Various stratigraphic and structural studies show that the CTFB has not developed synchronously. In general, the fold belt has grown progressively westward, toward the deformation front [*Johnson and Alam*, 1991; *Steckler et al*., 2008; *Maurin and Rangin*, 2009]. Many of the folds in the west have been active only from the late Pliocene or later. Many of the folds in the eastern part of the CTFB appear to no longer be active, even though they are clearly evident on the SRTM imagery. The rate of propagation of the deformation front has been about 100 mm/yr through the past 2 million years [*Maurin and Rangin*, 2009], far greater than the current rate of convergence across the fold belt.

This rapid propagation of the deformation front helps to explain the broad curvature of the CTFB between 24°N and the Shillong plateau. As the fold belt has propagated into the basin over the past 2 million years, it has not been able to propagate over the continental crust of the Shillong plateau, which has been rising and thrusting southward out over the basin through the past five million years. The sweep of the fold belt thus reflects the impediment to westward propagation imposed by the Shillong plateau.

Figure 6 shows in black those anticlines and related faults that do not appear to have been active recently. Those anticlines and related faults mapped in red have evidence for recent activity. In the case of the faults, evidence for activity consists of unusually steep flanks on the related anticline, which suggests that a fault has propagated to, or close to, the surface. In the following paragraphs, we describe the evidence for recent activity of some of the anticlines.

Published seismic reflection profiles across several anticlines reveal growth strata that constrain the initiation of folding. In some places the age of the growth strata constrain the initiation of anticlinal growth to Pliocene

or younger. The initiation of the Sylhet, Habiganj, Patiya, Jaldi, and two offshore anticlines (labeled S, H, P, and J, respectively, in Figure 6a) are so constrained [*Johnson and Alam*, 1991; *Steckler et al*., 2008; *Maurin and Rangin*, 2009].

Evidence of even more youthful activity exists for a few other folds. These include the Maheshkhali anticline, whose upper surface formed during the Last Glacial Maximum, when the fluvial plain extended many kilometers out onto the current seafloor but now sits far above the modern floodplain (M, Figure 6a). *Sharif Hossain Khan et al*. [2005] interpret this to indicate uplift in the past 18,000 years. Possible support for activity of this anticline is a report of extensional cracks that developed atop this anticline during a small (m_b 5.2) earthquake in 1999 [*Ansary et al*., 2000]. *Steckler et al*. [2008] plausibly interpret these as an indication of "coseismic slip on a blind ramp-flat fault with extension in the hanging wall block as it moved through the kink." *Sharif Hossain Khan et al*. [2005] also propose that the nearby Jaldi anticline is active, as evidenced by the young age of the soil on its crest. Their luminescence date from the crestal surface of the anticline implies a rise in fluvial base level in the past 35,000 years.

Other clear evidence of youthful vertical deformation along the western portion of the CTFB is resolvable from the SRTM 90 m digital elevation model and from optical satellite imagery. Sandwip Island, at the mouth of the Ganges, is a good example (SW in Figure 6a). A nearby radiocarbon date [*Goodbred and Kuehl*, 1999] suggests to us that its upper surface is about 7000 years old or younger. That surface displays an anticlinal warp of ~5 m above sea level (Figure 6b). This is likely representative of the entire Comilla Tract immediately to the north. The surface of this large tract at the front of the modern delta is 3–4 m above the modern surface of the delta [*Steckler et al*., 2008] and appears to be very gently folded from the global digital elevation model (CT, Figure 6a). Further west, published structural maps show several N-S trending anticlines between the Ganges River and the Comilla Tract [e.g., *Khan*, 1991] (Figure 6a). Although we do not find clear evidence of surface warping above these anticlines from the digital elevation model, the existence of these structures suggests that the active deformation front has propagated as far west as the active Ganges-Brahmaputra River delta.

Two other young uplifts are clear in SRTM topography and optical imagery farther south. The anticline at the southern tip of Bangladesh (Dakhinpara) has a terrace ~ 5 to 10 m above the current fluvial and coastal plain (Da, Figure 6a). Farther south, St. Martin Island sports at least two marine terraces, which imply incremental uplift since the mid-Holocene (SM, Figures 4 and 6a).

Although the earthquake history of the Chittagong-Tripura fold belt is ambiguous, large, destructive earthquakes are well known and have been frequent. One recent large event is the M_w ~ 7.5 Srimangal Earthquake of 1918, which strongly shook the northwestern part of the CTFB and adjacent Ganges-Brahmaputra delta. An isoseismal map [*Stuart*, 1920] shows clearly that the highest intensity occurred just east of the Rashidpur anticline (R, Figure 6a), where most of the buildings were leveled to the ground. The distribution of high intensities during the Srimangal Earthquake suggests that it was caused by a fault beneath the northwestern part of the fold belt, most likely the fault associated with uplift of the Rashidpur anticline.

Other large earthquakes within the Chittagong-Tripura fold belt may have resulted from slip on the megathrust itself. The area of Chittagong was so badly damaged by the Arakan earthquake of 1762 that some have suggested that the megathrust ruptured from the Ramree domain through the southern portion of the Dhaka domain [e.g.,*Cummins*, 2007; *Gupta and Gahalaut*, 2009]. Another earthquake in 1548 also wreaked havoc across nearly the entire Dhaka domain. Based on its widespread high seismic intensities, *Steckler et al*. [2008] suggest that this earthquake resulted from rupture of the megathrust north of the 1762 rupture patch. However, paleoseismological investigations along the southern flank of the Shillong Plateau suggest that the earthquake resulted from slip on the north-dipping Dauki fault [*Morino et al*., 2011]. Their evidence consists of a folding event that has an age consistent with the date of this historical earthquake. Another earthquake around 1663 and 1664 may also have resulted from rupture of a structure within the Dhaka domain. This earthquake resulted in widespread ground deformation (e.g., liquefactions) about 150 km from the Dhaka [*Ambraseys*, 2004].

3.2.2. The High Indoburman Range

A ~170 km long right-lateral oblique-slip fault is clearly evident in the topography of the high Indoburman range near Imphal (Figure 6a). Along the western flank of the Imphal basin, many of the eastward flowing rivers and basins exhibit dextral deflections and warping along the Churachandpur-Mao fault (Figure 7). This

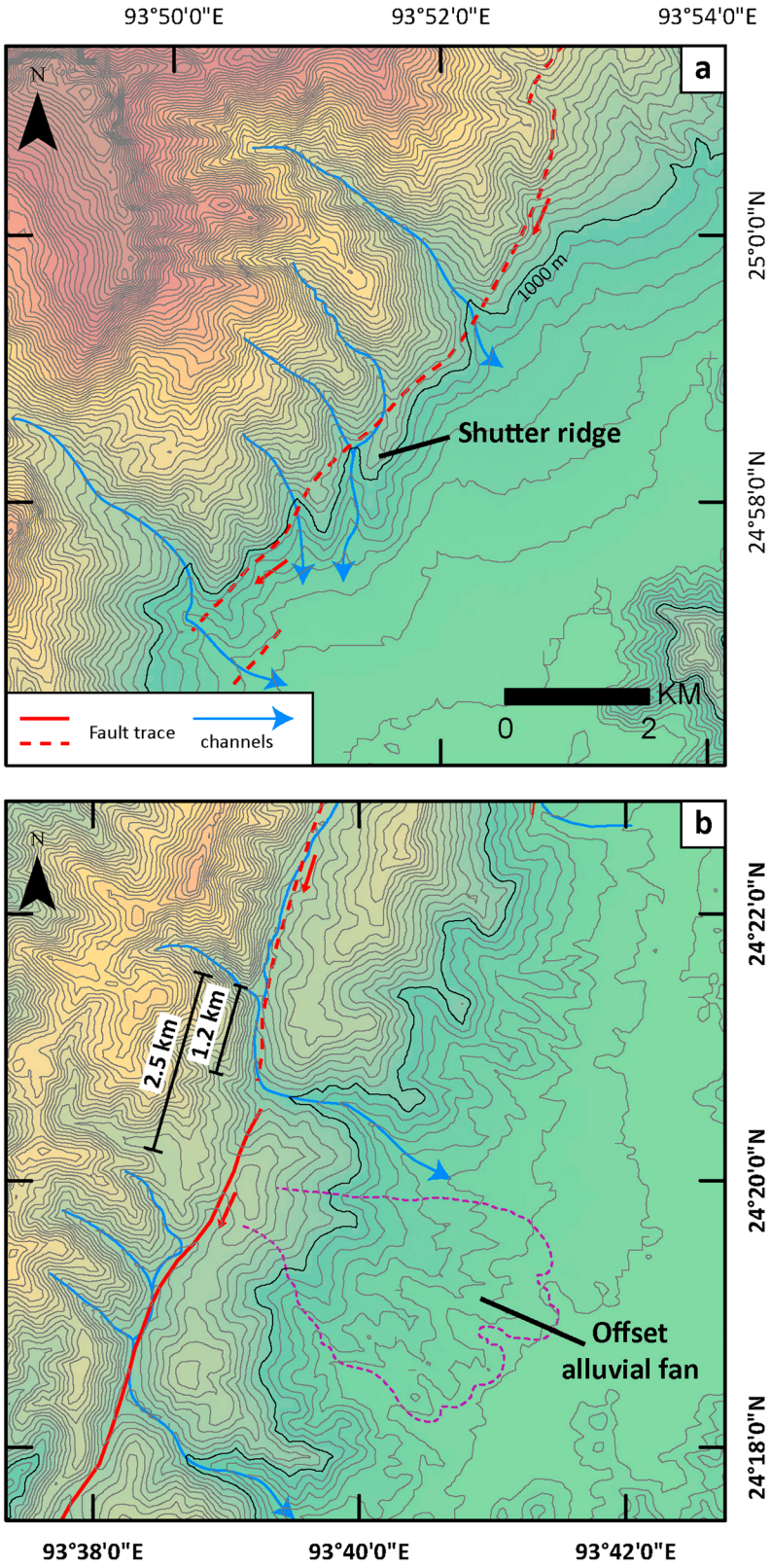

Figure 7. Geomorphological features of the Churachandpur-Mao fault at two different locations reflect clear dextral motions along the fault. (a) Clear right-lateral channel deflections on the 25 m contour map from SRTM topography along the northwestern margin of the Imphal basin. (b) Eroded and beheaded alluvial fan and nearest plausible source basin about 2.5 km to the northeast along the fault.

NNE-SSW-striking fault also shows a clear vertical component in the SRTM topography, as the range rises up steeply more than 1000 m from the basin floor to the mountain crest. We find the largest dextral geomorphic offset is about 3 km along the fault trace, whereas the vertical offset is likely more than 1.5 km (Figures 7a and 7b). Both the vertical and right-lateral offsets diminish northward and southward, and the geomorphological evidence becomes less compelling north and south of the basin.

The latitudinal span of the Churachandpur-Mao fault is almost perfectly coincident with the span over which the CTFB narrows from south to north. This spatial correlation suggests that the fault has resulted from the impediment posed by the Shillong block to westward motion of the Indoburman range. If the high Indoburman range is not moving westward as fast in the north as it is in the south, then a dextral-slip fault with the orientation of the Churachandpur-Mao fault could be a consequence and manifestation of that differential motion.

This neotectonic scenario also suggests that the initiation of the Churachandpur-Mao fault would have been much later than the formation of the high Indoburman range. Geomorphic features within the Imphal basin support this hypothesis. For example, wind gaps along the western flank of the basin suggest that the drainage basins west of the Imphal basin originally extended east into the basin. Moreover, the burial of highly eroded ridges in the eastern part of the basin indicates that it became the depositional center after formation of these ridges. Both of these observations support that initiation of the Churachandpur-Mao fault occurred long after initiation of uplift and erosion of the high Indoburman range.

If the fault initiated a million years ago and the 3 km dextral and 1.5 km vertical offsets represent its total offset, then average slip rate of the fault is about 4 mm/yr. This guess of its very long-term rate is much lower than the differential motion seen in geodetic measurements across the high Indoburman range. GPS vectors suggest that modern motion across the Churachandpur-Mao fault could be about 16 mm/yr and that motion is wholly strike slip [*Jade et al*., 2007; *Kumar et al*., 2011; *Gahalaut et al*., 2013]. About 5 mm/yr of this dextral motion appears to be accommodated by shallow creep on the fault. The remaining motion across the high Indoburman range could be accommodated either by a deeply locked Churachandpur-Mao fault or by strike-slip motion on the underlying megathrust. Thus, the 16 mm/yr rate calculated by *Gahalaut et al*. [2013] represents the maximum plausible strike-slip rate across this fault.

3.2.3. East Flank of the Indoburman Range and Beyond

The tectonic morphology of the eastern flank of the Indoburman range within the Dhaka domain is very different than that throughout the Ramree domain. In addition to an impressive east-facing escarpment, the eastern flank includes the basin of the Kabaw valley, which is flanked on the east by a range of narrow, low hills (Figure 6a). This implies that the east-dipping fault that traverses the eastern side of the Kabaw valley is raising the hills faster than sediment streaming out of the Indoburman range can bury the hanging wall block of the fault.

We call this the Kabaw fault system, as originally proposed by *Win Swe et al*. [1972]. Others have used this name in reference to west-dipping thrust faults along the entire eastern flank of the Indoburman range [e.g., *Hla Maung*, 1987; *Curray*, 2005]. In this work, we conform to the original use of the name.

The youthful appearance on SRTM and ASTER images of the eastern flank of the Kabaw valley between 22°N and 24.8°N suggests that the Kabaw fault system is active. Closer inspection of the southern half of the valley with 1:25,000-scale aerial photographs revealed no evidence for offset of an elevated erosion surface along a steeply dipping strike-slip fault in the center of the valley (Figure 8). Moreover, evidence of thrust-fault scarps on the eastern side of the low hills was equivocal. We therefore believe that the slip rate of the Kabaw fault system is equal to, or lower than, rates of sedimentation and erosion in this N-S-running narrow basin.

3.3. Naga Domain

A fundamental change in the Indian-Burma collision occurs at 25°N, where the Dauki thrust intersects the western flank of the Indoburman range (Figure 1). As the folds of the Chittagong-Tripura fold belt approach the Dauki thrust from the south, they swing eastward and the width of the belt narrows from about 240 to about 160 km (Figure 6a). North of the Dauki fault the CTFB is absent, and in its place along the steep western flank of the Naga Hills is a fold and thrust belt that is an order of magnitude narrower (Figure 9a). We refer to this segment of the Indo-Burman collision as the Naga domain, after the eponymous mountains that span the 430 km distance between the Shillong plateau and the Himalayan syntaxis.

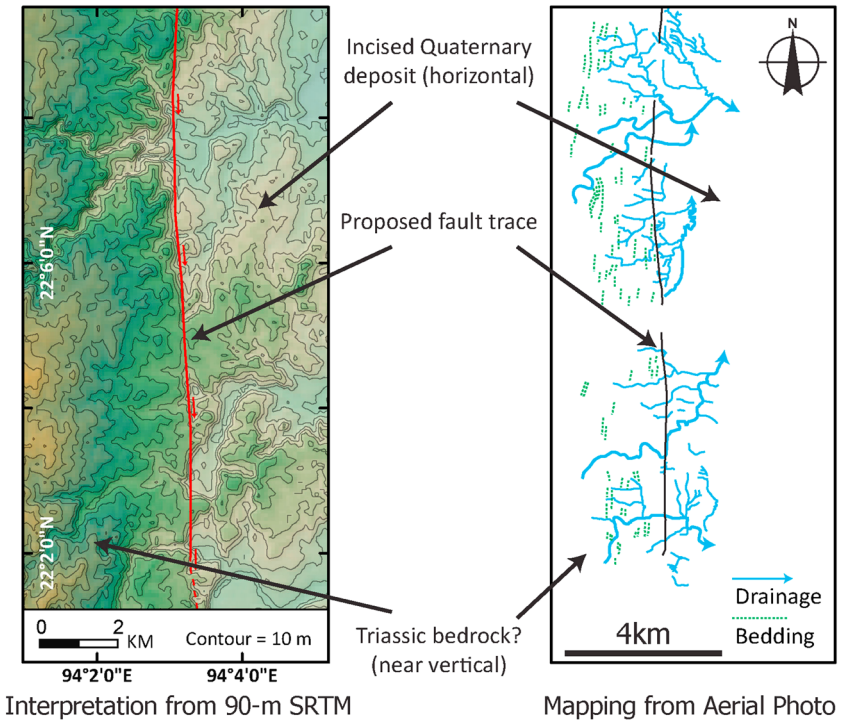

Figure 8. Fault and drainage map in the southern part of the Kabaw valley shows no young offset features along a strike-slip element of the fault. This indicates a very low slip rate along this dextral-slip fault.

This dramatic change in the structural and topographic expression of collision at 25°N reflects the dramatic change in nature of the footwall block across the Dauki fault. As we have just described, collision south of the Dauki fault in the Dhaka domain is extending rapidly westward, out into the thick pile of Gangetic delta sediments that rest atop transitional and foundering oceanic crust (Figure 1). North of the Dauki fault the Naga Hills override a very different footwall—recently uplifted continental crust of the Shillong Plateau and (farther east) the narrow continental shelf of the Assam block [e.g., *Verma et al.*, 1976; *Clark and Bilham*, 2008].

The stark geomorphologic contrast between Chittagong and Naga domains appears to reflect shallow crustal differences in collision rather than deep-seated ones. The nature of the higher Indoburman range does not change markedly across the domain boundary, nor do isobaths drawn on the top of Wadati-Benioff zone beneath the mountains show any clear bend or tear across the domain boundary below depths of ~60 km. The narrower width of the shallow portions of the Wadati-Benioff zone beneath the Naga Hills is consistent with the lack of a wide, CTFB-like fold and thrust belt and underlying décollement.

Beneath the Naga Hills, the Wadati-Benioff zone extends to depths of ~160 km, as far as 150 km from the mountain front. This implies subduction of at least a couple hundred kilometer of oceanic lithosphere before the thrust faults of the Naga hills began to ramp up onto the continental shelf of the Assam block in the early Miocene [*Kent et al.*, 2002].

The Naga Hills reflect convergence of the Burma plate and the Assam block across the 430 km that separate the Shillong Plateau from the Himalayan syntaxis. The narrowing of the hills from about 170 km in the southwest to 90 km in the northeast (Figure 9a) may imply a northeastward diminishment in total shortening across the range.

Geomorphological expression of the Naga thrust is very clear along the front of the Naga Hills, and its presence there is well known from geological and geophysical surveys [e.g., *Mathur and Evans*, 1964]. The fault trace appears as several arcuate lobes along the range front. Along its southwestern 100 km, a linear scarp clearly marks the location of the fault. An anticline and 5 km wide piggyback basin sit on the hanging wall block, and nested terraces imply incremental uplift. The highest terrace projects ~200 m above the range front, suggesting late Quaternary uplift of at least that amount (Figure 9b). Younger terraces display uplifts ranging from 20 to 50 m.

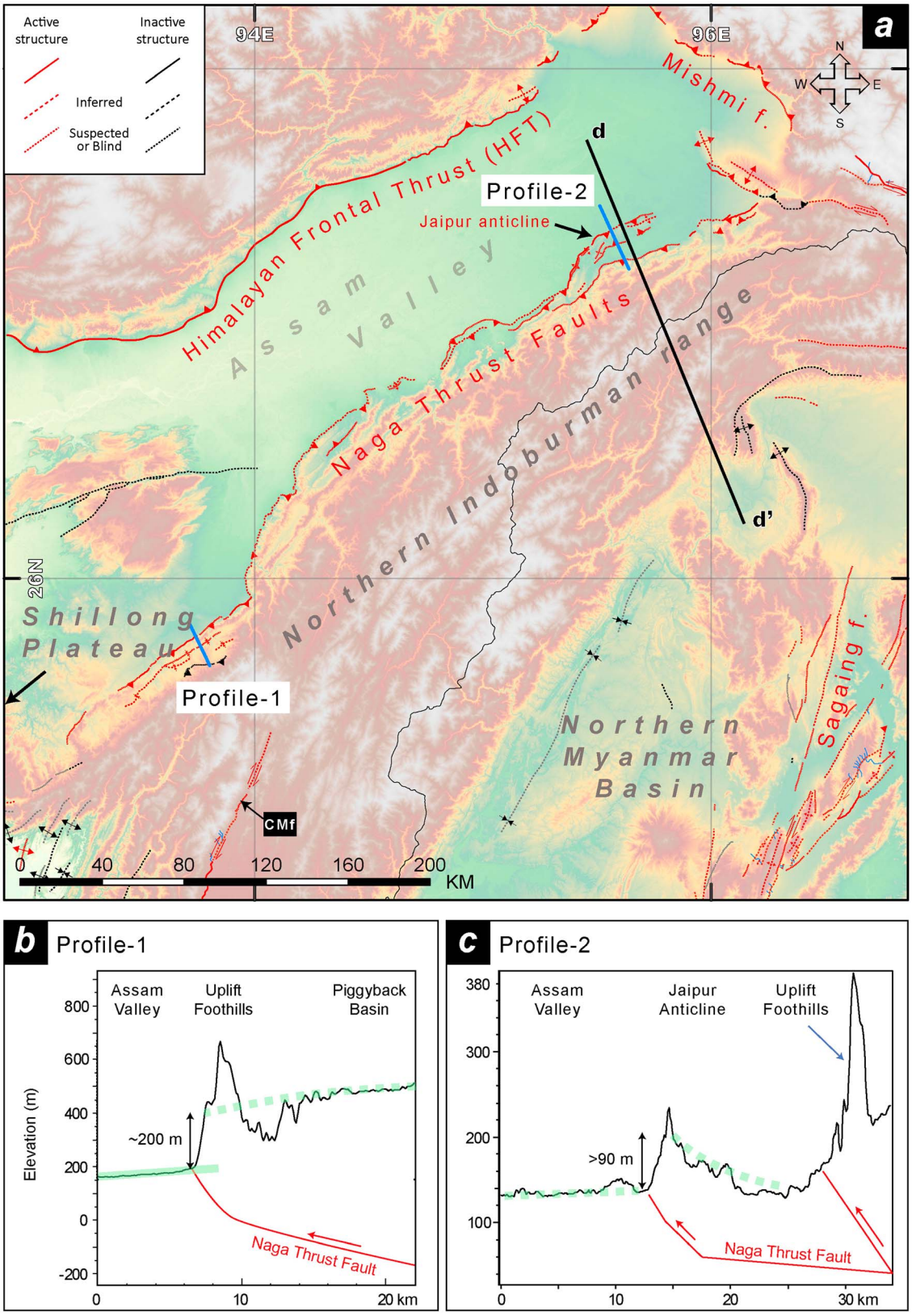

Figure 9. Map and cross sections of the Naga thrust fault system. (a) Map of traces of the fault visible in SRTM imagery shows three distinct lobes along its ~400 km length. (b and c) The geomorphic profiles show the thrust fault system deforms late Quaternary depositional surfaces and offsets them vertically by more than 90 m. Cross-section DD′ appears in Figure 19. The scale at depth is not equal to the scale of topographic profiles.

Geological mapping and seismic reflection lines at ~95.5°E illuminate the nature of the fault system. The fault dips moderately to steeply and breaks the surface at the position shown in Figure 9a. It thrusts folded lower Miocene rocks over undeformed upper Pliocene to Quaternary beds [*Kent et al*., 2002]. Recent field investigations show the Naga thrust overrides Quaternary alluvium at the mountain front [*Aier et al*., 2011]. Northwest of the main thrust fault, the geometry of the Jaipur anticline implies that it developed as a fault-propagation fold that was eventually breached by propagation of the fault to the surface. The clear geomorphological expression of the anticline implies that it is still active and that the dip of the thrust fault decreases at depth (Figure 9c).

The Naga thrust system terminates at 96°E where it appears to be cut by a NW-striking thrust fault and associated anticlines. This short fault appears to be the westernmost element in a system of thrust faults associated with westward thrusting of the Eastern Himalayan syntaxis over the Assam valley and Naga Hills. We infer from the topographic profile of the crest of the Naga Hills that slip on the Naga thrust dies out over ~100 km as it approaches this termination.

3.4. The Sagaing Domain

The Sagaing fault system performs the classic role of a ridge-trench transform fault as it traverses the 1400 km distance between the Andaman Sea spreading center in the south and the eastern Himalayan syntaxis in the north (Figure 1) [*Yeats et al*., 1997]. Total dextral offsets since the Miocene, estimated from bedrock matches, river offsets across the fault and the total opening of the Andaman Sea range from about 203 to 460 km [e.g., *Mitchell*, 1977; *Curray et al*., 1982; *Hla Maung*, 1987; *Armijo et al*., 1989; *Myint Thein et al*., 1991]. The central and southern parts of the Sagaing fault also approximate the western boundary of the Sunda block during its eastward and southward extrusion in an early (~34 to ~17 Ma) phase of the Indian-Asian collision [e.g., *Leloup et al*., 2007]. It is recognized as the region's major tectonic divide, separating disparate rocks of the Burma plate from those of the Sunda plate [*Mitchell*, 1977; *Curray et al*., 1982].

The recent slip rate of the Sagaing fault, assessed from an offset Pleistocene basalt and from GPS measurements, is about 20 mm/yr [*Bertrand et al*., 1998; *Vigny et al*., 2003; *Socquet et al*., 2006; *Maurin et al*., 2010]. Given its high slip rate, it is no surprise that the fault is well expressed geomorphically along most of its length. Isoseismal maps and seismic analyses of historical earthquakes show that about half of the Sagaing fault has ruptured during many large earthquakes over the past nine decades [e.g., *Coggin Brown and Leicester*, 1933; *Hurukawa and Phyo Maung Maung*, 2011] (Table 1).

Like the San Andreas fault, but in contrast to the Sumatran fault, the Sagaing fault system is unbroken by large step overs or complications along most of its length [e.g., *Yeats et al*., 1997]. This unbroken geometry is probably due to the fault's large accumulation of slip [*Wesnousky*, 1988; *Stirling et al*., 1996; *de Joussineau and Aydin*, 2010]. The northern 400 km of the fault system, however, is very complex. It comprises several distinct faults arranged in a complex horsetail pattern that fans out northward to a width of about 100 km. This complex geometry likely reflects both the lengthening of the fault system to accommodate India's northward motion and the extrusion of Asia around the eastern Himalayan syntaxis.

Between about 18°N and the Himalayan syntaxis, the Sagaing fault forms a broad concave-eastward arc (Figures 1 and 2). The fact that the arc mimics the curvature of the eastern flank of the Indoburman range to the west and coincides with the belt of sinistral-slip faults to the east intimates a shared cause—likely the westward extrusion of the Sichuan-Yunnan block around the syntaxis. The fast slip rate of the Sagaing fault overwhelms erosional and depositional activity along most of its trace, so abundant tectonic landforms enable us to map and characterize most of the fault well. We divide the fault in to various segments based on the geomorphical expression of the fault and its historical seismicity [e.g., *Barka and Kadinsky-Cade*, 1988]. We begin with segments along the southern subaerially exposed and relatively simple portion of the fault and then proceed to the complex horsetail of the northern few hundred kilometer.

3.4.1. The Southern Section of the Sagaing Fault

Although a synoptic view of most of the Sagaing fault leads one to think that its geometry is simple, careful geomorphic mapping justifies its division into five distinct segments between 16.5° and 23.5°N (Figure 10). What distinguishes these segments are bends, splays, and distinct secondary features, as well as the terminations of historical ruptures.

Table 1. Significant Earthquakes Within the Study Area Since the Late Nineteenth Century[a]

Date (YYYY/MM/DD)	Latitude	Longitude	M	M_{type}[b]	Location	Type of Records[c]	Reference
Indoburman Range and Central Burma Basin							
1762/4/2	19	93.5	> 8.5	M_{fault}	Sunda megathrust	Int + G	H; O; W1
1858/3/23	19.3	95	7.7	M_{int}	Central Burma basin	Int	O; A&D
1906/6/24	15	92	7.3	M_{unk}	Near megathrust	S	A
1918/7/8	24.5	91	7.5	M_w	Bangladesh	Int + S	S; E&V
1927/12/17	17.5	95.5	~ 6?	M	North of Yangon	Int	C.B. [1929]
1943/10/23	26	93	7.1	M_w	Assam Valley	S	E&V
Sagaing Fault							
1839/3/23	22	96	> 7	M	Near Mandalay	Int	O
1929/8/8	19.2	96.2	~7	M	Near Taungoo	Int	B2
1930/5/5	17.78	96.73	7.2	M_w	Bago	Int + S	C.B., 1931; E&V; H&P
1930/12/3	18.12	96.76	7.3	M_w	Pyu	Int + S	C.B. et al., 1933; E&V; H&P
1931/1/27	25.41	97.02	7.6	M_w	Kamaing	Int + S	C&R; E&V; H&P
1946/9/12	24.02	96.09	7.3	M_w	Sagaing fault	S	E&V; H&P
1946/9/12	22.35	96.24	7.7	M_w	Sagaing fault	S	E&V; H&P
1956/7/16	22.06	95.9	7.1	M_w	Sagaing	S + Int	E&V; H&P
1991/1/5	23.59	95.97	6.9	M_w	Tagaung	S	E&V; H&P; GCMT
2003/9/21	19.91	95.63	6.6	M_w	Taungdwingyi	S	E&V; H&P; GCMT
2012/11/11	22.755	95.708	6.8	M_w	Singu	S + G	NEIC; GCMT
Shan Domain							
1912/5/23	21	97	7.7	M_w	Kyaukkyan fault	Int + S	C.B. [1914]; E&V
1923/6/22	22.589	98.681	7.2	M_w	Eastern Myanmar	S	E&V
1925/12/22	20.538	101.667	6.8	M_{unk}	Mae Chan fault ?	S	A
1935/11/1	21.148	103.082	6.8	M_{unk}	close to DBPF	S	E&V
1941/5/16	23.7	99.4	6.9	M_s	Nanting fault	S + Int + G	*Lee et al.* [1978]; GNSIZM [1979]
1941/12/26[d]	21.08?	99.14?	7	M_s	Yunnan-Myanmar	Int + S	GNSIZM [1979]; E&V
1942/2/1	23.1	100.3	6.8	M_{unk}	Yunnan	Int + S	X; A
1950/2/2	21.758	99.97	7.1	M_w	Jinghong fault ?	Int + S	X; A
1976/5/29	24.509	98.913	6.7	M_w	Yunnan	Int + S	GNSIZM [1979]; A; GCMT
1976/5/29	24.52	98.502	6.6	M_w	Yunnan	Int + S	GNSIZM [1979]; A; GCMT
1983/6/24	21.721	103.265	6.2	M_w	close to DBPF	Int + S	*Trieu et al.* [2008]; A; GCMT
1988/11/6	22.869	99.571	7	M_w	Lancang fault	S + Int + G	*Yu et al.* [1991]; A; GCMT
1992/4/23	22.422	98.887	6.1	M_w	Myanmar	S	A; GCMT
1992/4/23	22.41	98.821	6.1	M_w	Myanmar	S	A; GCMT
1995/7/11	21.89	99.22	6.8	M_w	Myanmar-Yunnan, Menglian fault ?	Int + S	*Chen et al.* [2002]; A; GCMT
2007/3/10	24.727	97.597	5.5	M_w	Myanmar-Yunnan, Daying River fault	S	NEIC; GCMT; *Lei et al.* [2012]
2007/6/2	23.02	101.01	6.1	M_w	Yunnan, Wuliang Shan fault	S	A; GCMT
2007/5/16	20.47	100.69	6.3	M_w	Laos, Mae Chan fault	S	A; GCMT
2011/3/24	20.62	100.02	6.8	M_w	Myanmar, Nam Ma fault	S + G	W2; GCMT

[a]Reference: A: *Allen et al.* [2009]; A&D: *Ambraseys and Douglas* [2004]; C&R: *Chhibber and Ramamirtham* [1934]; E&V: *Engdahl and Villasenor* [2002]; H: *Halsted* [1841]; H&P: *Hurukawa and Phyo Maung Maung* [2011]; O: *Oldham* [1883]; S: *Stuart* [1920]; W1: *Wang et al.* [2013b]; W2: *Wang et al.* [2013a] X: *Xie and Tsai* [1983]; C.B. [1914, 1929, 1931, 1933]: *Coggin Brown* [1914, 1929,]; *Brown et. al.* [1931]; *Brown and Leicester* [1933].
[b]M_{fault}: estimate from the fault slip model; M_{int}: estimate from the seismic intensity record; M_{unk}: instrumental record, type of magnitude unspecified. M: speculate from historical seismic intensity records.
[c]Type of records: Int: intensity; S: instrument; G: ground deformation.
[d]The epicenter location is consistent with the isoseismal map.

3.4.1.1. Bago Segment

The Bago segment extends northward at least 170 km from the Myanmar coast, across the young, southward-propagating delta of the Sitong River [*Tsutsumi and Sato*, 2009; *Wang et al.*, 2011]. We do not know how much further it extends southward on the submarine portion of the delta. However, regional structural maps show that the Bago segment connects to a series of E-W-running normal faults several tens of kilometer south of the current coastline [e.g., *Replumaz*, 1999; *Pubellier*, 2008]. Its northern limit coincides with an abrupt 10° westward bend at 18°N (Figure 10). *Tsutsumi and Sato* [2009] and *Wang et al.* [2011] mapped in detail the tectonic landforms of this segment, from aerial photos and satellite imagery. The last major earthquake produced by the Bago segment was the M_w 7.2 Pegu earthquake of May 1930 (Table 1) [*Pacheco and Sykes*, 1992]. Measurement of small offsets led *Tsutsumi and Sato* [2009] to suggest that the maximum offset during this earthquake was at

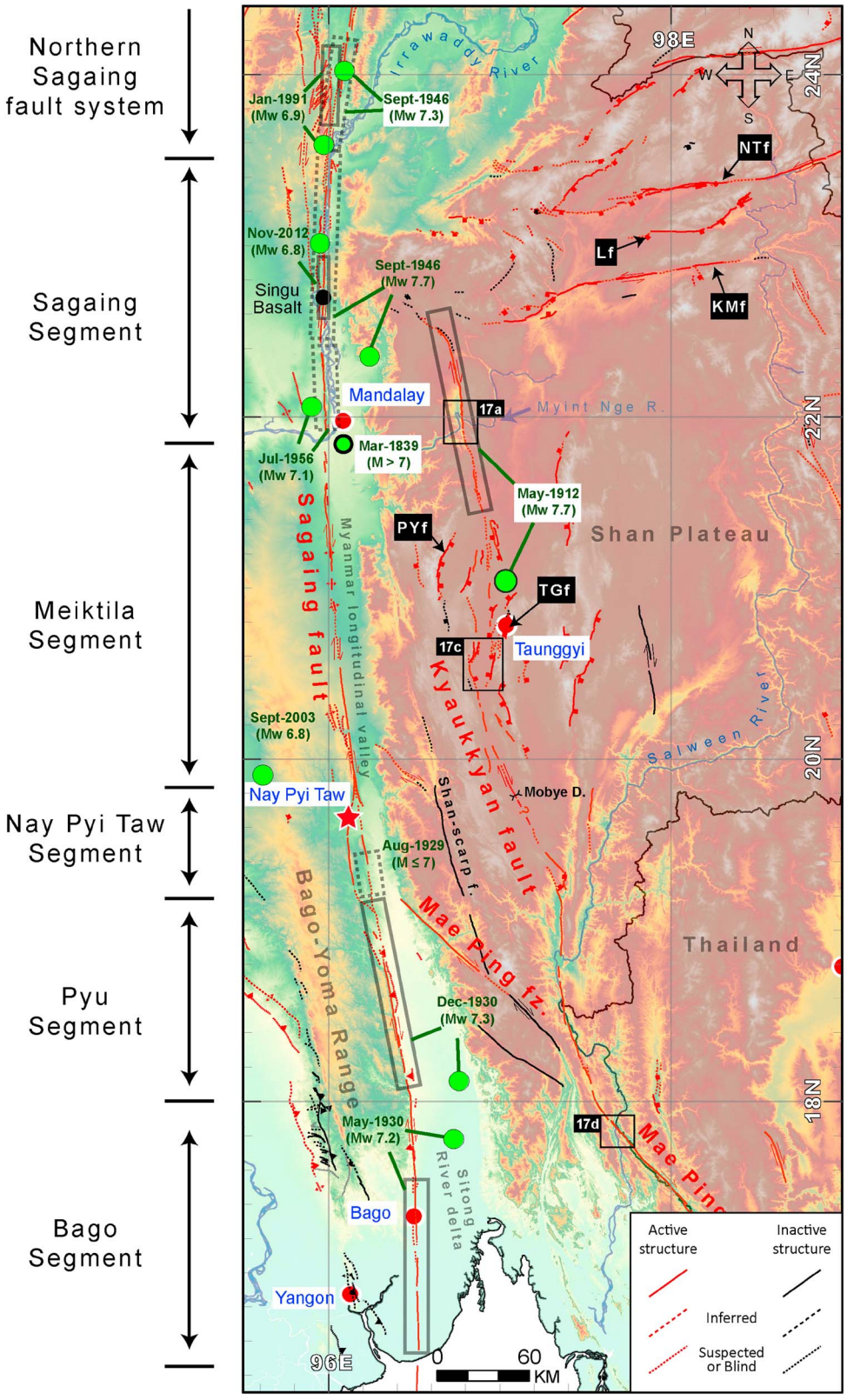

Figure 10. Fault segments and historical earthquakes along the central and southern parts of the Sagaing fault. Green dots show relocated epicenters from *Hurukawa and Phyo Maung Maung* [2011]. Dashed and solid gray boxes surround segments of the fault that ruptured in historical events. NTf = Nanting fault; Lf = Lashio fault; KMf = Kyaukme fault; PYf = Pingdaya fault; TGf = Taunggyi fault.

least 3 m. *Wang et al.* [2011] suggest a rupture length of about 100 km, extending from the southern coastline to ~20 km north of Bago city, based on field investigations and their interpretation of isoseismals published by *Coggin Brown et al.* [1931]. Measurements of an offset ancient wall and related paleoseismic work north of Bago led *Wang et al.* [2011] to propose an earthquake recurrence scenario for the Bago segment.

3.4.1.2. Pyu Segment

The Pyu segment extends ~130 km, from the sharp bend at 18°N to a bifurcation at 19.1°N. Along this reach, the main trace of the Sagaing fault skirts the base of the escarpment of the Bago-Yoma range (Figure 10). SRTM imagery clearly shows that most fluvial channels and alluvial fans from the Bago-Yoma range are offset right laterally at the mountain front (for details, see supporting information Figure S2). An elongate terrace lies east of the central part of this segment. The terrace rises on the hanging wall block of a west-dipping reverse fault that crops out on the east flank of the ridge [*Replumaz*, 1999]. This reverse fault and the escarpment are manifestations of a minor component of transpressional shortening across the Pyu segment [*Replumaz*, 1999; *Wang et al*., 2011]. This transpression is consistent with the 10° counterclockwise deviation of this section of the Sagaing fault from its overall strike.

The last major earthquake generated by the Pyu segment is the M_w 7.3 Pyu earthquake, which occurred in Dec 1930, just a few months after the similar-sized rupture of the Bago segment to the south (Table 1). The relocated epicenter of the Pyu earthquake is close to the segment's southern boundary [*Hurukawa and Phyo Maung Maung*, 2011]. The isoseismals drawn by *Coggin Brown and Leicester* [1933] clearly show that the highest intensities of the earthquake span the entire Pyu segment. We therefore propose that the majority of the Pyu segment ruptured during the December 1930 earthquake.

3.4.1.3. Nay Pyi Taw Segment

At 19.1°N, the Sagaing fault splays into two parallel fault traces that span the entire ~70 km length of the Nay Pyi Taw segment (Figure 10). The relief across the fault along this segment is much more subdued than it is along the Pyu segment. This indicates less vertical motion. Both traces of the Nay Pyi Taw segment offset channels and alluvial fans, so slip is significantly partitioned between these two branches. In the north, both traces traverse the ~30 km long basin in which the new capital, Nay Pyi Taw, was established in 2005. The western trace cuts through the eastern edge of the new capital and sports a ~5 m high east-facing scarp.

This segment does not appear to have produced a large earthquake in recent times. The moderate Swa earthquake of August 1929 (Table 1) severely damaged the railroad and bridges about 40 km south of the new city [*Coggin Brown*, 1932; *Chhibber and Ramamirtham*, 1934]. The highest intensities occurred along the eastern branch south of Myanmar's new capital city [*Coggin Brown*, 1932]. However, because the earthquake does not appear in the early global seismic catalog and was only felt in a limited area, we believe its magnitude is likely to have been smaller than M_w 7.

3.4.1.4. Meiktila Segment

The Meiktila segment traverses a ~220 km reach of the fault between Nay Pyi Taw and Mandalay. Its very simple trace runs almost uninterrupted from just north of Nay Pyi Taw to the southern side of the Irrawaddy river. Our choice for the northern boundary of the Meiktila segment is a bit arbitrary but is coincident with a greater prominence of transpressional secondary features north of the river.

Unlike the Pyu and the Nay Pyi Taw segments, the Meiktila segment does not run along the eastern base of the Bago-Yoma Range; instead, it traverses a broad valley (Figures 10 and S2). Narrow linear ridges are common along the fault trace as it traverses the fluvial valley fill. These probably reflect shallow shear dilatation of the faulted sands and gravels of the floodplain [e.g., *Gomberg et al*., 1995]. The utter lack of elevation differences across the fault shows that along this segment the Sagaing fault has no vertical component of slip. The largest clear right-lateral offset is ~2.4 km across a channel at 20°N.

There is no clear historical record of rupture of the Meiktila segment. The most recent plausible such event would be the Ava earthquake of 1839, so named for the ancient capital that straddles the fault on the southern bank of the Ayeyarwady River. Records written by British officers in nearby Mandalay indicate that the earthquake caused catastrophic damage and liquefaction east and south of the Ayeyarwady River, especially in Ava [*Oldham*, 1883; *Chhibber and Ramamirtham*, 1934].

3.4.1.5. Sagaing Segment

The namesake of the Sagaing segment is a small city on the fault just north of the Ayeyarwady River. It is the tectonic morphology of this section of the fault that led to the fault's discovery by *Win Swe* [1970]. The

northern limit of the Sagaing segment is at 23.5°N, where the fault steps left approximately 2 km from the eastern bank to the western bank of the Ayeyarwady (Figures 10 and S2). The northern limit of the Sagaing segment also marks the location where the fault splays into multiple traces. Further to the south, in the low Sagaing hills, east of the fault and north of the Ayeyarwady crossing are the southernmost outcrops of metamorphic rocks on the eastern flank of the fault.

Like the Meiktila segment, the Sagaing segment is relatively straight and simple. However, along its southern extent, the elongate ridges that comprise the Sagaing hills are larger than the ridges in the young fluvial sediments of the Meiktila segment and display more structural relief. Perhaps this greater relief is an indication that the formation of the Sagaing hills began well before the fault-zone ridges to the south, where they involve disruption only of young sediment and rocks. Between 21.9°N to 22.6°N, the Sagaing segment runs along the western bank of the Irrawaddy River and offsets a series of post-Pliocene alluvial fans along a 20 km reach [*Myint Thein et al*., 1991].

North of the Singu basalt, SRTM topography suggests that the Sagaing fault comprises two parallel fault traces, west and east of the Ayeyarwady River. Farther north, the western trace becomes what we term the Tawma segment, after it splits to two northward-diverging faults. A 5 to 10 m high east-facing scarp on a fluvial surface attests to the recent activity of the eastern trace.

The northern two thirds of the Sagaing segment may have produced the magnitude 7.6 earthquake of September 1946 (Figure 10 and Table 1). The relocated epicenter of the earthquake implies that the event initiated south of the Singu basalt [*Hurukawa and Phyo Maung Maung*, 2011] (Figure 10). A field investigation after the Shwebo earthquake of 11 November 2012 revealed ground cracks along the youthful-looking small scarps that we mapped from SRTM (Saw Ngwe Khaing, personal communication, 2012; Watkinson, personal communication, 2013). We therefore suggest that this part of the fault may have ruptured during both the September 1946 earthquake and this most recent event. The southern third of the segment may have ruptured during a smaller, M_w 7.1 earthquake in July 1956, during which buildings were damaged severely in the Sagaing-Mandalay area [*Win Swe*, 2006]. Unfortunately, no field investigations were conducted or isoseismal maps made after the 1946 or 1956 events. Based on the historical records of shaking, however, we speculate that the part of the Sagaing segment that runs along the western flank of Sagaing hills ruptured during the 1956 Sagaing earthquake.

3.4.2. The Northern Section of the Sagaing Fault

Beginning at 23.5°N, the Sagaing fault system fans northward as four distinct active fault zones that terminate sequentially from west to east between about 25° and 27°N (Figure 11). Geomorphological evidence for the westernmost fault zone ceases at about 25°N, whereas evidence for the easternmost one extends as far north as ~27°N and nearly connects to active structures between the Sagaing fault system and the Naga thrust. Because slip is distributed among these four subparallel fault traces, their geomorphic expressions are not as clear as those of the southern strands. The four fault zones of the northern Sagaing fault system comprise six discrete segments, distinguished by their geometries and discontinuities. In the paragraphs below, we describe each, starting with the southern and western ones and moving north and east.

3.4.2.1. Tawma and Ban Mauk Segments

The Tawma segment extends northward from a complex of faults at 23.5°N (TMs in Figure 11). The Tawma segment is the northward continuation of the western fault trace of the northern part of the Sagaing segment (see Figure S2 for details). The Tawma segment strikes northward nearly along the base of an east-facing escarpment. Some of the drainages flowing across the escarpment show right-lateral deflections across the fault.

The geomorphic expression of the segment disappears at ~24°N, at a left step over to the Ban Mauk segment, which is 10 km farther west (BMs, Figure 11). The step over between the two segments is complicated. SRTM imagery shows an array of NE-SW-striking faults across a 10 km wide transpressional ridge. Some of these faults may have a normal component of slip. The lengths of these secondary faults are mostly less than 20 km, and their subtle expression suggests they have low slip rates, compared to the rates of the main traces of the Sagaing fault.

A M_w 6.9 earthquake in 1991 may have resulted from rupture of the Tawma segment. Its relocated epicenter is near the segment's southern termination [*Hurukawa and Phyo Maung Maung*, 2011] (Figure 11). The (GCMT) Global Centroid-Moment-Tensor solution is consistent with dextral slip on a nearly N-S-striking fault. This

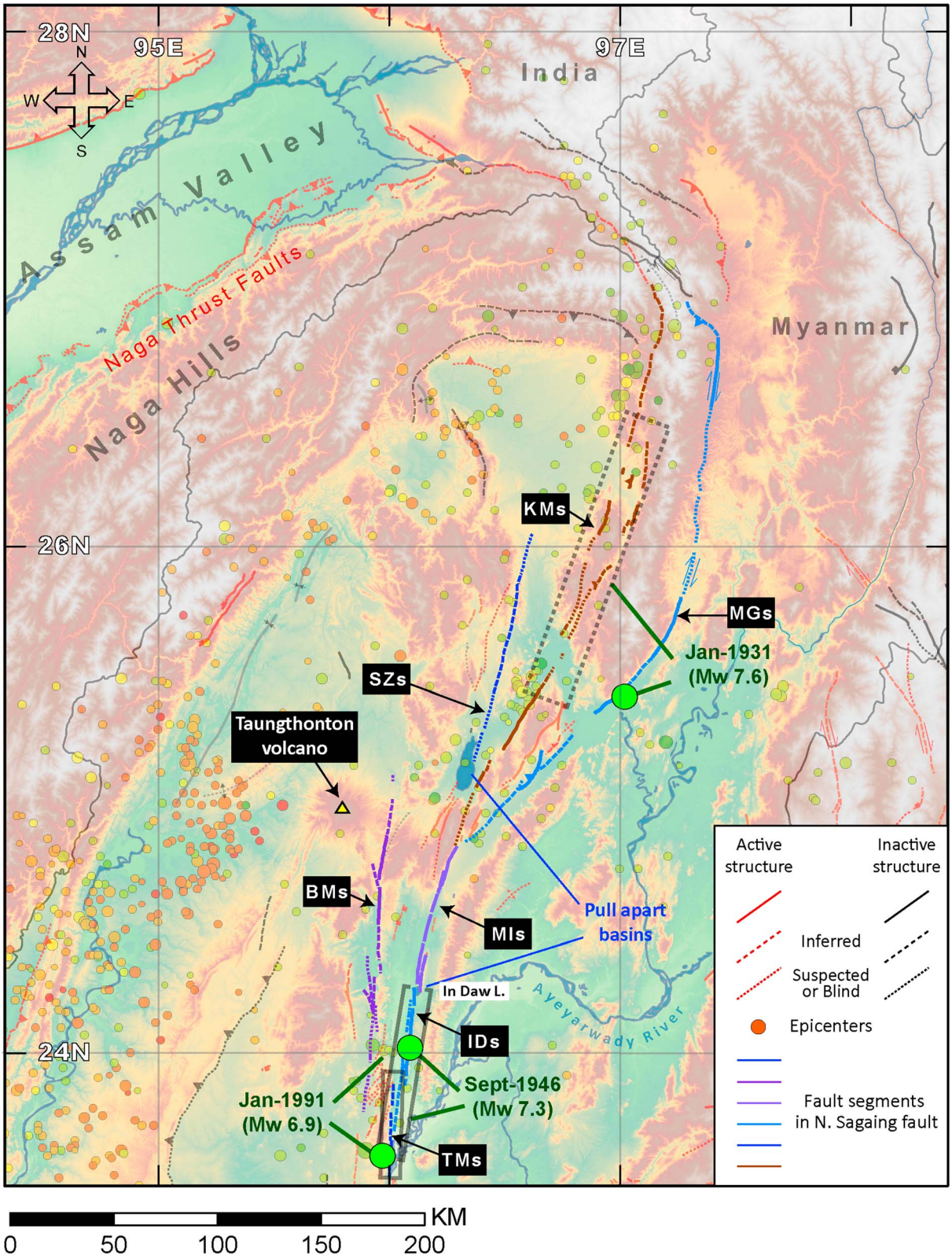

Figure 11. Fault segments of the northern Sagaing fault, differentiated by purple, blue, and brown colors. Lettering in black boxes show the abbreviated names of the segments. Green dots are relocated epicenters of major earthquakes from *Hurukawa and Phyo Maung Maung* [2011]. Gray boxes show inferred rupture patches during these earthquakes. BMs = Ban Mauk segment; TMs = Tawma segment; IDs = In Daw segment; MIs = Mawlu segment; SZs = Shaduzup segment; KMs = Kamaing segment; MGs = Mogang segment.

orientation is more consistent with the strike of the Tawma segment than the strike of the active In Daw segment to the east (IDs in Figure 11). Moreover, the length of the Tawma segment is comparable to typical rupture lengths for an earthquake of this magnitude [*Wells and Coppersmith*, 1994].

The Ban Mauk segment extends ~150 km northward from approximately 23.8°N (BMs in Figure 11). It separates Neogene volcanic rocks on the west from Miocene sedimentary rocks on the east [*Bender and Bannert*, 1983]. Geomorphological expression of the Ban Mauk segment is more muted than along segments to the south and east; clear geomorphic evidences, such as offset channels and offset drainage basins, are rare. Thus, we posit that the right-lateral slip rate of the Ban Mauk segment is significantly lower than the rates of neighboring faults. The northern terminus of the Ban Mauk segment is east of Taungthonton volcano, at 25°N. It appears that the fault trace there is covered by the apron of clastic deposits from Taungthonton volcano based on the SRTM topography. This is another indication of the low rate of slip of the Ban Mauk segment at least through the late Quaternary period.

The scant evidence of youthful activity along the Ban Mauk and Tawma segments is consistent with recent analysis of geodetic data, which implies that most strain across the Sagaing fault system is accumulated on fault segments farther east [*Maurin et al*., 2010].

3.4.2.2. In Daw and Mawlu Segments

The In Daw and Mawlu segments extend northnortheastward 170 km from the Sagaing segment. They form the eastern boundary of the fault system between ~24° and ~25°N (Figure 11). The In Daw segment separates from Tawma segment on the northern bank of Ayeyarwady River at 23.7°N, striking 7° more easterly than the Tawma segment. Farther north, at 24.25°N, a 3 km wide pull-apart basin, holding In Daw Lake, separates the In Daw segment from the Mawlu segment, which continues northnorthwestward another 90 km. The northern limit of the Mawlu segment coincides with several fault traces that cut Cretaceous to Eocene ultramafic rocks.

The InDaw and Mawlu segments are much more clearly expressed geomorphically than their western neighbors, the Tawma and Ban Mauk segments. We find the largest dextral geomorphologic offset across the In Daw/Mawlu segments to be about 4 km, 4 to 5 times larger than the largest geomorphologic offset across the Tawma and Ban Mauk segments. Furthermore, recent geodetic analysis implies strain accumulation equivalent to ~2 cm/yr of dextral slip across the InDaw and Mawlu segments [*Maurin et al*., 2010]. These two independent observations imply that the slip rate across these eastern segments has been substantially higher than the slip rates of the western segments through at least the past few thousand years.

Although their epicenters were separated by 200 km, the In Daw segment produced a M_w 7.3 foreshock 3 min before the Sagaing segment's M_w 7.7 earthquake of September 1946 [*Pacheco and Sykes*, 1992] (Table 1 and Figures 10 and 11). The size of the 7.3 earthquake is consistent with the 80 km length of the In Daw segment, so we suspect that the entire In Daw segment ruptured during this foreshock.

3.4.2.3. Shaduzup, Kamaing, and Mogang Segments

The northern termination of the Mawlu segment is at ~ 24.8°N, where the fault system trifurcates and fans northward in the shape of a horse's tail (Figure 11). From west to east, we call these strands of the horse's tail the Shaduzup, Kamaing, and Mogang segments (SZs, KMs, and MGs in Figure 11).

The obscurity of geomorphic evidence for activity along the westernmost of these suggests that it accommodates less strain than its two neighbors. Although the Shaduzup segment truncates Tertiary geological units and structure, we did not find clear evidence of drainages offset across the fault. The northern termination of the Shaduzup segment is not well defined in the coarse SRTM topography north of 26°N, so it appears that its total length is no more than 120 km.

The Kamaing segment traverses the western flank of a ridge composed of Precambrian and Miocene rocks [*Bender and Bannert*, 1983] and displays clear geomorphologic evidence of youthful activity along its middle reach. The Kamaing segment extends much farther north than the Shaduzup segment, well into the eastern border of the Naga Hills, north of 26.7°N. Several drainages along the eastern side of the Naga Hills show clear dextral offset near the northern termination of the Kamaing segment. Farther northwest, the northwestern extension of the Kamaing segment connects to the thrust fault system that bounds the eastern margin of the Assam valley (Figure 11).

The Kamaing segment has been seismically active over the past four decades, but no earthquakes larger than *M*6 appear in the global catalog. A cluster of moderate (*M*5 to *M*6) earthquakes forms a lineation parallel

and almost beneath the fault trace between 26° and 27.4°N. Another set of earthquakes clusters along it around 25.4°N. If generated by this segment, these clusters may indicate partial decoupling of this reach of the Kamaing segment, a notion supported by a modern geodetic analysis that implies very shallow locking of this segment [*Maurin et al*., 2010].

The easternmost of the active horsetail faults is the Mogang segment. It extends in a broad arc from ~24.8°N to ~26.8°N. Northward from 24.8°N, it forms an arcuate boundary between hills of Precambrian and Miocene rocks on the west and a broad valley on the east. Along the eastern flank of the hills, deflections of a series of drainages that incise the Miocene formation suggest up to 10 km of dextral offset. This implies that the Mogang segment has also been active during the late Quaternary Period. The Mogang segment terminates at 26.8°N, east of the Naga domain, along strike of a NW-SE-running thrust fault that bounds Precambrian and Cretaceous units of the eastern Himalayan syntaxis (Figure 11).

Unlike the Kamaing segment, the Mogang segment has been seismically silent in the past several decades. The last major earthquake to originate near these segments is the M_w 7.6 earthquake of January 1931 [*Pacheco and Sykes*, 1992; *Engdahl and Villasenor*, 2002] (Table 1). Its relocated epicenter is within kilometers of the arcuate Mogang segment (Table 1). The magnitude of the earthquake suggests a surface rupture of about 100 km, short enough to be associated with either the Mogang or the Kamaing segment (Figure 11). The lack of a reliable isoseismal map for this earthquake precludes us from confident assignment of the earthquake to either of the two segments. We favor the Kamaing segment as the source, however, because earthquake intensities were higher near the Kamaing segment than along the Mogang segment [*Chhibber and Ramamirtham*, 1934]. However, we cannot rule out the possibility of a Mogang source of this event, as the seismic intensity records were sparse for this event.

3.5. The Shan Domain

The Shan domain embodies a plexus of active predominantly left- and right-lateral faults between the Sagaing and Red River faults (Figure 2). North- to north-northwest-striking dextral-slip faults dominate the western and central eastern parts of the domain. West- to northeast-striking sinistral-slip faults dominate the central corridor of the domain, from its northwestern corner, near the northern Sagaing fault, to the arcuate Dien Bien Phu fault, about 750 km to the southeast (Figure 1). The geometry of these faults and GPS vectors drawn relative to the Sunda block [e.g., *Simons et al*., 2007] show that these faults accommodate southwestward rotational extrusion of the northern part of the Sunda block at rates that increase northwestward, toward the eastern Himalayan syntaxis. This extrusion appears to be driven by the ongoing extrusion of eastern Tibet's Sichuan-Yunnan block, which is bounded on the east by the Xianshuihe-Xiaojiang fault system [see *Tapponnier et al*., 1982] (Figure 1). In the past 4 to 5 million years, the Xianshuihe-Xiaojiang fault has experienced about 60 km of left-lateral motion, which is consistent with the broad 40 to 60 km bend of the Red River fault [e.g., *Allen et al*., 1984; *Wang et al*., 1998]. The presence of significant dextral-slip faults and a few normal faults within the region southwest of the Red River fault implies that the Shan domain is also extending slightly in an east-west direction (Figure 12).

The Sunda block has an earlier Cenozoic tectonic history involving its eastward and southward extrusion during an earlier phase of collision of India into Asia [e.g., *Tapponnier et al*., 1982; *Leloup et al*., 2007]. Many of the structures related to this earlier collision remain visible in the topography of the Shan domain but by and large appear to be inactive. Some of these earlier structures served as dextral-slip faults in the earlier phase of extrusion but have been moving left laterally throughout at least the past 5 million years [*Lacassin et al*., 1998].

In the paragraphs below, we describe evidence for activity of the faults of the Shan domain, beginning with the larger left-lateral faults and then the larger right-lateral fault systems.

3.5.1. The Left-Lateral Faults

3.5.1.1. Summary

Large left-lateral faults dominate the Shan domain (Figure 12). In general, these left-lateral faults (like the GPS vectors) arc around a pivot point near the eastern Himalayan syntaxis, with fault curvature decreasing away from the syntaxis.

Many of these left-lateral faults distinctly offset major river courses of Southeast Asia, particularly the Salween and Mekong Rivers and their tributaries. These sharp offsets imply a long and ongoing history. Some of

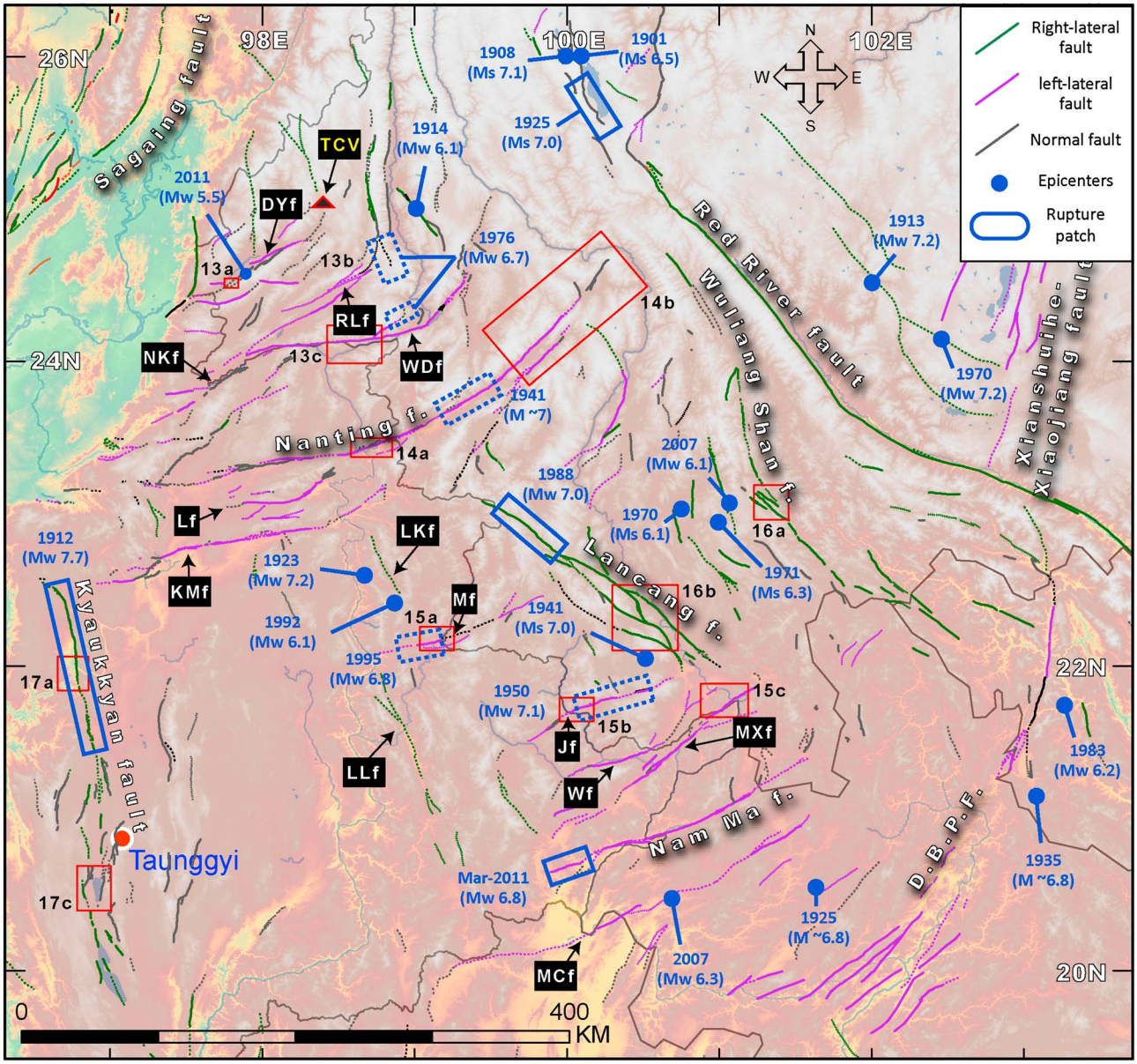

Figure 12. Active faults and associated historical earthquakes within the Shan domain. Purple = left-lateral faults. Green = right-lateral faults. Dark–gray = normal faults. Blue dots and boxes show locations of earthquake and ruptures of the past century. Red boxes are the locations of coming up figures. TCV = Tengchong Volcano; DYf = Da Yingjiang fault; RLf = Ruili fault; WDf = Wanding fault; NKf = Namkham fault; Lf = Lashio fault; KMf = Kyaukme fault; LKf = Loi Kwi fault; Mf = Menglian fault; LLf = Loi Lung fault; Jf = Jinghong fault; Wf = Wan Ha fault; MXf = Mengxing fault.

these offsets have a hairpin shape that implies a regional reversal of slip from right to left lateral sometime between 5 and 20 Ma [*Lacassin et al.*, 1998].

To facilitate a structured discussion, we separate these left-lateral faults into four geographical subgroups. Those in the first group, including the Daying River, Ruili, Wanding, and nearby smaller faults, slice through the northwestern corner of the Shan domain. These exhibit left-lateral shear and are associated with west-northwest normal faults. Those in the second group, including the Nanting, Lashio, and Kyaukme faults, are farther southeast and show almost purely westward left-lateral motion. The third group is still farther southeast and much shorter. The southeastern limit of the domain is defined by the long Dien Bien Phu fault zone.

3.5.1.2. Daying River, Ruili, and Wanding Faults

The Daying River fault, Ruili fault, and Wanding fault cut the northwesternmost portion of the Sunda plate (Figure 12). Two common characteristics are that each connects to a N-S-striking normal-dextral fault in the

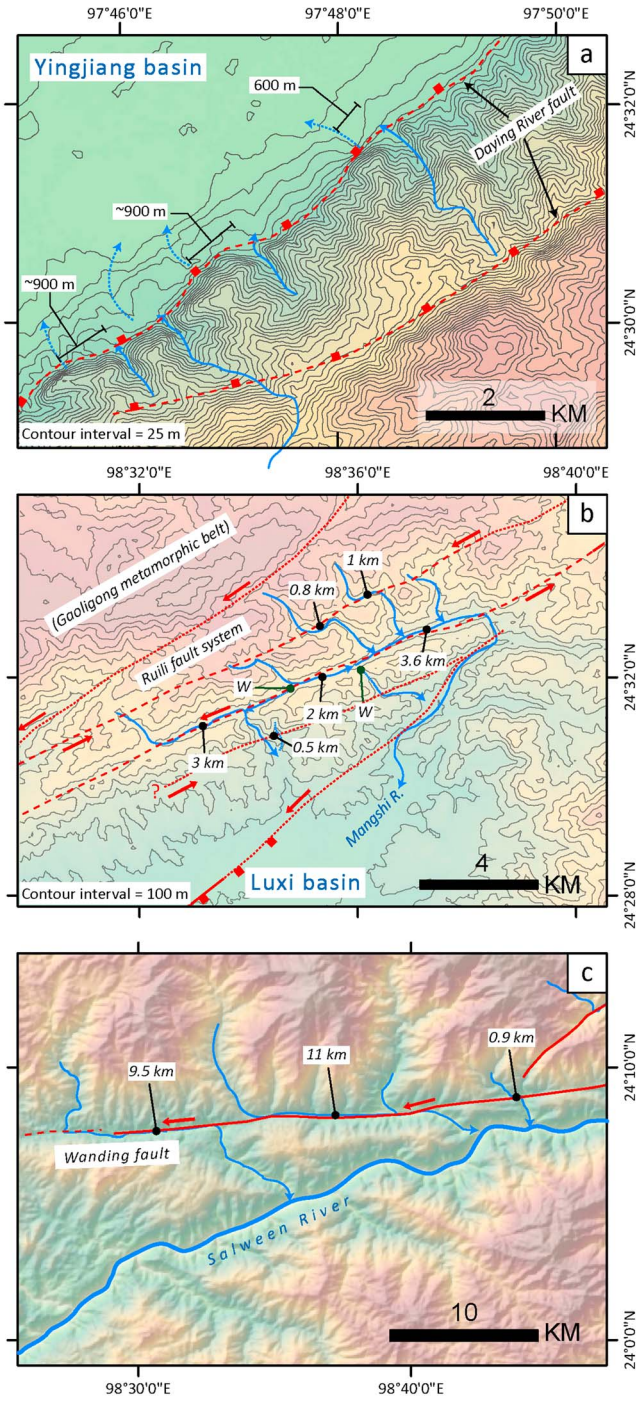

Figure 13. Selected examples of the geomorphological expression of active faults of the Shan domain, from SRTM topography and LANDSAT imagery. Blue lines = streams. Red lines = fault traces. (a) The Daying River fault appears as a trace with large vertical displacements within the mountain range and a trace with left-lateral displacements at the mountain front. (b) Offsets along multiple strands of the left-lateral Ruili fault total 10 to 11 km. W = wind gap. (c) Matches of tributaries of the Salween River suggest left-lateral offsets of ~11 km along the Wanding fault.

northeast and that each has a clear normal-slip component in the southwest. These characteristics show that this corner of the Shan domain is extending roughly east-west.

The *Daying River fault* is the northwesternmost of these three principal left-lateral faults. It courses southwestward about 135 km from the Tengchong Volcanic field in Yunnan (TCV, Figure 12) to the western escarpment of the Shan plateau in northern Myanmar. Along its traverse of the southeastern margin of the Yingjiang basin, it shows well-developed triangular facets indicative of a normal-slip component and clear left-lateral channel deflections (Figure 13a).

A field survey along the Daying River fault that enabled thermoluminescence (TL) dating determination of 10 and 20 ka ages for alluvial surfaces showed that left lateral slip rates are ~1.2 to 1.6 mm/yr [e.g., *Guo et al*., 1999b; *Chang et al*., 2011].

A M_w 5.5 earthquake that struck the region in March 2011 also indicates that the Daying River fault is active (Figure 12 and Table 1). Both the focal mechanism and relocated aftershocks are consistent with the strike and sense of slip on the Daying River fault [*Lei et al*., 2012]. Judging from the lateral extent of the aftershock sequence, the 2011 earthquake may have resulted from rupture of an approximately 12 km long section of the fault.

The *Ruili fault* (also known as Longling-Ruili fault) parallels the Daying River fault to the south. It roughly follows the highly sheared Gaoligong metamorphic belt and extends more than 140 km from Yunnan to northeastern Myanmar (Figure 12) [*Socquet and Pubellier*, 2005; *Wang et al*., 2008; *Huang et al*., 2010]. We map the fault splitting in the east into several northward-striking faults and connecting to N-S-striking normal-dextral faults (Figures 12 and S2). The Ruili fault merges southwestward with the E-W-striking Wanding fault.

Figure 13b illustrates some of the complexity of the Ruili fault in the east, at the north margin of the Luxi basin. There the fault comprises at least two major active fault traces. These parallel faults cut the highly sheared Goligong metamorphic belt and offset a series of incised drainages that are separated by wind or water gaps (W, Figure 13b). Left-lateral channel deflections along the southern of the two faults range from 2 to 3.6 km, but the wind and water gaps along the trace allow for a plausible offset as large as 11 km. The northern of the two faults could accommodate an additional kilometer of slip and a lesser fault nearer the mountain front could have slipped 0.5 km. The down-to-the-southeast steps across these faults imply a normal-slip component to the fault zone here as well.

The geomorphic features in the west are not as clear as those in the east. Perhaps slip is transferred to a normal fault at the left step of the fault across the Ruili basin. This 60 km long normal and left-lateral Namkham fault (NKf, Figure 12) forms the southern margin of the Ruili basin and dies out near the western escarpment of the Shan plateau.

An alluvial fan surface offset near the eastern end of the Ruili fault and shown to be 33 kyr old by luminescence dating has been offset about 70 m [*Huang et al*., 2010]. This and a nearby channel deflection of about 20 m on a 10 kyr old alluvial fan suggest the left-lateral slip rate of approximately 2 mm/yr.

The 170 km long *Wanding fault* is southeast of the Ruili fault. It bends northward near its eastern end and terminates at a N-S-striking normal fault. The Wanding fault connects with the Ruili fault at its western end. Topographic relief across the Wanding fault is small, perhaps because its strike is not oblique to the direction of regional extension.

Lacassin et al. [1998] and *Wang et al*. [1998] report 9 and 10 km left-lateral offsets of the Salween River across the Wanding fault. Tributaries of the Salween River are offset similar amounts (Figure 13c). This observation indicates that the horizontal displacement along the entire Wanding fault is roughly constant.

Field investigations and a survey of aerial photography shows that the Wanding fault offsets a series of young fluvial terraces of the Salween River [*Chang et al*., 2012]. They derive an average left-lateral slip rate of about 2 mm/yr based on the thermoluminescence (TL) ages from the offset sediments. This confirms the earlier estimate of *Lacassin et al*. [1998], which was based upon the assumed age of incision of the Salween River.

On 29 May 1976, M_w 6.7 and M_w 6.6 earthquakes struck the region between the Ruili and Wanding faults in quick succession, causing severe destruction in local villages (Table 1 and Figure 12). Focal mechanisms match the strike of the Ruili fault, but no fault surface ruptures were found along the fault trace. An isoseismal map of the second earthquake centers on the intersection of the Ruili fault and a normal fault [*Compilation Group of China Seismic Intensity Zoning Map SSB*, 1979]. We speculate that the M_w 6.6 event resulted from rupture of the easternmost portion of the Ruili fault. The isoseismal contours of the first earthquake are close to the Wanding fault. One of the high-intensity zones is coincident with a secondary normal and left-lateral fault of the Wanding fault system, so we suspect it to be the cause of this earlier event.

3.5.1.3. Nanting, Lashio, and Kyaukme Faults

These faults comprise an arcuate 400 km long system of left-lateral faults that cuts across nearly the entire width of the Shan plateau. SRTM topography and Landsat imagery show that this system terminates near but slightly east of the western escarpment of the plateau. The fault traces sport geomorphological features typical of strike-slip faults without a large component of dip slip: linear ridges, narrow and localized pull-apart basins, laterally offset stream channels and alluvial fans, and the like [*Yeats et al*., 1997].

The longest of these faults, in fact the longest within the entire Shan domain, is the *Nanting* (*Nan Tinghe*) *fault*. An abundance of offset features demarcate its trace. Within the Yunnan area, two traces mark the eastern section of the fault. Both traces clearly exhibit large channel offsets. The southeastern of the two is the less linear, less continuous, and shorter of the two, which indicates that the northwestern branch is structurally more mature; that is to say, it has accommodated more slip. This is supported by the fact that most of the young depositional basins align along the northwestern trace [*Zhu et al*., 1994]. Along the western margin of the Shan Plateau, geomorphically obvious fabric within the Mogok metamorphic belt shows clear sinistral warping near the termination of the Nanting fault, indicating that its left-lateral fault slip has been accommodated by diffuse deformation within the metamorphic belt and that the fault does not extend as far west as the Sagaing fault [e.g., *Socquet and Pubellier*, 2005].

The geomorphic evidence for recent activity of the Nanting fault has been long recognized [e.g., *Zhu et al*., 1994; *Wang and Burchfiel*, 1997; *Lacassin et al*., 1998; *Wang et al*., 1998; *Socquet and Pubellier*, 2005; *Wang et al*., 2006], but there is no agreement on the total slip across the Nanting fault. *Lacassin et al*. [1998] suggest that left-lateral offset is greater than 8 km, based on the offset of the channel of the Salween River. *Wang and Burchfiel* [1997] suggest the northeastern part of Nanting fault offsets the Mengliang ophiolitic suture about 40 to 50 km, 5 to 6 times greater than the Salween River offset along the central section of the fault. A later study from *Wang et al*. [1998] suggests that the southern branch of the Nanting fault may accommodate 17 km of left-lateral offset, based on the left-lateral warping of a major river.

In an attempt to resolve the dispute between the proponents of the 8 km and 40 km offsets, we reexamined the geomorphic evidence for offset of the Salween River. We note that a wide wind gap east of the 8 km measurement would permit an offset as great as at least 15 km (Figure 14a). This wind gap is wide enough to have accommodated the Salween River before it migrated to its current channel south of the fault. Moreover, a plausible restoration of channels at the eastern end of the fault implies a left-lateral offset as large as 21 ± 1 km across the Nanting fault (Figures 14b and 14c). This 21 km offset estimation magnitude of left-lateral offset could also apply to the Salween River offset. Nonetheless, this value would still be no more than half the 40 to 50 km bedrock offset suggested by *Wang and Burchfiel* [1997].

The last major earthquake in the vicinity of the Nanting fault is a $M \sim 7$ event in May 1941 (Figure 12 and Table 1). The eastern part of the Nanting fault intersects the zone of highest intensities [*Compilation Group of China Seismic Intensity Zoning Map SSB*, 1979]. *Wang et al*. [2006] argue from the historical earthquake reports that surface rupture of an at least 12 km long section of the fault is plausible. No other sections of the 370 km long fault can be associated with large earthquakes of the twentieth century. Indeed, for that eastern part of the fault within Yunnan province, Chinese historical data reveal no other destructive events in their written history [*Wang et al*., 2006], which for this region extends at least prior to the Qing dynasty (~seventeenth century).

South of and parallel to the western part of the Nanting fault are the left-lateral Lashio and Kyaukme faults. The two faults also exhibit clear geomorphic evidence of activity but not to the degree that the Nanting fault does. This comparison suggests comparatively lower slip rates.

The 85 km long *Lashio fault* lies 30 km south of the Nanting fault (Figure 12). The match of bedrock ridges, channel deflections, and the width of a transtensional basin suggest a plausible total left-lateral offset between 2.5 and 6.5 km. The eastern part of this E-W fault curves to the northeast and splits into a group of southeast-dipping normal faults. Along the Lashio fault's western span, geomorphic evidence of horizontal displacement gradually diminishes westward, which suggests that left-lateral slip may disperse into secondary faults that we cannot identify in the SRTM and ASTER imagery.

The Kyaukme and Nanting fault have an en echelon relationship to each other, whereby the former runs parallel to but lies to the south and west of the latter (Figure 12). Like the shorter Lashio fault, the Kyaukme fault curves northward along its eastern part.

The approximately 210 km long *Kyaukme fault* does not show any clear horizontal deflection of the current channel of the Salween River, although the river does have a gentle left-curving channel south of an ~300 m high fault scarp. A series of small, beheaded channels at the base of this scarp suggests left-lateral offsets greater than 1 km. The western portion of the fault traverses the northern margin of two large basins, and there shows left-lateral deflections of rivers flowing into the basins. The largest geomorphic offset that we see in SRTM topography is approximately 2.6 km, along the central and western parts of the fault (for locations, see Table 2).

With one possible exception, both the Lashio and Kyaukme faults were seismically quiet throughout the twentieth century. An M_w 7.2 earthquake on 22 June 1923 may have resulted from failure of one of these faults, as the epicenter from global earthquake catalog falls southeast of the Kyaukme fault (Figure 12 and Table 1). However, the lack of an isoseismal map or a damage report impedes firm assignment of a source.

3.5.1.4. Menglian, Jinghong, Wan Ha, and Mengxing Faults

Still farther southeast, a group of left-lateral faults occupies the central part of the Shan domain (Figure 12). The most prominent of these are the Menglian, Jinghong, Wan Ha, Mengxing, Nam Ma, and Mae Chan faults. All of these faults are more limited in their eastern and western extent that the large fault systems just

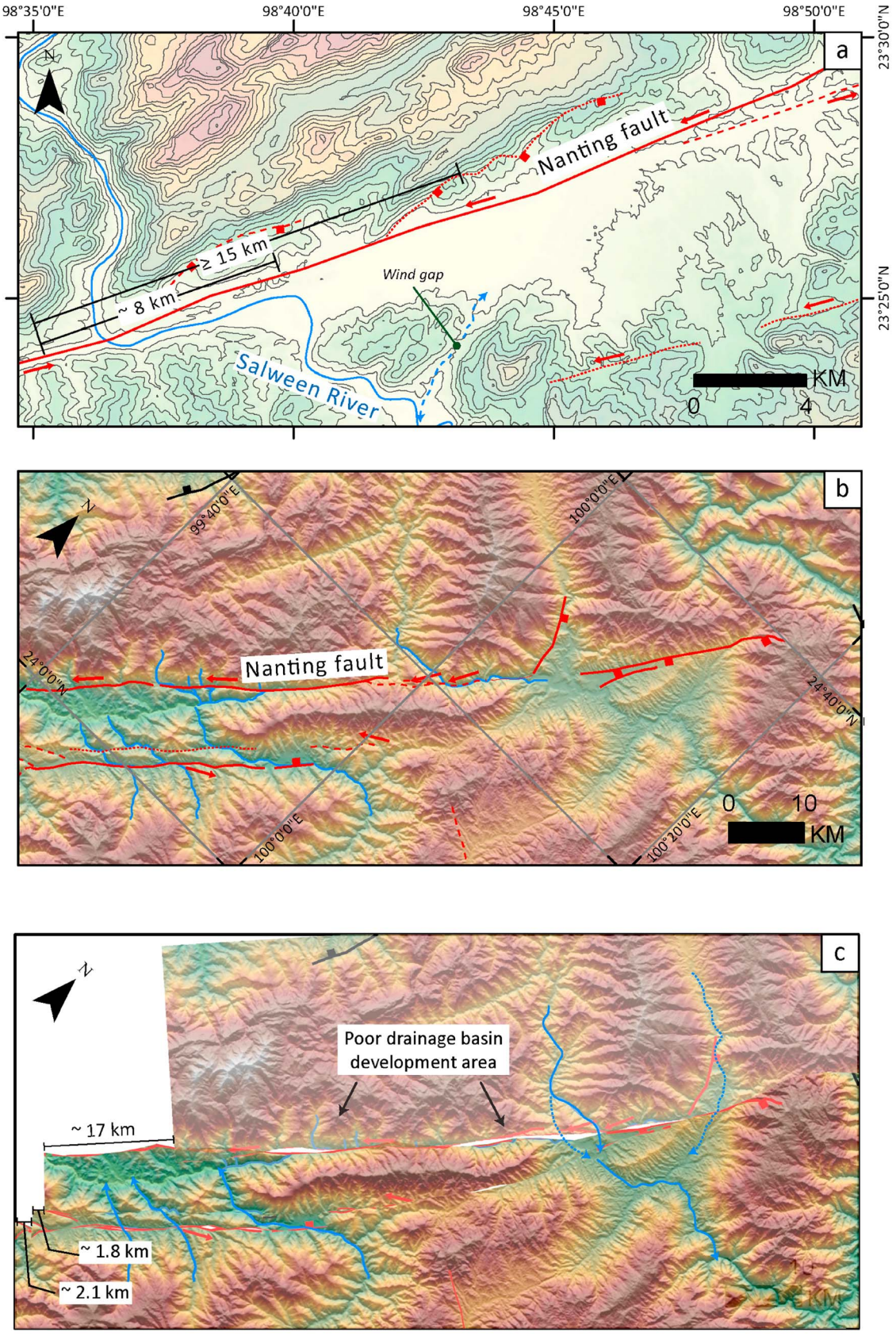

Figure 14

discussed. Three features in common are that they strike NE-SW, their lengths range from roughly 100 to about 200 km, and they terminate to the northwest just shy of a prominent NW-SE-striking fault. In this section, we will discuss together the geomorphic evidence for the Menglian, Jinghong, Wan Ha, and Mengxing faults, the smallest of the six.

The 120 km long *Menglian fault* straddles the border between China and Myanmar and shows clear geomorphic evidence for activity (Mf; Figure 12). On the east, it terminates before reaching the major NW-SE-running dextral Lancang fault. On the west, the fault ends near where it crosses the Salween River.

The total left-lateral offset of the Menglian fault is approximately 5 km. *Lacassin et al*. [1998] suggest that it offsets the Nam Hka River about 2.5 km at the hairpin loop that led them to propose an earlier 5 km offset as well (Figure 15a). However, a tributary of Nam Hka River, west of the Nam Hka's hairpin, shows a left-lateral deflection of about 5 km (Figure 15a). At the eastern part of the Menglian fault, a tributary of the Nam Loi River (Nanlei River) shows approximately 5.5 km left-lateral deflection (for location, see Table 2). Smaller left-lateral deflections and warps are also evident in the drainage networks traversed by the fault.

The Menglian fault is the likely source of an M_w 5.9 foreshock and M_w 6.8 earthquake mainshock in the China-Myanmar border region in July 1995. Both epicenters and the aftershock cluster are ~20 km south of the Menglian fault. Both focal mechanisms are consistent with left-lateral slip on the Menglian fault. The mapped region of highest intensity roughly coincides with the fault near the border [*Chen et al*., 2002]. Thus, we suggest that the western part of the Menglian fault produced the mainshock.

Eighty kilometer southwest of the Menglian fault is a very similar structure, the 110 km long *Jinghong fault*. As with the Menglian fault, the Jinghong fault terminates just before reaching the dextral-slip Lancang fault (Figure 12). Coincident with the intersection of these two active faults is a triangular shaped basin. Beyond the Jinghong's western termination is a normal fault that may relate to the termination of the Jinghong fault.

The Jinghong's largest geomorphic disruption is an 11 km sinistral deflection along its central part. There the Taluo River, which flows along the China-Myanmar border, bends left laterally along the fault (Figure 15b). Both upstream and downstream, its channel is deeply incised into bedrock, so this likely represents an offset. Further support for this hypothesis is the fact that a nearby contact between granitic intrusive rocks and Paleozoic rocks displays a left-lateral offset that is similar to that of the nearby river [*Bureau of Geology and Mineral Resources of Yunnan*, 1993]. Smaller offsets of fans and channels indicate that the Jinghong fault continues to be active.

A M_w 7.1 earthquake on 2 February 1950 was most likely caused by rupture of the Jinghong fault. The epicenter of mainshock is very close the central part of the fault, and several Chinese cities north of the Jinghong fault were damaged [*Xie and Tsai*, 1983]. Unfortunately, though, Chinese intensity data are too sparse to enable construction of an isoseismal map that might confirm the source. Two more recent and more moderate earthquakes (M_w 5.6 and M_w 5.4) on 23 June 2007 may also have resulted from failure of parts of the Jinghong Fault. Their GCMT focal mechanisms are consistent with the fault's strike.

Further southeast, the Wan Ha and Mengxing faults form a complicated left-lateral fault system. They come within about 10 km of each other in their central reaches but diverge toward the southwest (Wf and MXf; Figure 12). Both curve southward near their southwestern termini and transform into southeast-striking normal faults. To the northwest, the nexus of these and the dextral-slip Lancang fault zone are series of extensional basins.

Two major river channels that flow across the ~140 km long *Wan Ha fault* show left-lateral deflections of several kilometer. *Lacassin et al*. [1998] suggest that the Nam Loi River, which flows across the central part of the Wan Ha fault, is left-laterally offset about 5 km. Farther east, the Mekong River has a similar sized left-lateral curve along the easternmost trace of the fault (Figure 15c). Matching the shape of these two river channels and the crest of a bedrock ridge, we derive a 5 to 6 km geomorphological left-lateral offset of the Wan Ha fault. Along its northeastern part, where the Wan Ha fault strikes nearly NNE-SSW along the eastern

Figure 14. Tectonic geomorphological expressions of select locations along the Nanting fault. Conventions same as in previous figures. (a) Plausible 15 km offset along the central part of the Nanting fault, based upon recognition of a wind gap between the fault and the Salween River. (b and c) Current and restored stream-channel patterns along the northeastern reach of the Nanting fault suggest a 20 km offset.

Journal of Geophysical Research: Solid Earth

10.1002/2013JB010762

Table 2. Summary of Maximum Fault Offset in the Shan Domain Fault System

Fault Name	Fault Length (km)	Fault Type[a]	Location[b]		Type of Offset	Maximum Offset (km)	Reference[c]	Note
			Longitude	Latitude				
Daying River fault	135	L + N	97.95	24.65	River channel	4.1 ± 0.3		Min. offset
Huna fault	60	L + N	97.65	24.38	River channel	5 ± 0.4		
Manda fault	> 30	L	98.09	24.52	Ridge crest	4 ± 0.3		
Ruili fault (Eastern)	100	L + N	98.57	24.43	River channel	> 5; ≤ 11		
Ruili fault (Western)	40	L + N	97.76	23.98	Small channels	> 1.7 ± 0.3		*Poor correlation*
Namkham fault	60	L + N	97.47	23.79	River channel	> 0.6 ± 0.1		*Poor correlation*
Wanding fault	170	L	98.63	24.14	Salween River system	10.5 ± 1	LAC; WANG	
Nanting fault	380	L	100.17	24.52	Ridge crests and river offsets	21 ± 1		
Lashio fault	85	L	97.99	23.07	Ridge crest and basin	> 2.5; < 6.5		*Poor correlation*
Kyaukme fault	> 200	L	98.13	22.88	River channel	2.6 ± 0.3		Min. offset
Menglian fault	120	L	99.53	22.32	River channel	5.5 ± 0.3		
Jinghong fault	110	L	100.05	21.7	River channel	10 ± 1		
Wan Ha fault	140	L	100.18	21.34	Nam Loi River; ridges	5.8 ± 0.4	LAC	
Mengxing fault	180	L	100.63	21.38	Nam Loi River; ridge crests	24 ± 1	LAC	
Nam Ma fault	215	L	100.58	20.88	Mekong River	13 ± 1	LAC	
Mae Chan fault	310	L	100.71	20.508	Ridge crest and channels	4 ± 0.8		Max. offset
Dien Bien Phu fault (Northern)	150	L	103.15	20.02	River channel	12 ± 1	LAI	Single fault
Dien Bien Phu fault (Southern)	~110	L	101.6	19.9	Mekong River	< 60		Multiple faults, Max offset
Wuliang Shan fault zone	~400	R	101.4	22.98	Tributary of Mekong River	~6		Multiple faults
Lancang fault	210	R	100.52	22.28	Nanguo River	~17		Multiple faults
Northern Kyaukkyan fault	~160	R	99.77	21.99	Myint Nge River and tributary	4.8 ± 0.3		

[a]N = Normal fault; L = Left-lateral fault; R = Right-lateral fault.
[b]The location is roughly the center point of the offset feature along the fault.
[c]LAC = *Lacassin et al.* [1998]; WANG = *Wang et al.* [1998]; LAI = *Lai et al.* [2012].

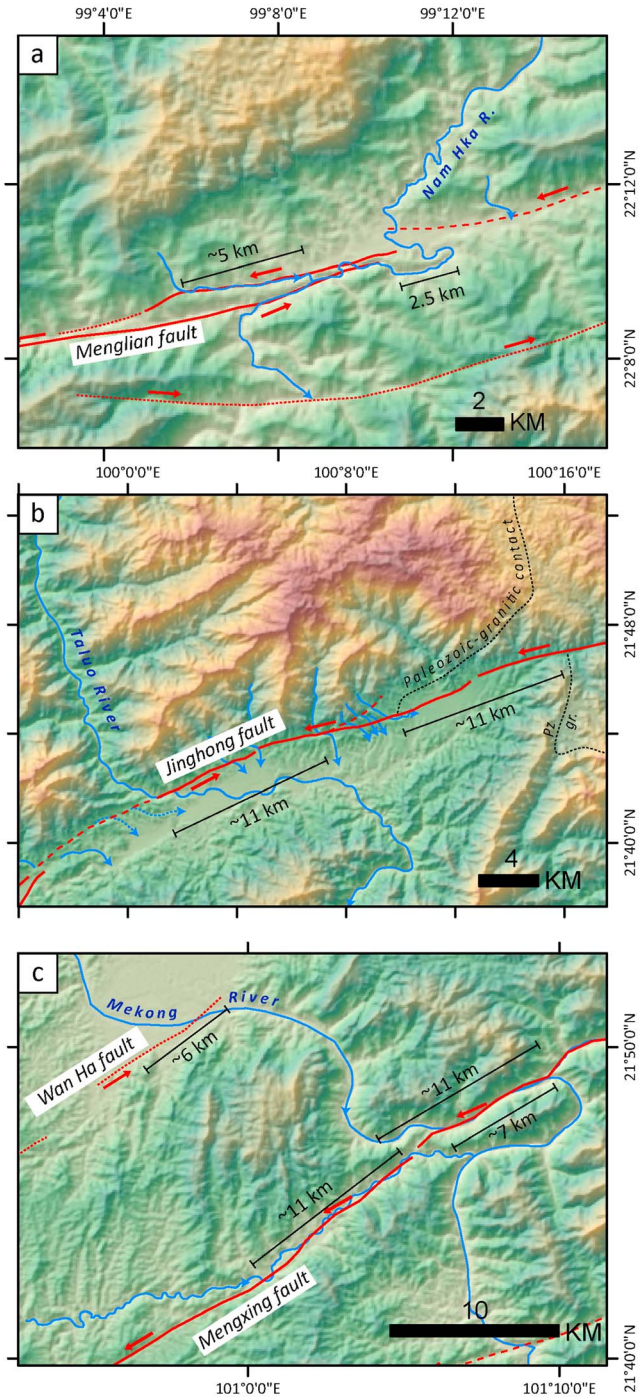

Figure 15. Tectonic geomorphological expressions of the Menglian, Jinghong, and Mengxing faults. (a) Deflections of the Nam Hka River and a tributary imply 2.5 and 5 km left-lateral offsets along the Menlian fault. (b) Deflections of the Taluo river imply an 11 km left-lateral offset along the Jinghong fault, which roughly matches the 11 km left-lateral offset of a bedrock contact. (c) Left-lateral deflections of the Mekong river and a tributary imply an 11 km offset by the Menxing fault.

margin of a transtensional basin, SRTM topography shows clear left-lateral bends and deflections of channels. These small tectonic landforms imply activity of the fault during the Quaternary period.

The *Mengxing fault* traverses more than 180 km from near the Lancang fault to the Myanmar-Thailand border region, where both the Mekong and Nam Loi Rivers display a large left-lateral offset (Figure 15c). *Lacassin et al.* [1998] noted the hairpin shape of the Nam Loi River and suggested that the sense of slip reversed from right to left lateral about 20 to 5 Myr ago. We estimate the left-lateral deflection of the Mekong River to be between 7 and 11 km and that of a small tributary just to the southwest to be ~11 km. This small tributary and the Mekong River are separated by a wind gap at the Mengxing fault (Figure 15c). The Nam Loi River hairpin loop, however, shows 24 ± 1 km of left-lateral deflection 56 km farther southwest. Both upstream and the downstream sections of the Nam Loi River are deeply incised into bedrock, so it is reasonable to surmise that the river has had little space to meander from its ancient to its current course. Moreover, there seems to be little possibility for this deflection to have been caused by river capture. The 24 km bend may be the largest geomorphological left-lateral offset on the Mengxing fault. This would imply that the smaller 11 km offset of the Mekong River and its tributary result from river capture after the initiation of left-lateral slip.

3.5.1.5. Nam Ma and Mae Chan Faults

We now consider two larger left-lateral faults farther to the southeast in the central Shan domain (Figure 12). The *Nam Ma fault* appears as a narrow 215 km long fault zone in the region of the Lao-Myanmar border, with a 12–14 km left-lateral offset of the Mekong River channel at the central part of the fault [*Lacassin et al.*, 1998]. The hairpin geometry of the Mekong River channel here implies that a larger 30 km right-lateral offset preceded this left-lateral

phase [*Lacassin et al*., 1998]. Left-lateral offset across the 310 km long Mae Chan fault is smaller; landforms visible in SRTM topography suggest an offset of about 4 km (Table 2).

The Nam Ma fault terminates on both ends in transtensional basins. Consistent with the fault's left-lateral sense of slip, the basin at the northeastern terminus is in the block north of the fault, whereas the basin at the southeastern terminus is in the block to the south.

Two hundred to 400 m left-lateral deflections of small river channels crossing the fault that we identify from SRTM and LANDSAT imagery imply that the fault is still active. Rupture of the westernmost 30 km of the fault during the March 2011 M_w 6.8 Tarlay earthquake proved that the fault is still active [*Soe Thura Tun et al*., 2013; *Wang et al*., 2013a].

Tectonic landforms along the *Mae Chan fault* are less clear than those along the Nam Ma fault. Perhaps this implies that the fault is slipping at a lower rate, as its smaller total geomorphic offset also implies. SRTM topography suggests that the fault has multiple traces west and south of the Mekong River. Farther west, the fault cuts through a Quaternary basin, within which it exhibits a ~50 m high north-facing scarp.

The epicenter of the M_w 6.3 earthquake of 16 May 2007 is midway along the Mae Chan Fault, and the focal mechanism of the earthquake is consistent with the strike of the fault. A larger, *M*6.8 earthquake in 1925 may have resulted from rupture of the eastern part of the Mae Chan fault (Table 1). However, neither an isoseismal map nor earthquake reports are available to constrain better the 1925 earthquake source.

3.5.1.6. Dien Bien Phu Fault

The Dien Bien Phu fault forms the southeastern boundary of the Shan domain (Figures 2 and 12). It is the southeasternmost active left-lateral fault between the right-lateral Red River and Sagaing faults. The fault is nearly but not quite colinear with the left-lateral Xiaojiang fault system on the opposite (north) side of the Red River fault and is southeast of the 40 to 60 km left-lateral bend of the Red River fault that has resulted from extrusion of the Sichuan-Yunnan block [e.g., *Wang et al*., 1998]. Along its southern reaches, the Dien Bien Phu fault exists within the Triassic Nan Suture zone, and multiple linear valleys imply that it fans into multiple left-lateral faults within a wide deformation belt.

Tectonic landforms are prominent along the southwestern and northern thirds of the 370 km long Dien Bien Phu fault. The central section of the fault may, in fact, not be active. SRTM topography along the northern (Vietnam) segment and the southern (Mekong) segment clearly shows river channel and alluvial fan offsets. The largest left-lateral geomorphological offset along the Vietnam segment is about 12.5 km [*Lai et al*., 2012]. Numerous kinks in the Mekong River canyon parallel the Mekong River segment and may indicate large left-lateral offsets there as well. However, we are not confident that these left-lateral bends reflect left-lateral motion because we cannot restore small drainages and regional geomorphic or bedrock patterns in any consistent way.

The central (Nam Hou) segment of the Dien Bien Phu fault separates the Vietnam and Mekong segments by a 110 km stretch, along which evidence of young fault activity is weak. Young fluvial landscapes dominate the low-relief topography, and the best evidence for the fault seems to be contrasts of bedrock. We find only weak geomorphic evidence of fault activity. Moreover, the Nam Hou River shows no evidence for tectonic warping where it crosses the fault. We suggest that the Nam Hou segment has experienced only very small left-lateral motions and that what deformation has occurred is distributed across a wide zone.

Some historical earthquakes may have been caused by the Dien Bien Phu fault. The M_w 6.8 earthquake of November 1935 occurred near the southern end of the Vietnam segment (Figure 12). Moreover, the M_w 6.2 earthquake of 24 June 1983 has a focal mechanism that is consistent with the strike of the fault.

3.5.2. The Right-Lateral Faults

3.5.2.1. Summary

Two right-lateral fault systems define the western and northeastern flanks of the Shan domain (Figures 2 and Figure 12). The western of these systems is nearly parallel to the Sagaing fault and extends about 200 km into the Shan domain (Figure 10). The northeastern set of faults is subparallel to the Red River fault and extends nearly 300 km into the Shan domain. These systems extend along most of the western and northeastern flank of the domain but notably terminate northward near the Nanting fault system (Figure 12).

3.5.2.2. Wuliang Shan Fault Zone

The Wuliang Shan fault zone is a diffuse, dextral shear zone 50 to 100 km southwest of the Red River fault. It extends nearly the entire 400 km length between the Nanting and Dien Bien Phu fault zones as a set of

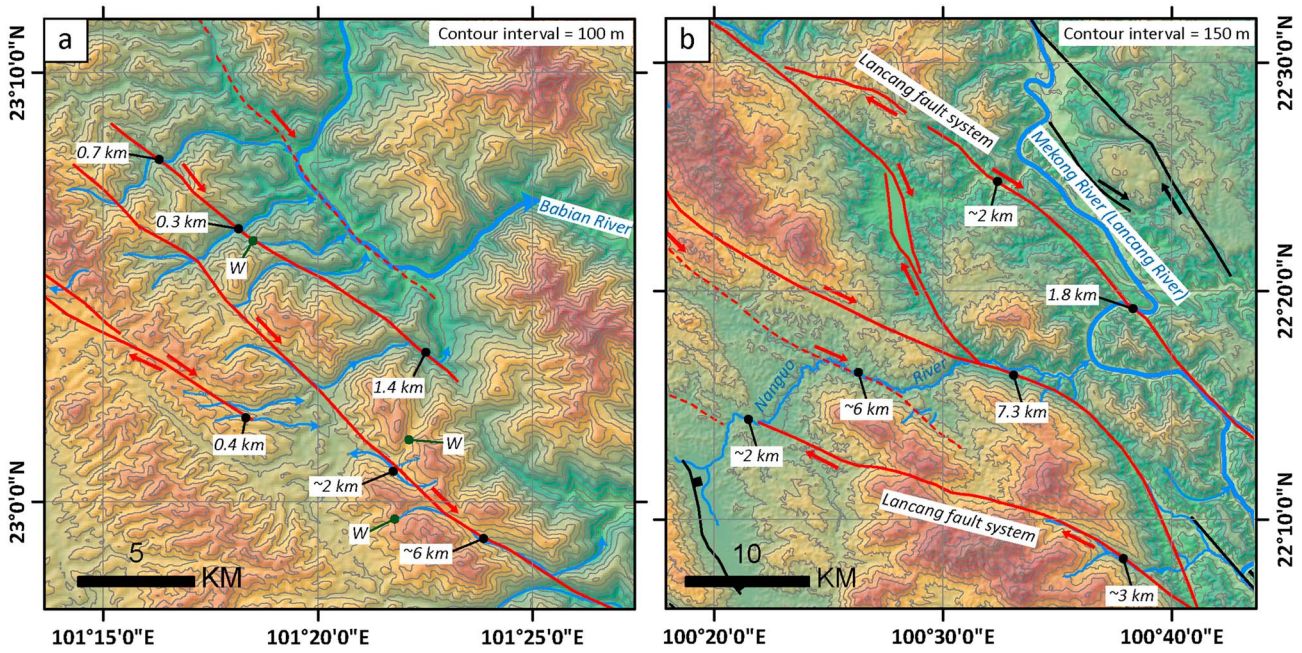

Figure 16. Tectonic geomorphology along parts of the right-lateral Wuliang Shan fault and Lancang fault system. (a) Maximum deflection of drainages across the Wuliang Shan fault zone is about 6 km here. (b) Deflections of the Nanguo river across a complicated set of faults suggest ~ 17 km of dextral offset across the Lancang fault system here.

discontinuous dextral and normal faults. The strand that courses along the eastern flank of the Wuliang Shan range shows very large and significant dextral offset of the river channels. Dextral offsets there range from 300 m to more than 3 km. The largest dextral offset in SRTM topography is approximately 6 km, along the central part of the fault (Figure 16a). Field investigations and interpretations of aerial photography support our observation, suggesting right-lateral offsets of several hundred meters on several NNW-running faults within the Wuliang Shan fault zone [e.g., *Guo et al*., 1999a].

The Wuliang Shan fault zone was very active in the twentieth century. The last of five moderate earthquakes along the fault zone was an M_w 6.1 on 2 June 2007, near the city of Ning'er (Table 1). Both the GCMT focal mechanism of the mainshock and the distribution of the relocated aftershocks [*Lu and Zhou*, 2011] are consistent with the general strike of and sense of slip on the Wuliang Shan faults. Other recent earthquakes, such as the M_w 6.0 of 15 March 1979 and the M_w 5.6 of 26 January 1993, also show GCMT focal mechanisms that are consistent with the strike and the slip sense of the Wuliang Shan fault.

3.5.2.3. Lancang Fault Zone

The right-lateral Lancang fault zone traverses a distance of about 210 km, between the left-lateral Nanting and Mengxing faults (Figure 12). It forms the boundary between sets of left-lateral and right-lateral faults. The fault zone comprises a simple strand in the north but a complex set of anastomosing faults in the south. Although a regional geological map shows that the Lancang fault offsets the Lincang batholith 30 km left laterally [e.g., *Wang and Burchfiel*, 1997], geomorphic offsets are clearly right lateral. This implies a history of slip inversion as previously hypothesized for currently left-lateral faults in this region [*Lacassin et al*., 1998].

We estimate right-lateral slip across the Lancang fault system to be about 17 km, based on a series of right-lateral bends of the Nanguo River valley (Figure 16b). If this offset began to accrue around 5 Ma, in concert with initiation of right-lateral slip on the Red River fault and left-lateral slip on the Xiaojiang fault [*Lacassin et al*., 1998; *Wang et al*., 1998; *Leloup et al*., 2007], then the average fault slip rate of the Lancang fault system is approximately 3.4 mm/yr. This rate is close to the higher bound of the 2 ± 2 mm/yr dextral rate estimated from geodetic data [*Shen et al*., 2005].

The best seismic confirmation of the activity of the Lancang fault is a M_w 7.0 earthquake that occurred on 6 November 1988 (Table 1). An approximately 45 km long rupture occurred along the northern part of the fault accompanied the earthquake [*Yu et al*., 1991]. A postearthquake field survey found clear dextral slip at two locations along the main trace of the fault. At one of these locations, offset reached 1.4 m [*Wang et al*., 1991; *Yu et al*., 1991].

3.5.2.4. Kyaukkyan Fault Zone

The Kyaukkyan fault zone is a complex 500 km long right-lateral fault zone that lies within the western Shan plateau between ~18° and 22.5°N, 100 to 150 km east of the Sagaing fault (Figure 10). Its northern terminus nearly coincides with the western terminus of the left-lateral Kyaukme fault. The fault zone includes a 40 km wide right step with prominent active normal faults in the vicinity of Taunggyi. At 18°N, it intersects the Mae Ping fault zone, which arcs southeastward into Thailand [*Morley et al*., 2007]. We separate the Kyaukkyan fault zone into three distinct segments, based primarily on its step overs and geomorphic expression.

3.5.2.5. Myint Nge Segment

The northern 160 km of the Kyaukkyun fault is east of Mandalay and north of Taunggyi, the capital of the Shan states [*Le Dain et al*., 1984]. Tectonic landforms along this reach demonstrate clearly that it is an active dextral-slip fault (Figures 17 and S2). The largest of these is the offset of the Myint Nge River (Figure 17a). This deeply incised river flows westward from the Shan plateau and down the Shan escarpment. At the fault crossing, it has a hairpin geometry that implies initial sinistral motion of 8 to 10 km followed by dextral offset of approximately 5 km (Figures 17a and 17b).

The Northern segment of the Kyaukkyun fault produced one of the largest earthquakes in Myanmar's history, on 23 May 1912 [*Coggin Brown*, 1914; *Chhibber and Ramamirtham*, 1934]. Earlier reports assign it a magnitude of 8 [*Gutenberg and Richter*, 1954], but later studies reassess its magnitude and revise it downward to M_s 7.7 to 7.6 [e.g., *Abe and Noguchi*, 1983; *Pacheco and Sykes*, 1992]. The area of highest intensities encompasses the entirety of the Northern segment but does not extend close to Taunggyi [*Coggin Brown*, 1914; *Wang et al*., 2009] (Figure S4). The distribution of highest intensities and the size of the earthquake are consistent with rupture of the entire northern segment.

3.5.2.6. Taunggyi Segment

Geomorphological expression of the Kyaukkyun fault zone becomes obscure as it extends southward toward Taunggyi, likely because it splays into several less-rapidly slipping traces (Figures 10 and 12). From 21.5°N, the fault zone widens into several obscure strands that extend southward into a 50 km wide transtensional basin. This basin extends 100 km from north to south, to 20.3°N. The most obvious active faults associated with the basin are the two normal faults that bound it—the Pindaya fault on the west and the Taunggyi fault on the east.

Both of these two bounding normal faults show clear, youthful vertical displacements. The steep limestone escarpment of the east-facing Pindaya fault is at least 350 m high, and the west-facing Taunggyi escarpment rises about 400 m near the city of Taunggyi. Farther south, Inle Lake shows an asymmetric geometry that suggests eastward tilt of the basin associated with motion of the Taungyi fault. The western side of the lake is significantly shallower than the eastern side (Figure 17c).

Although the limestone escarpment that extends from Taunggyi to Inle Lake is steep and rugged, we were unable in the field to find any small scarps along its base that might have indicated rupture within the past few centuries or millennia. Nonetheless, triangular facets and faulted alluvium indicate activity in the late Quaternary Period (Figure 17c).

3.5.2.7. Salween Segment

The Southern segment of the Kyaukkyun fault extends from the southern end of the transtensional basin southward ~220 km to the Mae Ping fault zone at the Salween River (Figure 10). The maximum offset we found along this segment is an ~4.7 km offset of a bedrock ridge and an ~5.4 km offset of the Salween River. These are nearly identical to the maximum offset we found along the northern segment of the Kyaukkyan fault. The main fault trace passes through the western embankment of Moybe dam (Figure 10) and is covered by young fluvial deposits south of the reservoir. Further south, the fault trace bends nearly 20° westward at 19.2°N and creates a narrow transtensional basin along the Salween River. The southern segment of the Kyaukkyan fault connects to the Mae Ping fault zone at about 18.2°N. After this merger, the Mae Ping fault continues ~170 km southeastward along the Thailand-Myanmar border and may later enter the Mekong basin north of the Bangkok [e.g., *Morley et al*., 2007]

3.5.2.8. Mae Ping Fault Zone

We also find clear geomorphic evidence along the northwestern part of the Mae Ping fault of dextral slip. However, maximum channel offsets are smaller than those along the Sagaing and the Kyaukkyan faults. The amount of dextral motion is smaller based on the maximum channel offsets we found along its fault trace.

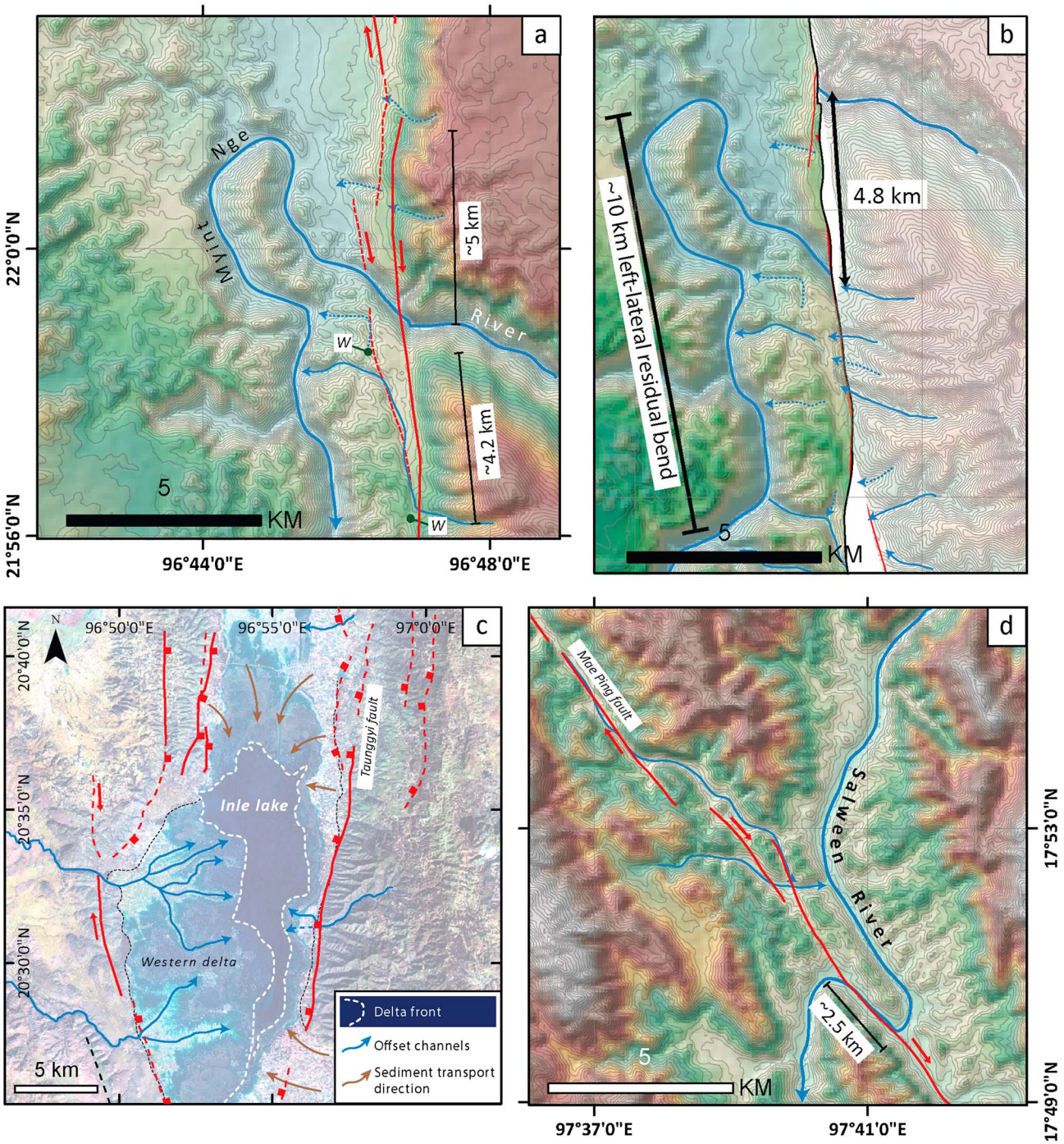

Figure 17. Geomorphological expression of particularly informative parts of the right-lateral Kyaukkyan fault system. (a) The hairpin geometry of the Myint Nge river channel, along the northern reach of the Kyaukkyan fault, shows clear evidence for normal and dextral displacement along the fault. (b) Restoration of a 5 km recent right-lateral component of slip leaves a remaining, earlier 10 km left-lateral bend. (c) LANDSAT imagery of the Inle lake region showing the complex geometry of Taunggyi normal fault. (d) The Mae Ping fault zone offsets the Salween river channel and tributaries about 2.5 km.

Between the Sagaing fault and the southern Kyaukkyan fault, the largest dextral offset is ~1.2 km. East of 97.5°N, the maximum dextral offset is ~2.5 km (Figure 17d).

3.5.2.9. Partially Reactivated Faults of the Shan Escarpment

A dramatic linear valley parallel to and lying between the Sagaing and Kyaukkyun faults within the Shan escarpment suggests the presence of a large strike-slip fault (Figure 10). The question for us is whether or not

Table 3. Scaling Relationships for Fault Length and Magnitude That Is Used in This Study

Equation	Reference	Note
Reverse Fault		
$M_w = 4.16 + 1.75 \times \log10(L)$	*Blaser et al.* [2010]	
$M = 5.00 + 1.22 \times \log10(SRL)$	*Wells and Coppersmith* [1994]	
$M = 4.49 + 1.49 \times \log10(RLD)$	*Wells and Coppersmith* [1994]	For blind structure
$M_w = 4.868 + 1.392 \times \log10(L)$	*Strasser et al.* [2010]	For subduction interface
Normal Fault		
$M_w = 3.67 + 1.92 \times \log10(L)$	*Blaser et al.* [2010]	
$M = 4.86 + 1.32 \times \log10(SRL)$	*Wells and Coppersmith* [1994]	
$M = 4.34 + 1.54 \times \log10(RLD)$	*Wells and Coppersmith* [1994]	For blind structure
Strike-Slip Fault		
$M_w = 4.20 + 1.56 \times \log10(L)$	*Blaser et al.* [2010]	
$M = 5.16 + 1.12 \times \log10(SRL)$	*Wells and Coppersmith* [1994]	
$M = 4.33 + 1.49 \times \log10(RLD)$	*Wells and Coppersmith* [1994]	For blind structure

this large fault is active. The lack of disruption of small landforms along most of its trace implies that most of it is inactive. Perhaps it was an active element of the early to mid-Cenozoic extrusion of the Sunda block. In those few places where small drainages show right-lateral deflections, we show the fault as active in Figure 10.

4. Earthquakes Past and Future

The two principal motivations of our neotectonic study of Myanmar have been to understand the past occurrences of and future potential for large earthquakes in the Myanmar region. Throughout the previous pages, we have accomplished the former by constructing a new neotectonic map that helps to make sense of many of the large earthquakes of the past century or so.

Looking to the future, public seismic safety will depend to a large extent on understanding the potential for other large earthquakes throughout this region. Our neotectonic map assists in this goal as well. Many of the active faults within the region have not produced large earthquakes during the past century or more of human record keeping, so what is their potential for the future?

Although what we have presented is by no means complete, our geomorphologic mapping augmented by seismic, geodetic, and other relevant geological data provides a fundamental basis for a simple evaluation of the predominant seismic sources for each of the three active tectonic domains of Myanmar and its neighboring countries. In this section we utilize our neotectonic understanding of these active faults to assess their potential for future rupture. The current scarcity of published structural information, high-quality seismological and geodetic data, and paleoseismological information limits this effort to a pretty basic level. Nonetheless, we provide below a synoptic, first-order estimate of plausible earthquake scenarios within each domain.

Wells and Coppersmith [1994] (W&C) provide equations that relate rupture length to earthquake magnitude. *Blaser et al.* [2010] improved upon these scaling relationships by using an enlarged historical earthquake database. They also incorporated thrust fault ruptures in subduction environments, thus enabling better estimates of earthquake magnitude for such faults. Length-magnitude scaling relationships for subduction megathrusts have also been given by *Strasser et al.* [2010]. These two independent scaling relationships help us to estimate the uncertainties in estimation of maximum earthquake magnitude produced by the megathrust along the western Myanmar coast and under eastern Bangladesh. Table 3 lists the parameters that we used to calculate potential earthquake magnitude.

Although we used structural discontinuities, jogs, and kinks to define structural segments and assumed that these segment boundaries delimit plausible future fault ruptures, we are well aware that fault ruptures sometimes propagate through such structural complications and thus produce larger earthquakes [e.g., *Wesnousky*, 2006]. Currently, however, paleoseismological and historical documentation of rupture lengths in the Myanmar region are too sparse to warrant a sophisticated consideration of multiple-segment ruptures. In this first effort, we simply estimate magnitudes associated with single-segment rupture for the mapped

faults. In some cases, we also use estimates of fault slip rate, published geodetic analyses, and regional earthquake histories to offer plausible average earthquake recurrence times for these full-segment ruptures. These simplistic first-order recurrence intervals provide a useful starting point for future investigations of the faults' true behaviors. These future studies will need to explore which of these faults have commonly ruptured partially, perhaps due to fault immaturity, and thus produced more frequent and smaller earthquakes than estimated from the full-segment rupture scenario. Moreover, future studies may find that those active faults in complicated tectonic regions, such the Shan Domain, have produced events clustered within a short time period, perhaps due to the fault-rupture interactions. We cannot evaluate either of these complications from our neotectonic mapping.

Table 4 summarizes the potential earthquake magnitudes we have calculated for all of the major structures. Below, we explain these results for the faults of each domain, starting in the west with the four domains of the Indoburman range and ending in the east with the Shan domain.

4.1. The Indoburman Range

We will assess the seismic potential of the four domains of the Indoburman range from south to north, in the same order that we described them in the preceding section. In addition to the surface manifestation of these domains that appear in the maps of Figures 3a, 4a, 6, and 9a, we utilize four schematic cross sections (Figures 18 and 19), based upon available geological and seismological data. Together, the maps and cross sections allow us to estimate the preliminary three-dimensional geometry of the megathrust and its relationship to large secondary structures. At this stage of our understanding of the geometries and kinematics of the region's active faults, it seems unwarranted to conduct a statistical analysis of plausible rupture areas, widths, and slip amounts. We attempt here merely a crude first cut at assessing earthquake potential of the region. So for example, we do not attempt to include the range of uncertainty in the depth of downdip rupture limits for the megathrust; instead, we mainly use the length of fault mapped from the surface to assess the plausible maximum earthquake magnitude on the subduction zone interface.

4.1.1. Coco-Delta Domain

We have described above a Coco-Delta domain dominated by a highly oblique plate interface that dips about 20° to 30° eastward [*Dasgupta et al*., 2003] (Figure 18a). The orientation of this section of the megathrust (early parallel to the vector of relative plate motion), its steep dip, and secondary features imply predominantly right-lateral slip across this oblique-reverse fault. A predominance of dextral slip within the domain, on the very northern part of the 2004 megathrust rupture [*Chlieh et al*., 2007], is consistent with this interpretation. The downdip limit of its seismic rupture is likely shallower than the ~50 km downdip limit of the adjacent megathrust farther south [*Chlieh et al*., 2007], as its motion contains a large component of strike slip. However, the downdip limit of the locked patch may still extend to about 20 or even 30 km, as the subducting oceanic lithosphere here is old and cold ($>$ 80 Ma) [*Müller et al*., 1997]. We use the reverse fault and megathrust equations from both *Blaser et al*. [2010] and *Strasser et al*. [2010] to estimate a M_w 8.6 to 8.9 range for the maximum earthquake that could be produced by this 480 km long segment (Table 4).

The fact that the southernmost part of this domain ruptured during the great 2004 earthquake [*Meltzner et al*., 2006] supports the suspicion that this section of the megathrust can accumulate tectonic strain and slip seismically. Moreover, large submarine landslides mapped by *Nielsen et al*. [2004] within this domain could well be evidence that the megathrust has produced high ground accelerations in the past. However, a complete rupture of the Coco domain megathrust segment would not be frequent (~10^3 years or longer), as the direction of the Indian-Burman plate motion is not optimized for the strain accumulation on the megathrust at this domain, and the oblique Indian-Sunda plate convergence rate at this latitude is slower than the rate at the Sumatran area.

In addition to the megathrust, we suggest that at least three other structures along the eastern flank of the Indoburman range may be capable of generating significant earthquakes (Table 4 and Figures 2 and 20). From their lengths, we estimate that M_w 7.6 to 7.7 earthquakes are plausible. Lacking reliable estimations of their slip rates, however, it would be speculative to estimate average return periods of such earthquakes.

4.1.2. Ramree Domain

The Arakan earthquake of 1762 may represent the maximum earthquake within the Ramree domain, because it appears to have resulted from failure of the megathrust in combination with large splay faults in the upper plate [*Wang et al*., 2013b]. If the megathrust ruptured across the entire length of the domain, from

AGU Journal of Geophysical Research: Solid Earth

10.1002/2013JB010762

Table 4. Proposed Major Seismic Structures of Myanmar and Surrounding Countries

Code	Name	Type[a]	Length (km)	Slip Rate (mm/yr)	Strike	Dip	$M_{W\&C}$ (length)	M_{Blaser} (length)	$M_{Strasser}$ (length)	Last Known Earthquake		
										Year	*M*	Partial /Entire
Coco-Delta Domain												
	Sunda megathrust (Coco-Delta section)	SS + R	480	8 to 28 [c]	N20E	20	8.3	**8.9**	**8.6**			
Paf	Pathein fault	R	95	<< 12[d]	N20E	45	**7.4**	**7.6**				
Elf[S]	East-limb fault (Southern section)	R	100	<< 12[d]	N20E	45	**7.4**	**7.7**				
	Seidaung fault	SS	>160	<< 5?	N20E	90	**7.6**	**7.6**				
Ramree Domain												
	Sunda megathrust (Ramree section)	R	450	< 23[d]	N35W	16	8.2	**8.8**	**8.6**	1762	8.5 to 8.8	Entire
WBf	West Bago-Yoma fault	R	65	> 0.4[ec]	N20W	45	**7.2**	**7.3**		1927?	~6?	Partial?
PDf	Paungde Fault	R	70	> 0.4[c]	N45W	45	**7.3**	**7.4**				
CKf	Chauk fault	R	70	—	N15W	45	**7.3**	**7.4**				
MBf	Minbya Fault	R	105	—	N20W	45	**7.5**	**7.7**				
LMf	Laymyo Fault	SS	175	~ 0.6[f]	N20W	90	**7.7**	**7.6**				
TCf	Thahtay Chaung fault	SS	>150	~ 2[f]	N15W	90	**7.6**	**7.6**				
Elf[C]	East-Limb fault (central section)	R	60	<< 9[d]	N45W	45	**7.2**	**7.3**				
Elf[N]	East-Limb fault (northern section)	R	~120	<< 9[d]	N25W	45	**7.5**	**7.8**				
Sdf	Sidoktaya Fault	R	70	<< 9[d]	N25W	45	**7.3**	**7.4**				
PTf	Pato fault	R	30	—	N45W	45	**6.8**	**6.7**		1858?	7.7	Entire?
Pyf	Pyay fault	R	90	—	N15W	45	**7.4**	**7.6**				
Dahaka and Naga Domains												
	Blinded Sunda megathrust (Dhaka section)	R	520	> 6[c]	N15W	5	8.3	**8.9**	**8.6**			
IPf	Churachandpur-Mao fault	SS	≧170	16[g]	N10E	90	**7.6**	**7.6**				
	Kabaw fault	R	~280	< 9[d]	N-S	45	**8.0**	**8.4**				
SM	St. Martin's Island	A	>16	1 to 3[h]	N10W	—	**6.3**	**6.3**				
Da	Dakshin Nila	A	40	1 to 3[h]	N30W	—	**6.9**	**7.0**				
M	Maheshkhali	A	50	1 to 3[h]	N20W	—	**7.0**	**7.1**		1999	5.2	Partial
J	Jaldi	A	40	1 to 3[h]	N20W	—	**6.9**	**7.0**				
P	Patiya	A	50	1 to 3[h]	N20W	—	**7.0**	**7.1**				
Si	Sitakund	A	65	1 to 3[h]	N25W	—	**7.2**	**7.3**				
SW	Sandwip	A	50	1 to 3[h]	N25W	—	**7.0**	**7.1**				
L	Lalmai	A	90	1 to 3[h]	N15W	—	**7.4**	**7.6**				
H	Habiganj	A	105	1 to 3[h]	N15W	—	**7.5**	**7.7**				
R	Rashidpur	A	62	1 to 3[h]	N5W	—	**7.2**	**7.3**		1918	7.5	Entire
S	Sylhet	A	22	1 to 3[h]	N70E	—	**6.5**	**6.5**				
F	Fenchunganj	A	45	1 to 3[h]	N10W	—	**7.0**	**7.1**				
Ha	Hararganj	A	80	1 to 3[h]	N15W	—	**7.3**	**7.5**				
Pa	Patharia	A	46	1 to 3[h]	N15W	—	**7.0**	**7.1**				
	Naga thrust fault	R	400	< 5[i]	N48E	23	8.2	**8.7**	**8.5**			
Sagaing Domain												
	Bago	SS	>170	18[j]	N-S	90	**7.7**	**7.7**		1930	7.2	Partial
	Pyu	SS	130	18[j]	N10W	90	**7.5**	**7.5**		1930	7.3	Entire
	Nay Pyi Taw	SS	70	18[j]	N10W	90	**7.2**	**7.1**		1929	~7	Partial
	Meiktila	SS	220	18[j]	N5W	90	**7.8**	**7.9**		1839?		Entire?
	Sagaing	SS	180	18[j]	N-S	90	**7.7**	**7.7**		1946/1956	7.6/7.0	Partial
BMs	Ban Mauk	SS	150	<< 20[k]	N5E	90	**7.6**	**7.6**				
TMs	Tawma	SS	60	<< 20[k]	N-S	90	**7.2**	**7.0**		1991	6.9	Entire
IDs	In Daw	SS	80	~20[k]	N10E	90	**7.3**	**7.2**		1946	7.3	Entire
Mls	Mawlu	SS	90	~20[k]	N10E	90	**7.3**	**7.2**				

AGU Journal of Geophysical Research: Solid Earth

10.1002/2013JB010762

Table 4. (continued)

Code	Name	Type[a]	Length (km)	Slip Rate (mm/yr)	Strike	Dip	$M_{W\&C}$ (length)	M_{Blaser} (length)	$M_{Strasser}$ (length)	Last Known Earthquake		
										Year	*M*	Partial /Entire
Szs	Shaduzup	SS	120	< 20[k]	N10E	90	**7.5**	**7.4**				
Kms	Kamaing	SS	170	~20[k]	N15W	90	**7.7**	**7.7**		1931	7.5	Partial?
Mgs	Mogang	SS	260	< 20[k]	N10W	90	**7.9**	**8.0**				
Shan Domain												
DYf	Daying River Fault	SS + N	135	1.4 ± 0.2[l]	N50E	90	**7.5**	**7.5**		2007	5.5	Partial
	Huna Fault	SS + N	60	~1[m]	N70E	90	**7.2**	**7.0**				
	Manda fault	SS	> 30	~0.9[m]	E-W	90	**6.8**	**6.5**				
RLf	Ruili fault (Eastern)	SS + N	100	~2[n]	N50E	90	**7.4**	**7.3**				
RLf	Ruili fault (Western)	SS + N	40	< 2[n]	N50E	90	**7.0**	**6.7**				
NKf	Namkham fault	SS + N	60	?	N50E	90	**7.2**	**7.0**				
Wdf	Wanding fault	SS	170	~2[o]	N40E–E-W	90	**7.7**	**7.7**				
NTf	Nanting fault	SS	380	4.2[m]	N50E–N80E	90	**8.0**	**8.2**		1941	7	Partial
Lf	Lashio fault	SS	85	1.3[m]	E-W	90	**7.3**	**7.2**				
KMf	Kyaukme fault	SS	165	~0.5[m]	N80E	90	**7.6**	**7.7**				
Mf	Menglian fault	SS	120	~1[m]	N70E	90	**7.5**	**7.4**		1995	6.8	Partial
Jf	Jinghong fault	SS	110	~2.2[m]	N70E	90	**7.4**	**7.4**		1950	7.1	Partial
Wf	Wan Ha fualt	SS	140	~1[m]	N70E	90	**7.6**	**7.5**				
MXf	Mengxing fault	SS	180	~4.8 K	N50E	90	**7.7**	**7.7**				
MNf	Nam Ma fault	SS	215	~2.6[m]	N70E	90	**7.8**	**7.8**		2011	6.8	Partial
MCf	Mae Chan fault	SS	310	~1[m]	N70E	90	**8.0**	**8.1**		2007	6.3	Partial
DBPf-V	Dien Bien Phu fault (Vietnam segment)	SS	150	2.5[m]	N10E	90	**7.6**	**7.6**		1935/1983	6.8/6.2	Partial
DBPf-M	Dien Bien Phu fault (Mekong segment)	SS	110	2.5[m]	N45E	90	**7.4**	**7.4**				
LKf	Loi Kwi fault	SS	50	~0.8[m]	N25W	90	**7.1**	**6.9**		1992	6.1	Partial
LLf	Loi Lung fault	SS	95	~0.7[m]	N20W	90	**7.4**	**7.3**				
KKF	Kyaukkyan fault (Myint Nge segment)	SS	160	~1[m]	N10W	90	**7.6**	**7.6**		1912	7.7	Entire
PYf	Pingdaya fault	SS	50	—	N10E	60	**7.1**	**6.9**				
TGf	Taunggyi fault	SS	45	—	N10E	60	**7.0**	**6.8**				
KKF	Kyaukkyan fault (Salween segment)	SS	480	~1[m]	N10W	90	**8.2**	**8.4**				
WLSf	Wuliang Shan fault zone	SS	105[b]	> 1.2[m]	N10W–N50W	90	**7.4**	**7.4**		2007	6.1	Partial
LCf	Lancang fault	SS	200	> 3.4[m]	N50W	90	**7.7**	**7.8**		1988	7	Partial
MPf	Mae Ping fault	SS	100	~0.5[m]	N45W	90	**7.4**	**7.3**				

[a]R: Reverse fault; N: Normal fault; SS: Strike-slip fault; A: Anticline with unknown type of blind faulting.
[b]The longest dextral fault trace within the Wuliang Shan fault zone.
[c]The rate is estimated from the Indian, Burma, and Sunda plate motion vectors (see Table S1).
[d]Inferred from *Socquet et al.* [2006].
[e]We assume the age of 30 m high uplift surface is ~100 ka.
[f]We assume the strike slip began to be active in 5 Ma.
[g]The rate is from *Gahalaut et al.* [2013].
[h]Speculate from the anticline uplift rates in this region.
[i]Speculate from the uncertainity of geodetic analysis.
[j]Slip rate is from *Vigny et al.* [2003].
[k]Slip rate is from *Maurin et al.* [2010].
[l]Average fault slip rate is from *Chang et al.* [2011].
[m]Rate = maximum offset / 5 Ma. We assume the fault slip began in 5 Ma, based on the regional tectonic history.
[n]Average fault slip rate is from *Huang et al.* [2010].
[o]Average fault slip rate is from *Chang et al.* [2012].

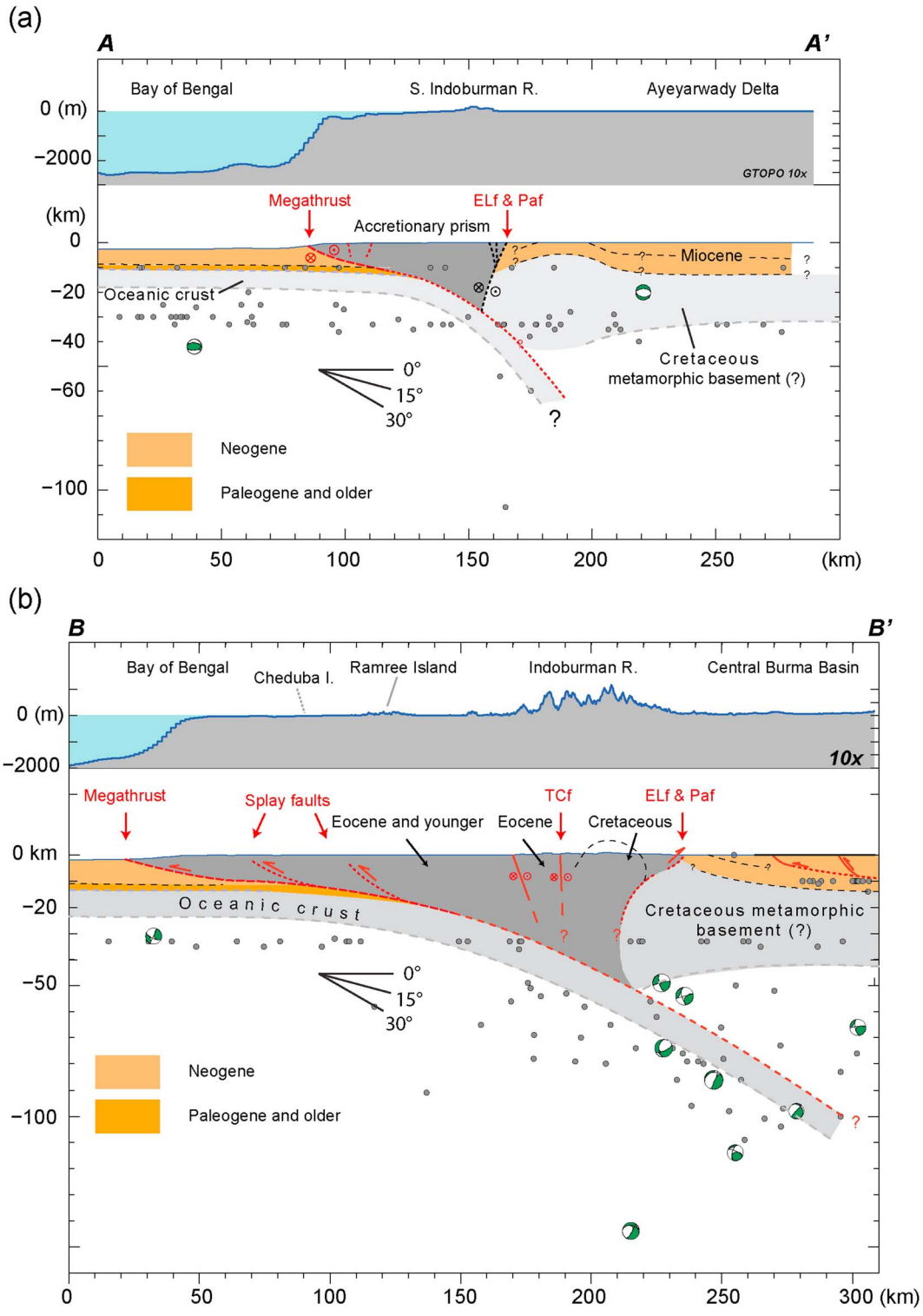

Figure 18. Schematic cross sections through two domains of the northern Sunda megathrust show the geometry of the megathrust and hanging wall structures. Gray dots the hypocenter locations from NEIC catalog since 1976. Green and white focal mechanisms are from GCMT database. (a) The megathrust along the Coco-Delta domain dips moderately and has secondary active structures near the deformation front. See Figures 2 and 3 for profile location. (b) The megathrust along the Ramree domain dips shallowly and is associated with splay thrust faults and strike-slip faults within the hanging wall block. See Figures 2 and 4 for location of the profile.

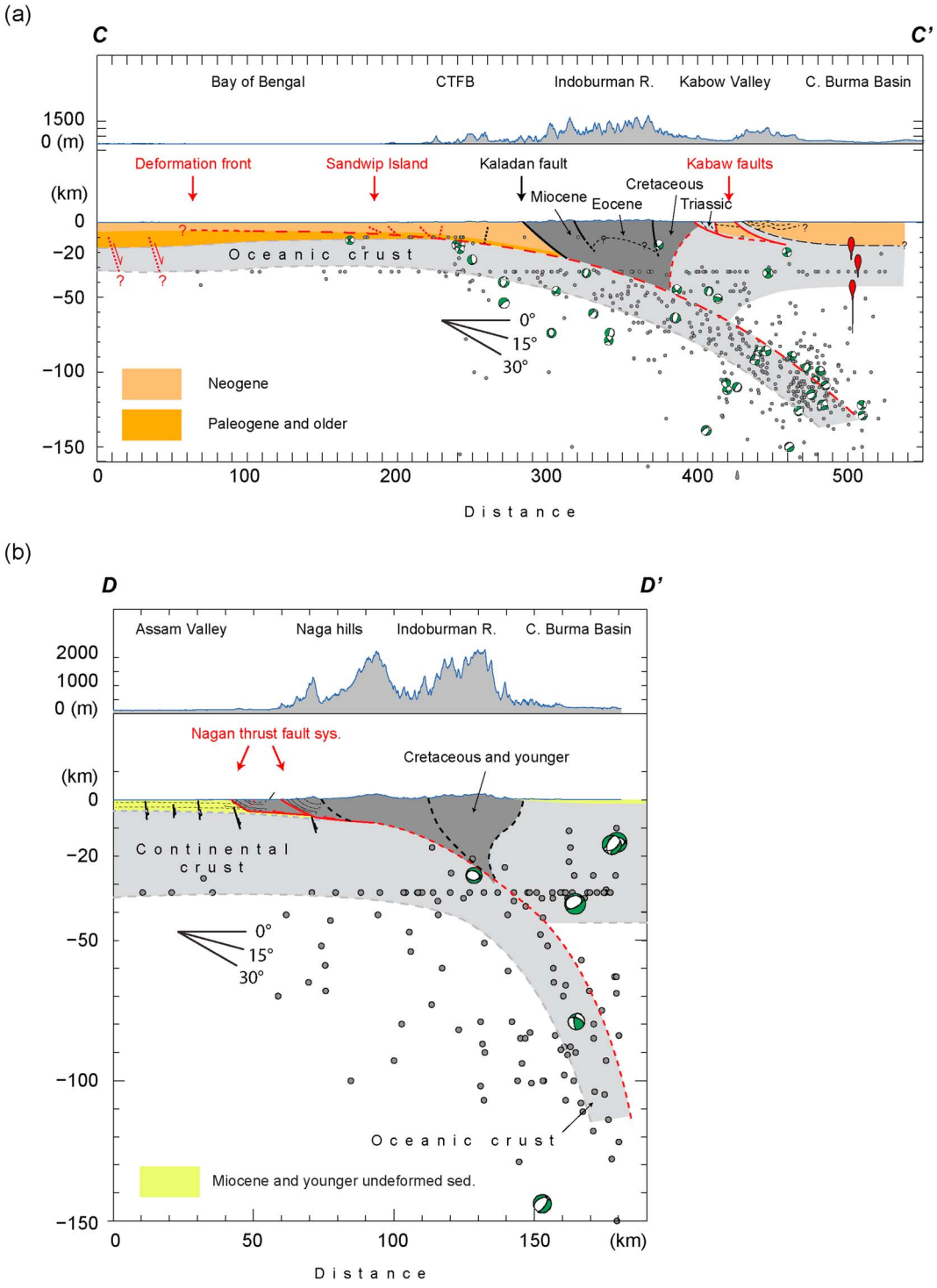

Figure 19. Schematic cross sections through two domains of the northern Sunda megathrust show the geometry of the megathrust and hanging wall structures. Symbols as in Figure 18. (a) The megathrust along the Dhaka domain dips very shallowly and has secondary active thrust faults within 120 km of the deformation front. See Figures 2 and 6 for profile location. (b) The megathrust along the Naga domain dips moderately and juxtaposes continental against continental crust but still has an attached subducting slab of Indian-plate oceanic crust. See Figures 2 and 9 for profile location.

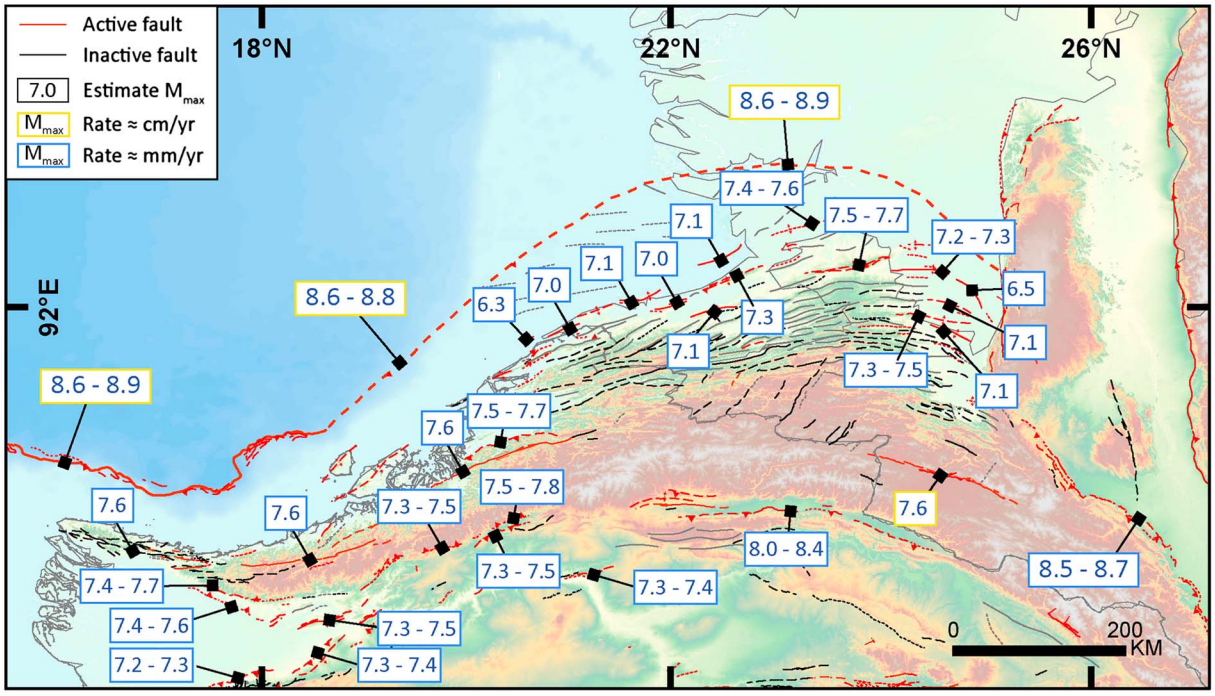

Figure 20. Map of potential maximum earthquake magnitudes (M_w) associated with shallow active faults of the four domains of the northern Sunda megathrust and Indoburman range. Blue numbers show earthquake magnitudes assuming complete rupture of each fault along its entire strike length. Red lines show the active structures mapped from digital elevation model and satellite imagery. Black lines show structures that we interpret to be inactive.

near Fouls Island to Chittagong (Figure 4), as *Cummins* [2007] suggests, and we use the average coseismic fault slips modeled by [*Wang et al.*, 2013b], then the magnitude would likely have been within the range M_w 8.5 to 8.8. This range of magnitudes is consistent with estimations of the maximum earthquake magnitude (M_w 8.6 to 8.8) using just fault length [*Blaser et al.*, 2010; *Strasser et al.*, 2010] (Table 4).

Terrace- and coral-uplift records yield recurrence intervals ranging between about 400 and 1000 years for earthquakes that involve uplift of Ramree and Cheduba Islands [*Shishikura*, 2009; *Wang et al.*, 2013b]. This range is about twice as long as the 190 to 550 year recurrence interval calculated for M_w 8.6 to 8.8 earthquakes if the 23 mm/yr oblique plate convergence is fully taken up by slip on the 450 km long megathrust [e.g., *Socquet et al.*, 2006]. This discrepancy implies either that the megathrust is not fully coupled or that the oblique Indian-Burman plate motion is partitioned between the megathrust and upper plate faults, such as the Thahtay Chaung fault within the Indoburman Range.

Upper plate structures may fail separately from the megathrust and generate smaller but nonetheless destructive earthquakes along the western Myanmar coast. The 1848 earthquake of northern Ramree Island [*Oldham*, 1883] may be such an event. It caused moderate damage to the city of Kyaukpyu, but the felt area was much more limited than that of the 1762 earthquake.

The great length of the right-lateral strike-slip Thahtay Chaung fault within the Indoburman Range (Figures 4a and 5) implies that this fault could generate the earthquake as large as M_w 7.6 (Figure 20) [*Wells and Coppersmith*, 1994; *Blaser et al.*, 2010]. The lack of reliable written history in this mountainous region precludes knowing whether such an event has happened within the past 250 years. Moreover, a lack of constraints on the slip rate of the fault precludes us from saying anything meaningful about an average recurrence interval. Nevertheless, the existence of this large strike-slip fault within the Indoburman range gives good reason to hypothesize that large, destructive shallow earthquakes are plausible from faults within the range.

The lengths of the west-dipping East Limb faults that crop out along the eastern flank of the Indoburman Range (Figures 4a and 18b) imply that they are capable of generating earthquakes between M_w 7.3 and 7.8 (Figure 20 and Table 4). It is likely that these two faults are connected in the subsurface by a blind thrust. If so,

combined rupture could generate an even greater earthquake. The average recurrence interval of such combined rupture along the eastern Indoburman Range would be greater than a thousand years, though, because GPS analysis shows the shortening rate across the eastern Indoburman Range and the central Burma basin is only several mm/yr [*Socquet et al*., 2006; *Steckler et al*., 2013].

Several active reverse faults between Thayet-Myo and Yangon could generate large earthquakes along the floodplain of the Ayerawaddy River, although the recurrence time for each individual fault must on the order of 10,000 years, given the likelihood that slip rates are ≤ 1 mm/yr. Within the Ramree domain, the southernmost of these is the West Bago-Yoma fault, on the eastern flank of the Ayerawaddy flood plain. The fault is likely a high-angle reverse fault that dips northeastward beneath the western flank of the Bago-Yoma Range. The length of the West Bago-Yoma fault implies a maximum magnitude of M_w 7.2 to 7.3 for earthquakes near the Ayerwaddy flood plain north of Yangon (Figure 20). The Paungde fault, farther north along the Ayerwaddy flood plain, is longer, so we estimate that it is capable of producing a M_w 7.3 to 7.4 earthquake in the vicinity of Prome. A related fault farther north likely produced the earthquake of 1858 and may have disrupted temporarily the flow of the Ayeyarwady River.

Before we leave the discussion of the Ramree domain, we should also note that rupture of faults within the downgoing Indian lithospheric slab could also produce damaging earthquakes in the region. Such hidden faults would not be manifest in our mapping of surface features, so we can say little more than that the existence of these should be contemplated in making a comprehensive seismic assessment of the region. The m_b 6.5 Bagan earthquake of 1975 was an event of this type. Its hypocentral depth was within the slab at a depth of about 120 km [*Engdahl and Villasenor*, 2002]. The earthquake ruined several temples in this ancient capital of Burma that are believed to have been built nearly a millennium ago.

4.1.3. Dhaka Domain

The Dhaka domain is defined by the length and width of the broad belt of folds of the Chittagong-Tripura fold belt. As such, it extends more than 500 km along strike from south to north and nearly 200 km from west to east. If the blind megathrust underlying this entire domain were to fail at once, the resulting earthquake would likely have a magnitude in the range M_w 8.6 to 8.9 [*Blaser et al*., 2010] (Figure 20 and Table 4). Whether such a large event is plausible is a matter of some debate. We discuss the range of seismic possibilities, below.

The existence of active anticlines above the megathrust requires that slip on it diminish westward toward zero at the deformation front, at least in the long term. This structural boundary condition is true whether the fault fails wholly in characteristic great earthquakes, partially in lesser earthquakes or wholly aseismically. As the megathrust extends westward beneath these anticlines, progressively more and more of the shortening between the Indian plate and the Indoburman range is taken up by the thrust faults and tilt panels associated with the folds. Concomitantly, slip on the megathrust diminishes westward. In general, there seem to be about three active anticlines along the western part of the Chittagong-Tripura fold belt at any particular latitudinal cross section across the domain (Figure 6). This westward bleeding of long-term slip off the megathrust and onto the lesser faults beneath the folds must be taken into account in developing seismic rupture scenarios for seismic hazard assessment.

Recent GPS studies constrain the rate of strain accumulation across the domain and thus the rate of accumulation of seismic potency across the megathrust and overlying secondary faults. Across the latitudes of the Dhaka domain, the Indoburman Range is moving westward between 5 and 14 mm/yr relative to the Indian plate [*Gahalaut et al*., 2013; *Steckler et al*., 2013]. *Steckler et al*. [2013] demonstrate that the 14 mm/yr gradient in westward motion can be fit by an elastic deformation model that consists of a locked shallow-dipping megathrust under the Chittagong-Tripura fold belt and the Indoburrman range. In this model, the downdip, aseismically slipping section of the megathrust is accumulating slip at 14 mm/yr. We use this rate, below, to estimate average recurrence intervals for a suite of rupture scenarios.

Figure 21 illustrates a broad range of behaviors for the megathrust and overlying faults and folds. The A1 and A2 scenarios depict wholesale rupture of the megathrust, with slip diminishing from 10 m in the east to zero at the deformation front. In A1, the auxiliary faults fail with the megathrust; in A2, they fail during separate events. Scenario A1 could well be akin to the 1964 Alaskan earthquake [*Plafker*, 1965] and the 1762 Arakan earthquake [*Wang et al*., 2013b], during which complete rupture of the megathrust was accompanied by rupture of two to three thrust faults in the accretionary prism. In A1, all elastic strains accumulated since the previous great earthquake are released during the multiple-source earthquake. In A2, westward-diminishing

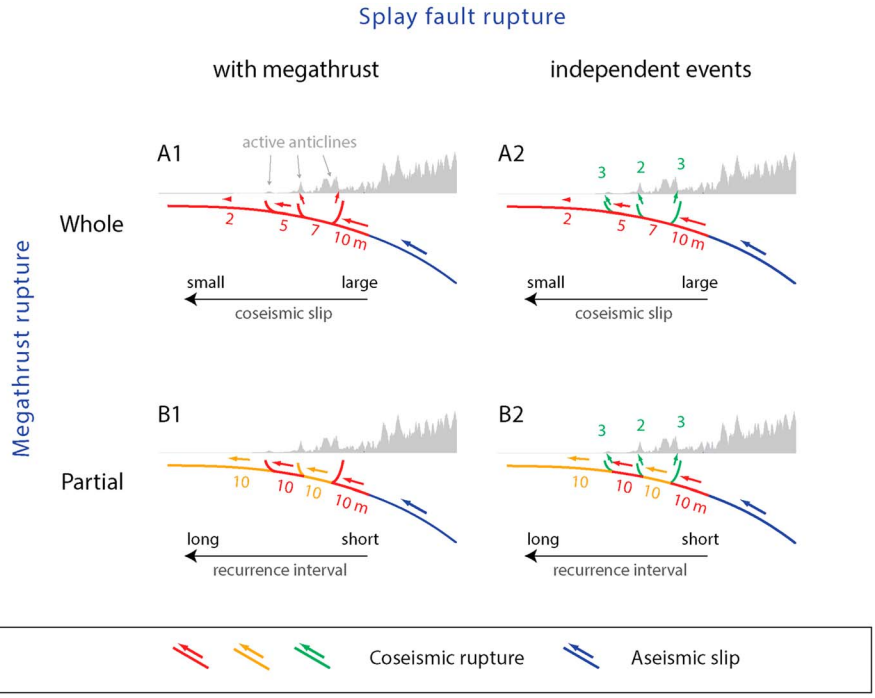

Figure 21. The simplified megathrust and upper plate-fault rupture scenarios in the Dhaka domain. Scenarios A1 and A2 show the wholesale rupture scenarios assuming the entire megathrust ruptured at once with the coseismic slip diminished toward the deformation front. Scenarios B1 and B2 show the partial megathrust-rupture scenarios with uniform coseismic slip. The recurrence intervals of increase westward as the long-term slip rate decrease toward the deformation front. The upper plate structures (i.e., splay faults) may either slip during the megathrust events (A1 and B1) or fail separately producing moderate but frequent earthquakes (A2 and B2).

seismic slip on the megathrust produces elastic strains in the overlying block, which are later relieved during ruptures of the overlying thrust faults and by folding.

In the two B scenarios, the megathrust fails during partial ruptures, in which updip and downdip limits are demarcated by the megathrust's intersections with overlying thrust faults. In B1, the partial ruptures are accompanied by large amounts of slip on an associated thrust fault. In B2, the overlying thrust faults fail more frequently during separate earthquakes. In each of the B scenarios, megathrust ruptures produce smaller earthquakes than in the A scenarios, because their rupture areas are smaller.

Let us consider now the recurrence characteristics of the A and B scenarios. If we adopt *Steckler et al.* [2013] loading rate of 14 mm/yr and the amounts of slip shown on the megathrust in Figure 21 (zero to 10 m), then wholesale megathrust ruptures would recur on average about every 700 years in both A scenarios. In A2, the secondary faults would produce large earthquakes in between these characteristic 700 year megathrust events. If slip on the megathrust is 2 or 3 times as large as shown in Figure 21, then the time between characteristic megathrust ruptures would be 2 or 3 times longer than 700 years.

In the B scenarios, we have arbitrarily chosen to assign 10 m of slip to each megathrust patch. Slip amounts might be similar on all patches if physical properties varied little across the fault plane. If this were the case, then ruptures of the western patch would occur less frequently than ruptures on the eastern patch, because the long-term accumulation of slip is occurring at slower rates in the west than in the east. If, for example, the long-term rate of slip on the westernmost section averages just 2 mm/yr, then 10 m slip events would recur on average every 5000 years. In contrast, if the long-term rate of slip on the easternmost locked section averages 14 mm/yr, then 10 m slip events would recur about every 700 years.

The historical record provides some constraints on the applicability of these four scenarios. First, at least a couple of moderate earthquakes appear to be associated with complete or partial failure of secondary thrust faults beneath active anticlines (the 1918 M_w 7.5 earthquake in the vicinity of the Rashidpur anticline and the 1999 m_b 5.2 earthquake near the Maheshkhali anticline). These occurrences support the idea that at least

some of the faults beneath the anticlines should be expected to fail independently of the megathrust, in earthquakes that range in size from M_w 6.3 to 7.7 (Table 4 and Figure 20). Second, the existence of only one large historical earthquake that can be plausibly associated with wholesale failure of the megathrust (AD 1548) [*Iyengar et al*., 1999; *Steckler et al*., 2008] suggests that ruptures of the megathrust occur very infrequently and that slip amounts are large. At 14 mm/yr, the easternmost part of the locked patch would have accumulated 6.5 m of potential slip since 1548. If the 1548 earthquake was not caused by the megathrust (as suggested by the paleoseismic work of *Morino et al*. [2011] on the Dauki fault), accumulated potential slip would be even higher. Given that the range of average slip magnitudes on megathrusts during earthquakes of M_w 8.5 and greater ranges from about 10 m to 20 m [*Wells and Coppersmith*, 1994], it seems quite likely that the return period for great failures of this megathrust are at least many hundreds and could well be over a thousand years. If the megathrust is not fully coupled [e.g., *Chlieh et al*., 2008; *Hsu et al*., 2012], it would take even longer for the megathrust to accumulate enough strain to generate a single or a cluster of great earthquakes.

Ruptures of faults within the downgoing Indian Ocean lithosphere farther east are another plausible source of destructive earthquakes. An example of such an event is the M_s 7.4 earthquake of 1954, east of the Indoburman Range. Its hypocentral depth of 180 km [*Engdahl and Villasenor*, 2002; *Allen et al*., 2009] puts it squarely within the Wadati-Benioff zone of the downgoing slab. These intraslab sources are farther than shallow ruptures from human infrastructure at the Earth's surface. Nonetheless, they can cause significant damage. Shallower sources, however, within the subducting Indian Ocean lithosphere west of the crest of the Indoburman range could cause destructive earthquakes within the populated regions of Bangladesh. Destructive earthquakes in Bangladesh in 1842 and 1885, for example, may have been intraslab earthquakes, as there is no geomorphic evidence of surface deformation near their proposed epicenters.

As in the Ramree domain to the south, the Dhaka domain has seismic faults within and east of the high Indoburman range. The Churachandpur-Mao fault is the most prominent of these. Judging by its 170 km length, wholesale failure of this right-lateral fault could produce an M_w 7.6 earthquake. The geodetic analysis of *Gahalaut et al*. [2013] suggests, however, the fault slips aseismically, at least in part. Aseismic slip along active strike-slip faults is usually associated with minor to moderate earthquakes [*Lienkaemper et al*., 1991]. However, we are not aware of any historical events that can be ascribed to rupture of the Churachandpur-Mao fault in the *Szeliga et al*. [2010] earthquake catalog, nor does the instrumental catalog show a high level of seismic activity along the fault. Thus, we suspect that the Churachandpur-Mao fault is creeping only very near the surface and is capable of generating a large earthquake in the vicinity of Imphal.

The ~280 km length of the eastward dipping Kabaw fault implies that it could generate an M_w 8.4 earthquake if it were to fail all at once (Table 4). The average interval between such earthquakes would be a millennium or longer, since geodetic analysis suggests the fault slip rate is only a few mm/yr [*Socquet et al*., 2006; *Steckler et al*., 2013], which is consistent with our observation that the slip rate must be lower than sedimentation and erosion rates.

4.1.4. Naga Domain

The southeastward-dipping Naga thrust fault is the principal seismic source within the Naga domain (Figure 9). The 400 km length of the fault implies a maximum earthquake within the range M_w 8.5 to 8.7 (Table 4). The structural cross section from *Kent et al*. [2002] suggests the dip of the Naga thrust fault is about 23°, higher than the dip angle of the megathrust of the Dhaka and Ramree domains. In addition to being distinguished by a steeper dip, the fault is also distinguished by the fact that it is the interface between two pieces of continental lithosphere (Figures 19b and 1a) rather than the boundary between oceanic and continental lithosphere.

Using the equations from *Blaser et al*. [2010] and *Strasser et al*. [2010], we estimate that the Naga thrust fault is capable of producing an M_w 8.5 to 8.7 earthquake, similar in size to the great Assam earthquake of 1950, which resulted from rupture of the Himalayan Frontal Thrust, just to the north. On the other hand, it is plausible that each of the three 100 to 150 km long arcuate lobes we have mapped commonly fail individually. In such a case, the magnitude of the largest Naga thrust earthquakes would be in the M_w 7.7 to M_w 8 range.

Neither vectors from GPS stations spanning the fault nor vectors from plate-motion models constrain the slip rate of the Naga thrust fault, because of the sparse coverage of geodetic networks in Assam and northern Myanmar. Improved estimates of the seismic potential of the Naga thrust will require additional geodetic and geological studies in the region.

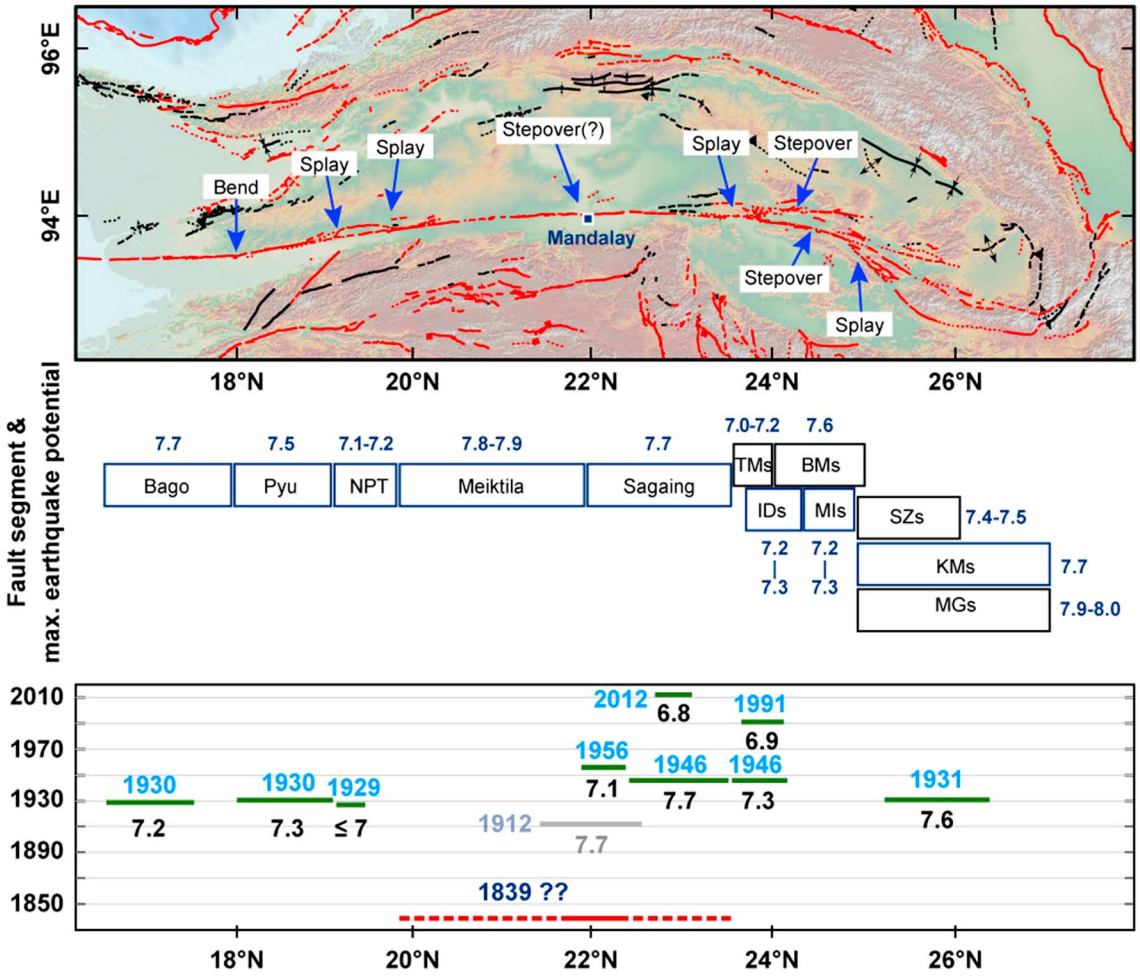

Figure 22. Map and chart of potential maximum earthquake magnitudes (M_w) associated with named segments of the Sagaing fault. Blue arrows show the boundaries of fault segments. Ruptures of the past century appear in the lower box. Green lines are the proposed rupture patches along the Sagaing fault since the beginning of the twentieth century; gray line shows the proposed rupture section along the Kyaukkyan fault, parallel to the Sagaing fault. Red line marks the possible rupture patch of the 1839 earthquake, inferred from historical data. BMs = Ban Mauk segment; TMs = Tawma segment; IDs = In Daw segment; MIs = Mawlu segment; SZs = Shaduzup segment; KMs = Kamaing segment; MGs = Mogang segment.

Although we did not find any evidence of active faults along the southeastern flank of or within the northern Indoburman range (Figure 9a), some intraslab earthquakes occur within the downgoing Indian plate beneath the range. Although the intraslab events in the Naga domain were not as frequent as those in the Dhaka domain, failure of faults within the subducting plate poses a potential hazard within the Naga domain. In addition, several earthquakes greater than magnitude 6 have occurred along the southeastern flank of the northern Indoburman range. These include a magnitude 7 earthquake in 1932 and an M_w 7.2 earthquake in 1988 [*Engdahl and Villasenor*, 2002]. Both of these two events originated at depths greater than 90 km. Although its hypocenter was deep, the 1988 earthquake did cause some damage.

4.2. The Sagaing Fault

The 60 to 260 km range of segment lengths along the right-lateral Sagaing fault implies a range of maximum magnitudes from M_w 7 to 8 (Table 4 and Figure 22). This is consistent with the observation that during the first half of the twentieth century, more than half of the fault appears to have ruptured in several earthquakes with magnitudes in the mid-seven range [*Coggin Brown and Leicester*, 1933; *Hurukawa and Phyo Maung Maung*, 2011] (Figure 22). This historical behavior of the Sagaing fault appears quite similar to that of the more highly segmented Sumatran fault through the first half of the twentieth century [*Daryono et al.*, 2012]. The early twentieth century clustering of large ruptures is also similar to the behavior of the North Anatolian fault, which produced several low- to high-*M*7 earthquakes in the twentieth century [e.g., *Stein et al.*, 1997].

One notably (and perhaps ominously) quiet section of the fault is the 220 km long Meiktila segment, between the large city of Mandalay and the new capital of Naw Pyi Daw. This long quiet section separates a southern cluster of ruptures in 1929 and 1930 from a northern cluster between 1931 and 2012. The length of the Meiktila segment implies that it is capable of producing an earthquake as large as M_w 7.8 to 7.9, if it ruptures all at once [*Wells and Coppersmith*, 1994; *Blaser et al*., 2010] (Figure 22 and Table 4).

We speculate, on the basis of sparse historical records of shaking, that the 1839 Ava earthquake may have resulted from the failure of Meiktila segment, in conjunction with the Sagaing segment, its neighbor on the north. If the Meiktila segment has been dormant since then, and the fault is fully coupled down to a depth between 12 and 15 km, as *Vigny et al*. [2003] and *Socquet et al*. [2006] suggest, then accumulated slip potency on the Meiktila segment after 1839 is enough to generate a M_w 7.6 earthquake.

The earthquake histories and complicated fault geometry of the northern half of the Sagaing fault imply a more complex behavior than that of the southern half of the fault. The segment lengths of the northern half of the fault yield a range of maximum earthquake magnitudes from about M_w 7.0 to 8.0 (Table 4 and Figure 22). These estimates may be high, however, because a recent geodetic analysis suggests that the locking depth of the northern Sagaing fault is just ~5 to 7 km [*Maurin et al*., 2010], far more shallow than for most of the faults used in the global length–magnitude scaling relationships.

We have chosen in our analysis of plausible earthquakes to assume that each segment will rupture completely during future earthquakes. Nonetheless, it is clear that this is not always the case. The November 2012 rupture of a short portion of the Sagaing segment is a recent example of the partial failure of a segment. This M_w 6.8 earthquake resulted from partial failure of a segment that most likely ruptured *en toto* during a larger M_w 7.7 earthquake in 1946 (Figure 22). Perhaps coincidentally, the slip potency accumulated on the 40 km long 2012 fault rupture in the years between 1946 and 2012 roughly equals the potency of the 2012 event, if the rupture extended to 12 km at depth. The 180 km long Sagaing segment illustrates well that our assumption of whole-segment rupture is a gross simplification of reality. Return periods of just decades are plausible for M_w 6.8 to M_w 7.0 partial failure events, and these events may be clustered over a short period. M_w 7.7 whole-segment failures would recur about every 300 to 400 years.

The historical seismic record of the northern half of the Sagaing fault may illustrate another complexity as well—multisegment rupture. One plausible example of this is the combined rupture of Meiktila and the Sagaing segment during the great 1839 earthquake. If fault ruptures commonly propagate across the boundary between the Meiktila and Sagaing segments, rupture length would be about 400 km. Length-magnitude relationships suggest that such long ruptures would generate earthquakes of M_w 8.1 to 8.3 [*Wells and Coppersmith*, 1994; *Blaser et al*., 2010]. Slip-magnitude relationships yield return times longer than 500 to 1000 years for such events.

4.3. Shan Domain

We have identified 27 active faults systems within the Shan domain. The lengths of these faults range from about 30 to more than 480 km (Table 2). Our mapping suggests that maximum geomorphically expressed offsets range from approximately 2.5 to 23 km for these strike-slip fault systems (Table 2 and Figure 23).

From length-magnitude relationships, we estimate maximum earthquake magnitudes that range from about M_w 6.5 to 8.4 [*Wells and Coppersmith*, 1994; *Blaser et al*., 2010] (Table 4 and Figure 23). Historical earthquake magnitudes have ranged from 5.5 to 7.7 (Tables 1 and 4 and Figure 12). This difference between estimated and actual maximum magnitudes suggests that most historical events have involved partial failures.

The 1988 M_w 7.0 Lancang earthquake is one example of a partial failure. The highest intensities (MMI ≥ VIII) and a ~45 km long surface rupture occurred along the northwestern part of the 200 km long dextral-slip fault [*Yu et al*., 1991] (Figure 12).

The 2011 M_w 6.8 Tarlay earthquake is another example of partial failure. Measurements of the surface rupture from satellite imagery and field measurements show clearly that only the westernmost 30 km of the Nam Ma fault ruptured during this earthquake. The rupture spanned the entire length of a segment of the fault that terminates eastward in a pull-apart basin [*Wang et al*., 2013a]. Other examples include partial failures of the Kyaukkyun fault during the 1912 M_w 7.7 earthquake and of the Nanting fault during a magnitude 7 earthquake in 1941. Although the surface ruptures of these early twentieth century earthquakes

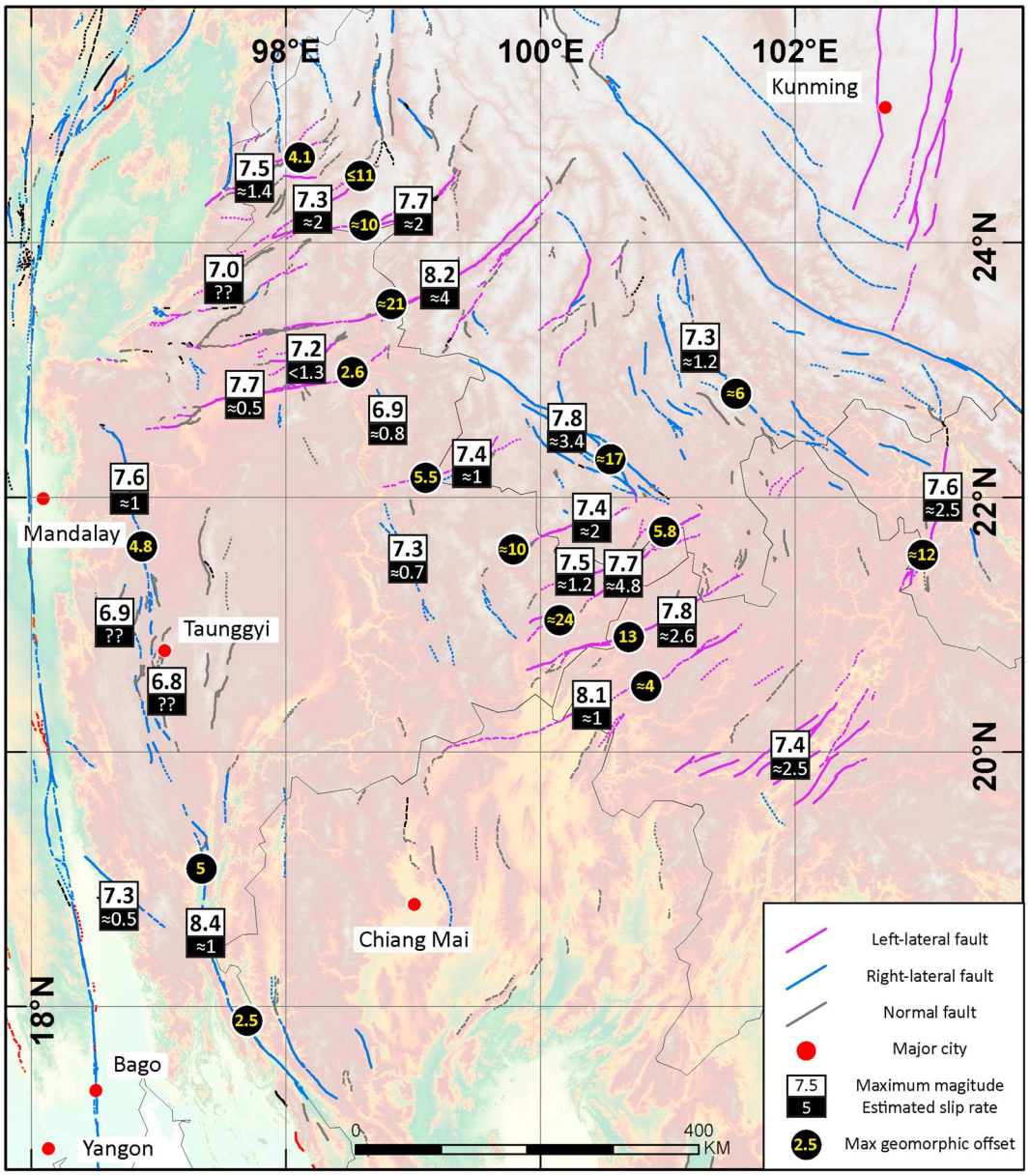

Figure 23. Map of total geomorphological evident offset (black dots) and potential maximum earthquake magnitudes (M_w) (white rectangles) associated with named faults of the Shan domain. The maximum earthquake magnitudes are based on the assumption that each fault will rupture along its entire length. Purple, blue, and gray lines represent left-lateral, right-lateral, and normal faults, respectively.

were not mapped in the field, isoseismal maps in both cases imply that rupture of the faults was partial [*Coggin Brown*, 1914; *Compilation Group of China Seismic Intensity Zoning Map SSB*, 1979] (Figure 12). These examples and the commonly moderate size of earthquakes along the strike-slip faults of the Shan domain show that partial rupture of these faults is typical.

It is not surprising that some of these faults have experienced partial rupture during the period of instrumental record, because many fault traces exhibit step overs and other structural complexities. The existence of these complexities is not surprising, given that fault complexity is inversely proportional to a fault's total offset [*Wesnousky*, 1988; *Stirling et al.*, 1996]. Cumulative offsets that we have estimated for faults in the Shan domain range from 10 to 20 km. This range in total offsets coincides with along-strike step over spacing between 25 and 40 km [*de Joussineau and Aydin*, 2010]. This is consistent with the Shan domain's

instrumental earthquake history—many destructive earthquakes have had magnitudes between M_w 6.7 and 7, consistent with ruptures less than 40 km long [e.g., *Wells and Coppersmith*, 1994].

However, this does not mean that the wholesale rupture of a longer fault is not possible in the Shan domain. Many large earthquakes have resulted from the rapid-fire rupture of two or more fault segments. The Landers earthquake in 1992 [*Sieh et al*., 1993], the El Mayor-Cucapah earthquake in 2010 [*Oskin et al*., 2012], and the off-Sumatra earthquake in 2012 [*Meng et al*., 2012] are just some of these examples. Thus, future seismic hazard evaluations of the Shan domain should include the possibility of both complete- and partial-rupture scenarios.

We now use the maximum geomorphically expressed offsets and an estimated ~5 Ma age of these offsets [*Lacassin et al*., 1998; *Wang et al*., 1998] to calculate fault-slip rates for the strike-slip faults of the Shan domain (Table 4). Thus calculated, most of the average fault-slip rates are lower than 4 mm/yr. Two exceptions are the 4 to 5 mm/yr rates of the Nanting fault and the Menglian fault. These estimated low fault-slip rates imply recurrence intervals of 10^3 to 10^4 years for each of the slower-slipping faults. For example, we estimate an average recurrence interval of 3000 years for the maximum (M_w 7.5) earthquake on the Daying River fault. The 180 km long Mengxing fault is one of the fastest moving faults, but the fault would take about 1300 years to accumulate enough slip potency to generate its maximum earthquake (M_w 7.7).

Although these low fault-slip rates imply long recurrence intervals for complete rupture of any one fault, the large number of faults and their common partial rupture mean that earthquakes are still very frequent throughout the domain. In fact, about 14 moderate to strong (M_w 6.7 to M_w 7.7) earthquakes occurred within the Shan domain during the past century—on average, about one every 8 years. If we assume that an average partial failure of these faults produces a M_w 7.0 earthquake, slightly smaller than the average earthquake magnitude of these 14 recent destructive earthquakes, we calculate a recurrence of about 15 years for the whole domain. This frequency is, however, about half the average frequency of the past century. This suggests that throughout the past century, the Shan domain has been experiencing an episode of activity than is higher than its average long-term level. This speculation is supported by the observation that total seismic moment released during these historical earthquakes is about 3 times higher than the seismic moment that would have been accumulated based on their fault slip rates.

5. Conclusions

Geomorphologically evident active faults and folds of the Myanmar region comprise three majors systems, which accommodate the northward translation of the Indian plate into the Eurasian plate and the extrusion of crust around the eastern syntaxis of the Himalaya. The western of these three systems comprises four distinct neotectonic domains, each distinguished by a unique geometry of the Sunda megathrust. Distinct active hanging wall structures within each of these four domains include large strike-slip faults and both blind and surface-rupturing thrust faults. The Sagaing fault comprises the second of the three systems. Second-order structural characteristics of this ~1200 km long domain suggest division into 12 segments. Historical seismicity confirms that to a large degree these structurally defined segments constrain seismic ruptures. The third of the neotectonic systems is the Shan domain, a large region of conjugate left- and right-lateral active faults that accommodate extrusion of material around the eastern Himalayan syntaxis.

Empirical global relationships between fault length and earthquake magnitude allow us to estimate maximum magnitudes for the active faults and fault segments in each of these domains. The lengths of these structures imply that most are capable of generating events greater than M_w 7.0. However, the historical and instrumental records show that smaller earthquakes are common, because of partial rupture of faults and fault segments is common. Each of the four megathrust segments is capable of producing an earthquake of M_w 8.5 or greater, but only one has done so in the period of historical record. Estimates of slip rates for the faults of the Shan domain and empirical relationships between fault length and magnitude suggest that recurrence intervals for complete rupture of these faults are typically several thousand years. Seismic moment release in this domain during the past century may have been greater than the millennially averaged rate. Empirical relationships and historical seismicity show that ruptures of segments of the Sunda megathrust and the Sagaing fault should occur every few hundred years, on average.

Our analysis of the active, seismogenic faults of the Myanmar region should serve as a foundation for more detailed evaluations of seismic hazard and for assessments of risk and exposure.

Acknowledgments

We have benefited greatly from discussions with Win Swe and other friends in Myanmar during our stays in Yangon. We also appreciate assistance from members of the Myanmar Geosciences Society (MGS), the Department of Meteorology and Hydrology (DMH) of Myanmar since 2006. This research was supported initially by the Caltech Tectonics Observatory and later by the Earth Observatory of Singapore (EOS), Nanyang Technological University, Singapore. This is Caltech Tectonics Observatory contribution 258 and Earth Observatory of Singapore contribution 56.

References

Abe, K., and S. I. Noguchi (1983), Revision of magnitudes of large shallow earthquakes, 1897–1912, *Phys. Earth Planet. Inter.*, *33*(1), 1–11.

Aier, I., K. Luirei, S. Bhakuni, G. T. Thong, and G. C. Kothyari (2011), Geomorphic evolution of Medziphema intermontane basin and Quaternary deformation in the schuppen belt, Nagaland, NE India, *Z. Geomorphol.*, *55*(2), 247–265, doi:10.1127/0372-8854/2011/0055-0048.

Alam, M. (1989), Geology and depositional history of Cenozoic sediments of the Bengal Basin of Bangladesh, *Palaeogeogr. Palaeoclimatol. Palaeoecol.*, *69*, 125–139, doi:10.1016/0031-0182(89)90159-4.

Allen, C., A. Gillespie, H. Yuan, K. E. Sieh, Z. Buchun, and Z. Chengnan (1984), Red River and associated faults, Yunnan Province, China: Quaternary geology, slip rates, and seismic hazard, *Geol. Soc. Am. Bull.*, *95*(6), 686–700, doi:10.1130/0016-7606(1984)95<686:RRAAFY>2.0.CO;2.

Allen, T. I., K. D. Marano, P. S. Earle, and D. J. Wald (2009), PAGER-CAT: A composite earthquake catalog for calibrating global fatality models, *Seismol. Res. Lett.*, *80*(1), 57–62, doi:10.1785/gssrl.80.1.57.

Amante, C., and B. W. Eakins (2009), *ETOPO1 1 Arc-Minute Global Relief Model: Procedures, Data Sources and Analysis*, US Department of Commerce, National Oceanic and Atmospheric Administration, National Environmental Satellite, Data, and Information Service, National Geophysical Data Center, Marine Geology and Geophysics Division, Boulder, Colo.

Ambraseys, N. (2004), Three little known early earthquakes in India, *Curr. Sci.*, *86*(4), 506–508.

Ambraseys, N. N., and J. Douglas (2004), Magnitude calibration of north Indian earthquakes, *Geophys. J. Int.*, *159*(1), 165–206, doi:10.1111/j.1365-246X.2004.02323.x.

Ansary, M. A., T. M. Al-Hussaini, and M. Sharfuddin (2000), Damage assessment of July 22, 1999 Moheshkhali Earthquake, Bangladesh, paper presented at 8th ASCE Specialty Conference on Probabilistic Mechanics and Structural Reliability, Indiana, U.S.A.

Armijo, R., P. Tapponnier, and T. Han (1989), Late Cenozoic right-lateral strike-slip faulting in southern Tibet, *J. Geophys. Res.*, *94*(B3), 2787–2838, doi:10.1029/JB094iB03p02787.

Banerjee, P., R. Bürgmann, B. Nagarajan, and E. Apel (2008), Intraplate deformation of the Indian subcontinent, *Geophys. Res. Lett.*, *35*, L18301, doi:10.1029/2008GL035468.

Barka, A., and K. Kadinsky-Cade (1988), Strike-slip fault geometry in Turkey and its influence on earthquake activity, *Tectonics*, *7*(3), 663–684.

Bender, F., and D. N. Bannert (1983), *Geology of Burma*, Science Publishers, Gebruder Borntraeger Verlagsbuchhandlung.

Bertrand, G., C. Rangin, R. Maury, H. Htun, H. Bellon, and J.-P. Guillaud (1998), The Singu basalts (Myanmar): New constraints for the amount of recent offset on the Sagaing Fault, *C.R. Acad. Sci., Ser. IIa: Sci. Terre Planets*, *327*(7), 479–484.

Blaser, L., F. Krüger, M. Ohrnberger, and F. Scherbaum (2010), Scaling relations of earthquake source parameter estimates with special focus on subduction environment, *Bull. Seismol. Soc. Am.*, *100*(6), 2914–2926.

Brune, J. N., J. Curray, L. Dorman, and R. Raitt (1992), A proposed super-thick sedimentary basin, Bay of Bengal, *Geophys. Res. Lett.*, *19*(6), 565–568.

Brunnschweiler, R. (1966), On the geology of the Indoburman ranges: (Arakan Coast and Yoma, Chin Hills, Naga Hills), *J. Geol. Soc. Aust.*, *13*(1), 137–194.

Burbank, D. W., and R. S. Anderson (2011), *Tectonic Geomorphology*, Wiley, Oxford, U. K.

Bureau of Geology and Mineral Resources of Yunnan (1993), Geological map of Yunnan, scale 1:500,000.

Bustin, A., R. Hyndman, H. Kao, and J. Cassidy (2007), Evidence for underthrusting beneath the Queen Charlotte Margin, British Columbia, from teleseismic receiver function analysis, *Geophys. J. Int.*, *171*(3), 1198–1211.

Chang, Z.-F., X.-W. An, and Y.-F. Zhang (2012), Study on late-quaternary activity and displacement of drainage systems along the Wanding Fault, *Seismolog. Geol.*, *2*, 228–239, doi:10.3969/j.issn.0253-4967.2012.02.003.

Chang, Z.-F., G. Chen, and J.-Q. Yu (2011), Geological evidence of activity along the Dayingjiang Fault since late Pleistocene, *Seismol. Geol.*, *33*(4), 877–888.

Chen, Q.-F., D. Zheng, G. Liu, and L. Ming (2002), *Earthquake Cases in China (1995–1996)*, Seismological Press, Beijing, China.

Chhibber, H. L., and R. Ramamirtham (1934), The geology of Burma, MacMillan, London, U. K.

Chlieh, M., et al. (2007), Coseismic slip and afterslip of the great M_w 9.15 Sumatra–Andaman earthquake of 2004, *Bull. Seismol. Soc. Am.*, *97*(1A), S152–S173, doi:10.1785/0120050631.

Chlieh, M., J. P. Avouac, K. Sieh, D. H. Natawidjaja, and J. Galetzka (2008), Heterogeneous coupling of the Sumatran megathrust constrained by geodetic and paleogeodetic measurements, *J. Geophys. Res.*, *113*, B05305, doi:10.1029/2007JB004981.

Clark, M. K., and R. Bilham (2008), Miocene rise of the Shillong Plateau and the beginning of the end for the Eastern Himalaya, *Earth Planet. Sci. Lett.*, *269*(3), 337–351.

Coggin Brown, J. (1914), The Burma earthquake of May 1912, *Memoir Geol. Surv India*, *13*, 1–147.

Coggin Brown, J. (1929), *The Rangoon Earthquakes of September and December 1927*, Records of the Geological Survey of India, vol. LXII, pp. 258–278.

Coggin Brown, J. (1932), *A Note on the Swa Earthquake of August 8th, 1929*, Rec. Geol. Surv. India, vol. LXVI, pp. 244–249, Calcutta, India.

Coggin Brown, J., and P. Leicester (1933), The Pyu earthquakes of 3rd and 4th December, 1930, and subsequent Burma earthquakes up to January, 1932, Geological Survey of India.

Coggin Brown, J., P. Leicester, and H. L. Chhibber (1931), A preliminary note on the Pegu earthquake of May 5th, 1930, *Rec. Geol. Surv. India*, *65*, 221–284.

Compilation Group of China Seismic Intensity Zoning Map SSB (1979), *Atlas of Chinese Earthquake Isoseismals*, Seismic Publishing House, Beijing.

Cummins, P. R. (2007), The potential for giant tsunamigenic earthquakes in the northern Bay of Bengal, *Nature*, *449*(7158), 75–78.

Curiale, J., G. Covington, A. Shamsuddin, J. Morelos, and A. Shamsuddin (2002), Origin of petroleum in Bangladesh, *AAPG Bull.*, *86*(4), 625–652.

Curray, J., F. Emmel, D. Moore, and R. Raitt (1982), Structure, tectonics, and geological history of the northeastern Indian Ocean, in *The Ocean Basins and Margins*, edited by A. M. Nairn and F. Stehli, pp. 399–450, Springer, New York, doi:10.1007/978-1-4615-8038-6_9.

Curray, J. R. (1991), Possible greenschist metamorphism at the base of a 22-km sedimentary section, Bay of Bengal, *Geology*, *19*(11), 1097–1100.

Curray, J. R. (2005), Tectonics and history of the Andaman Sea region, *J. Asian Earth Sci.*, *25*(1), 187–232, doi:10.1016/j.jseaes.2004.09.001.

Curray, J. R., D. G. Moore, L. A. Lawver, F. J. Emmel, R. W. Raitt, M. Henry, and R. Kieckhefer (1979), Tectonics of the Andaman Sea and Burma: Convergent margins, in *Geological and Geophysical Investigations of Continental Margins*, vol. 29, edited by J. S. Watkins, L. Montadert and P. W. Dickerson, pp. 189–198, Am. Assoc. of Pet. Geol. Mem., Tulsa, Okla.

Curray, J. R., F. J. Emmel, and D. G. Moore (2002), The Bengal Fan: Morphology, geometry, stratigraphy, history and processes, *Mar. Pet. Geol.*, *19*(10), 1191–1223, doi:10.1016/S0264-8172(03)00035-7.

Daryono, M. R., D. H. Natawidjaja, and K. Sieh (2012), Twin-surface ruptures of the March 2007 M > 6 earthquake doublet on the Sumatran fault, *Bull. Seismol. Soc. Am.*, *102*(6), 2356–2367.
Dasgupta, S., M. Mukhopadhyay, A. Bhattacharya, and T. K. Jana (2003), The geometry of the Burmese-Andaman subducting lithosphere, *J. Seismolog.*, *7*(2), 155–174.
de Joussineau, G., and A. Aydin (2010), Segmentation along strike-slip faults revisited, in *Mechanics, Structure and Evolution of Fault Zones*, pp. 1575–1594, Springer, London, U. K., doi:10.1007/978-3-0346-0138-2_3.
DeMets, C., R. G. Gordon, and D. F. Argus (2010), Geologically current plate motions, *Geophys. J. Int.*, *181*(1), 1–80.
Densmore, A. L., M. A. Ellis, Y. Li, R. Zhou, G. S. Hancock, and N. Richardson (2007), Active tectonics of the Beichuan and Pengguan faults at the eastern margin of the Tibetan Plateau, *Tectonics*, *26*(4), doi:10.1029/2006TC001987.
Engdahl, E. R., and A. Villasenor (2002) Global seismicity: 1900-1999, in *International Handbook of Earthquake Engineering and Seismology*, vol. 81A, edited by W. H. K. Lee et al., pp. 665–690, Academic Press, Boston, Mass.
Fitch, T. J. (1972), Plate convergence, transcurrent faults, and internal deformation adjacent to Southeast Asia and the western Pacific, *J. Geophys. Res.*, *77*(23), 4432–4460, doi:10.1029/JB077i023p04432.
Fuller, M. L. (1912), *The New Madrid Earthquake*, U.S. Government Printing Office, Washington, D. C.
Gahalaut, V. K., B. Kundu, S. S. Laishram, J. Catherine, A. Kumar, M. D. Singh, R. Tiwari, R. Chadha, S. Samanta, and A. Ambikapathy (2013), Aseismic plate boundary in the Indo-Burmese wedge, northwest Sunda Arc, *Geology*, *41*(2), 235–238.
Gomberg, J., P. Bodin, W. Savage, and M. E. Jackson (1995), Landslide faults and tectonic faults, analogs?: The Slumgullion earthflow, Colorado, *Geology*, *23*(1), 41–44.
Goodbred, S. L., and S. A. Kuehl (1999), Holocene and modern sediment budgets for the Ganges-Brahmaputra river system: Evidence for highstand dispersal to flood-plain, shelf, and deep-sea depocenters, *Geology*, *27*(6), 559–562.
Guo, S.-M., Y. Wang, and F.-J. Ji (1999a), Tectonic mechanism of moderate strong swarms in Yunnan's Simao-Pu'er region, *J. Seismolog. Res.*, *22*(2), 105–115.
Guo, S.-M., H.-F. Xiang, and X.-W. Xu (1999b), The preliminary study on late Quaternary activity of Dayingjiang fault zone, western Yunnan Province, *Research on Active fault*, *7*.
Gupta, H., and V. Gahalaut (2009), Is the northern Bay of Bengal tsunamigenic?, *Bull. Seismol. Soc. Am.*, *99*(6), 3496–3501.
Gutenberg, B., and C. Richter (1954), *Seismicity of the Earth*, 310 pp, edited, Princeton Univ. Press, Princeton, N. J.
Guzmán-Speziale, M., and J. F. Ni (2000), Comment on "Subduction in the Indo-Burma Region: Is it still active?" by S. P. Satyabala, *Geophys. Res. Lett.*, *27*(7), 1065–1066, doi:10.1029/1999GL005428.
Halsted, E. P. (1841), Report on the Island of Chedooba, *J. Asiatic Soc. Bengal*, *114*, 419–436.
Maung, H. (1987), Transcurrent movements in the Burma–Andaman Sea region, *Geology*, *15*(10), 911–912.
Hsu, Y.-J., S.-B. Yu, T.-R. A. Song, and T. Bacolcol (2012), Plate coupling along the Manila subduction zone between Taiwan and northern Luzon, *J. Asian Earth Sci.*, *51*, 98–108, doi:10.1016/j.jseaes.2012.01.005.
Huang, X.-M., Y. Du, S.-B. Shu, and F.-R. Xie (2010), Study of the late Quaternary slip rate along the northern segment on the south branch of Longling-Ruili fault, *Seismolog. Geol.*, *32*(2), 222–232.
Hurukawa, N., and Phyo Maung Maung (2011), Two seismic gaps on the Sagaing Fault, Myanmar, derived from relocation of historical earthquakes since 1918, *Geophys. Res. Lett.*, *38*, L01310, doi:10.1029/2010GL046099.
Iyengar, R., D. Sharma, and J. Siddiqui (1999), Earthquake history of India in medieval times, *Indian J. Hist. Sci.*, *34*, 181–238.
Jade, S., et al. (2007), Estimates of interseismic deformation in Northeast India from GPS measurements, *Earth Planet. Sci. Lett.*, *263*(3–4), 221–234, doi:10.1016/j.epsl.2007.08.031.
Jarvis, A., H. I. Reuter, A. Nelson, and E. Guevara (2008), Hole-filled seamless SRTM data V4, *International Centre for Tropical Agriculture* (*CIAT*).
Johnson, S. Y., and A. M. N. Alam (1991), Sedimentation and tectonics of the Sylhet trough, Bangladesh, *Geol. Soc. Am. Bull.*, *103*(11), 1513–1527.
Kent, W. N., R. G. Hickman, and U. Dasgupta (2002), Application of a ramp/flat-fault model to interpretation of the Naga thrust and possible implications for petroleum exploration along the Naga thrust front, *AAPG bull.*, *86*(12), 2023–2045.
Khan, F. H. (1991), *Geology of Bangladesh*, Wiley Eastern.
Kreemer, C., W. E. Holt, and A. J. Haines (2003a), An integrated global model of present-day plate motions and plate boundary deformation, *Geophys. J. Int.*, *154*(1), 8–34, doi:10.1046/j.1365-246X.2003.01917.x.
Kreemer, C., W. E. Holt, and A. J. Haines (2003b), An integrated global model of present-day plate motions and plate boundary deformation, *Geophys. J. Int.*, *154*(1), 8–34.
Kumar, A., M. Sanoujam, L. Sunil, and T. Dolendro (2011), Active deformations at the Churachandpur Mao Fault (CMF) in Indo Burma Ranges: Multidisciplinary evidences, *Int. J. Geosci.*, *2*(4), 597–609.
Lacassin, R., A. Replumaz, and P. H. Leloup (1998), Hairpin river loops and slip-sense inversion on southeast Asian strike-slip faults, *Geology*, *26*(8), 703–706, doi:10.1130/0091-7613(1998)026<0703:Hrlass>2.3.Co;2.
Lai, K.-Y., Y.-G. Chen, and D. Đ. Lâm (2012), Pliocene-to-present morphotectonics of the Dien Bien Phu fault in northwest Vietnam, *Geomorphology*, *173–174*(0), 52–68, doi:10.1016/j.geomorph.2012.05.026.
Le Dain, A. Y., P. Tapponnier, and P. Molnar (1984), Active faulting and tectonics of Burma and surrounding regions, *J. Geophys. Res.*, *89*(B1), 453–472, doi:10.1029/JB089iB01p00453.
Lee, W., F. Wu, and S. Wang (1978), A catalog of instrumentally determined earthquakes in China (magnitude ≧ 6) compiled from various sources, *Bull. Seismol. Soc. Am.*, *68*(2), 383–398.
Lei, J., G. Zhang, F. Xie, Y. Li, Y. Su, L. Liu, H. Ma, and J. Zhang (2012), Relocation of the 10 March 2011 Yingjiang, China, earthquake sequence and its tectonic implications, *Earthquake Sci.*, *25*(1), 103–110, doi:10.1007/s11589-012-0836-4.
Leloup, P. H., R. Lacassin, P. Tapponnier, U. Schärer, D. Zhong, X. Liu, L. Zhang, S. Ji, and P. T. Trinh (1995), The Ailao Shan-Red River shear zone (Yunnan, China), Tertiary transform boundary of Indochina, *Tectonophysics*, *251*(1–4), 3–84, doi:10.1016/0040-1951(95)00070-4.
Leloup, P. H., P. Tapponnier, R. Lacassin, and M. Searle (2007), Discussion on the role of the Red River shear zone, Yunnan and Vietnam, in the continental extrusion of SE Asia Journal, vol. 163, 2006, 1025–1036, *J. Geol. Soc.*, *164*(6), 1253–1260.
Li, C., R. D. Van der Hilst, A. S. Meltzer, and E. R. Engdahl (2008), Subduction of the Indian lithosphere beneath the Tibetan Plateau and Burma, *Earth Planet. Sci. Lett.*, *274*(1), 157–168.
Lienkaemper, J. J., G. Borchardt, and M. Lisowski (1991), Historic creep rate and potential for seismic slip along the Hayward Fault, California, *J. Geophys. Res.*, *96*(B11), 18,261–18,283, doi:10.1029/91JB01589.
Lu, X., and L.-Q. Zhou (2011), Accurate location of the 2007 M_s 6.4 Ning'er, Yunnan, earthquake sequence, *Seismolog. Geol.*, *33*(3), 560–567, doi:10.3969/j.issn.0253-4967.2011.03.006.
Müller, R. D., W. R. Roest, J. Y. Royer, L. M. Gahagan, and J. G. Sclater (1997), Digital isochrons of the world's ocean floor, *J. Geophys. Res.*, *102*(B2), 3211–3214.

Mallet, F. R. (1878), The mud volcanoes of Ramri and Cheduba, *Rec. Geol. Surv. India*, *11*, 188–207.
Martin, S., and W. Szeliga (2010), A catalog of felt intensity data for 570 earthquakes in India from 1636 to 2009, *Bull. Seismol. Soc. Am.*, *100*(2), 562–569.
Mathur, L. P., and P. Evans (1964), Oil in India, paper presented at 22nd Session International Geological Congress Proceedings, New Delhi, India.
Maurin, T., F. Masson, C. Rangin, U. T. Min, and P. Collard (2010), First global positioning system results in northern Myanmar: Constant and localized slip rate along the Sagaing fault, *Geology*, *38*(7), 591–594.
Maurin, T., and C. Rangin (2009), Structure and kinematics of the Indo-Burmese Wedge: Recent and fast growth of the outer wedge, *Tectonics*, *28*(2), TC2010, doi:10.1029/2008TC002276.
Mazzotti, S., H. Dragert, J. Henton, M. Schmidt, R. Hyndman, T. James, Y. Lu, and M. Craymer (2003), Current tectonics of northern Cascadia from a decade of GPS measurements, *J. Geophys. Res.*, *108*(B12), 2554, doi:10.1029/2003JB002653.
McCaffrey, R. (2009), The tectonic framework of the Sumatran subduction zone, *Annu. Rev. Earth Planet. Sci.*, *37*(1), 345–366, doi:10.1146/annurev.earth.031208.100212.
Meltzner, A. J., K. Sieh, M. Abrams, D. C. Agnew, K. W. Hudnut, J.-P. Avouac, and D. H. Natawidjaja (2006), Uplift and subsidence associated with the great Aceh-Andaman earthquake of 2004, *J. Geophys. Res.*, *111*, B02407, doi:10.1029/2005JB003891.
Meng, L., J.-P. Ampuero, J. Stock, Z. Duputel, Y. Luo, and V. Tsai (2012), Earthquake in a maze: Compressional rupture branching during the 2012 M_w 8.6 Sumatra earthquake, *Science*, *337*(6095), 724–726.
Mitchell, A. (1977), Tectonic settings for emplacement of Southeast Asian tin granites, *Bul. Persat. Geol. Malays.*, *9*, 123–140.
Morino, M., A. Maksud Kamal, D. Muslim, R. M. Ekram Ali, M. A. Kamal, M. Zillur Rahman, and F. Kaneko (2011), Seismic event of the Dauki Fault in 16th century confirmed by trench investigation at Gabrakhari Village, Haluaghat, Mymensingh, Bangladesh, *J. Asian Earth Sci.*, *42*(3), 492–498.
Morley, C., M. Smith, A. Carter, P. Charusiri, and S. Chantraprasert (2007), Evolution of deformation styles at a major restraining bend, constraints from cooling histories, Mae Ping fault zone, western Thailand, *Geol. Soc. Lond Spec. Publ.*, *290*(1), 325–349.
Mueller, K., and J. Pujol (2001), Three-dimensional geometry of the Reelfoot blind thrust: Implications for moment release and earthquake magnitude in the New Madrid seismic zone, *Bull. Seismol. Soc. Am.*, *91*(6), 1563–1573.
Ni, J. F., M. Guzman-Speziale, M. Bevis, W. E. Holt, T. C. Wallace, and W. R. Seager (1989), Accretionary tectonics of Burma and the three-dimensional geometry of the Burma subduction zone, *Geology*, *17*(1), 68–71.
Nielsen, C., N. Chamot-Rooke, and C. Rangin (2004), From partial to full strain partitioning along the Indo-Burmese hyper-oblique subduction, *Mar. Geol.*, *209*(1), 303–327.
Oldham, T. (1883), A catalogue of Indian earthquakes from the earliest time to the end of AD 1869, *Mem. Geol. Surv. India*, *19*(3), 53.
Oskin, M. E., J. R. Arrowsmith, A. H. Corona, A. J. Elliott, J. M. Fletcher, E. J. Fielding, P. O. Gold, J. J. G. Garcia, K. W. Hudnut, and J. Liu-Zeng (2012), Near-field deformation from the El Mayor–Cucapah earthquake revealed by differential LIDAR, *Science*, *335*(6069), 702–705.
Pacheco, J. F., and L. R. Sykes (1992), Seismic moment catalog of large shallow earthquakes, 1900 to 1989, *Bull. Seismol. Soc. Am.*, *82*(3), 1306–1349.
Pelayo, A. M., and D. A. Wiens (1989), Seismotectonics and relative plate motions in the Scotia Sea region, *J. Geophys. Res.*, *94*(B6), 7293–7320, doi:10.1029/JB094iB06p07293.
Penick, J. L. (1981), *The New Madrid Earthquakes*, Univ. of Missouri Press, Columbia, Mo.
Plafker, G. (1965), Tectonic deformation associated with the 1964 Alaska Earthquake: The earthquake of 27 March 1964 resulted in observable crustal deformation of unprecedented areal extent, *Science*, *148*(3678), 1675–1687.
Prawirodirdjo, L., and Y. Bock (2004), Instantaneous global plate motion model from 12 years of continuous GPS observations, *J. Geophys. Res.*, *109*, B08405, doi:10.1029/2003JB002944.
Pubellier, M. (2008), *Structural Map of Eastern Eurasia*, CCGM, Paris, France.
Rao, N. P., and Kalpna (2005), Deformation of the subducted Indian lithospheric slab in the Burmese arc, *Geophys. Res. Lett.*, *32*, L05301, doi:10.1029/2004GL022034.
Replumaz, A. (1999), *Reconstruction de la zone de collision Inde-Asie*, Étude centrée sur l'Indochine, PhD thesis, Université Paris 7-IPG, Paris, France.
Richards, S., G. Lister, and B. Kennett (2007), A slab in depth: Three-dimensional geometry and evolution of the Indo-Australian plate, *Geochem. Geophys. Geosyst.*, *8*, Q12003, doi:10.1029/2007GC001657.
Rudolf, B., A. Becker, U. Schneider, A. Meyer-Christoffer, and M. Ziese (2010), The new "GPCC Full Data Reanalysis Version 5" providing high-quality gridded monthly precipitation data for the global land-surface is public available since December 2010, *GPCC Status Report December*.
Rudolf, B., and U. Schneider (2005), Calculation of gridded precipitation data for the global land-surface using in-situ gauge observations, paper presented at Proceedings of the 2nd Workshop of the International Precipitation Working Group IPWG.
Satyabala, S. (1998), Subduction in the Indo-Burma Region: Is it still active?, *Geophys. Res. Lett.*, *25*(16), 3189–3192.
Sella, G. F., T. H. Dixon, and A. Mao (2002), REVEL: A model for Recent plate velocities from space geodesy, *J. Geophys. Res.*, *107*(B4), 2081, doi:10.1029/2000JB000033.
Sharif Hossain Khan, M., B. Parkash, and S. Kumar (2005), Soil–landform development of a part of the fold belt along the eastern coast of Bangladesh, *Geomorphology*, *71*(3), 310–327.
Shen, Z.-K., J. Lü, M. Wang, and R. Bürgmann (2005), Contemporary crustal deformation around the southeast borderland of the Tibetan Plateau, *J. Geophys. Res.*, *110*, B11409, doi:10.1029/2004JB003421.
Shishikura, M. (2009), Geomorphological evidence of great Holocene earthquakes of western Myanmar, paper presented at the International Workshop on Tsunami and Storm Surge Hazard Assessment and Management for Bangladesh.
Shyu, J. B. H., K. Sieh, Y. G. Chen, and C. S. Liu (2005), Neotectonic architecture of Taiwan and its implications for future large earthquakes, *J. Geophys. Res.*, *110*(B8), B08402, doi:10.1029/2004JB003251.
Sieh, K., L. Jones, E. Hauksson, K. Hudnut, D. Eberhart-Phillips, T. Heaton, S. Hough, K. Hutton, H. Kanamori, and A. Lilje (1993), Near-field investigations of the Landers earthquake sequence, April to July 1992, *Science*, *260*(5105), 171–176.
Sieh, K., and D. Natawidjaja (2000), Neotectonics of the Sumatran fault, Indonesia, *J. Geophys. Res.*, *105*(B12), 28,295–28,326, doi:10.1029/2000JB900120.
Simons, W. J. F., et al. (2007), A decade of GPS in Southeast Asia: Resolving Sundaland motion and boundaries, *J. Geophys. Res.*, *112*, B06420, doi:10.1029/2005JB003868.
Socquet, A., and M. Pubellier (2005), Cenozoic deformation in western Yunnan (China–Myanmar border), *J. Asian Earth Sci.*, *24*(4), 495–515, doi:10.1016/j.jseaes.2004.03.006.
Socquet, A., C. Vigny, N. Chamot-Rooke, W. Simons, C. Rangin, and B. Ambrosius (2006), India and Sunda plates motion and deformation along their boundary in Myanmar determined by GPS, *J. Geophys. Res.*, *111*, B05406, doi:10.1029/2005JB003877.

Soe Thura Tun, Y. Wang, S. N. Khaing, M. Thant, N. Htay, Y. M. Min Htwe, T. Myint, and K. Sieh (2013), Surface ruptures of the M_w 6.8 March 2011 Tarlay Earthquake, Eastern Myanmar.
Steckler, M. S., S. H. Akhter, and L. Seeber (2008), Collision of the Ganges–Brahmaputra Delta with the Burma Arc: Implications for earthquake hazard, *Earth Planet. Sci. Lett.*, *273*(3), 367–378.
Steckler, M. S., et al. (2013), GPS velocity field in Bangladesh: Delta subsidence, seasonal water loading and shortening across the Burma Accretionary Prism and Shillong Massif, Abstract # T13D-2565 presented at 2013 Fall Meeting, AGU, San Francisco, Calif.
Stein, R. S., A. A. Barka, and J. H. Dieterich (1997), Progressive failure on the North Anatolian fault since 1939 by earthquake stress triggering, *Geophys. J. Int.*, *128*(3), 594–604, doi:10.1111/j.1365-246X.1997.tb05321.x.
Stirling, M. W., S. G. Wesnousky, and K. Shimazaki (1996), Fault trace complexity, cumulative slip, and the shape of the magnitude-frequency distribution for strike-slip faults: A global survey, *Geophys. J. Int.*, *124*(3), 833–868, doi:10.1111/j.1365-246X.1996.tb05641.x.
Strasser, F., M. Arango, and J. Bommer (2010), Scaling of the source dimensions of interface and intraslab subduction-zone earthquakes with moment magnitude, *Seismol. Res. Lett.*, *81*(6), 941–950.
Stuart, M. (1920), The Srimangal Earthquake of 8th July, 1918, Mem. Geol. Surv. India, XLVI, 1-70, Calcutta, India.
Szeliga, W., S. Hough, S. Martin, and R. Bilham (2010), Intensity, Magnitude, Location, and Attenuation in India for Felt Earthquakes since 1762, *Bull. Seismol. Soc. Am.*, *100*(2), 570–584.
Tapponnier, P., G. Peltzer, A. Le Dain, R. Armijo, and P. Cobbold (1982), Propagating extrusion tectonics in Asia: New insights from simple experiments with plasticine, *Geology*, *10*(12), 611–616.
Tapponnier, P., X. Zhiqin, F. Roger, B. Meyer, N. Arnaud, G. Wittlinger, and Y. Jingsui (2001), Oblique stepwise rise and growth of the Tibet Plateau, *science*, *294*(5547), 1671–1677.
Than Tin Aung, K. Satake, Y. Okamura, M. Shishikura, W. Swe, H. Saw, T. Lwin Swe, S. Thura Tun, and Thura Aung (2008), Geologic evidence for three great earthquakes in the past 3400 years off Myanmar, *J. Earthquake Eng. Tsunami*, *2*(04), 259–265.
Thein, M., K. Tint, and A. K. Aung (1991), On the lateral displacement of the Sagaing fault, *Georeports*, *1*(1), 23–34.
Trieu, C., G. Panza, A. Peresan, F. Vaccari, F. Romanelli, N. Tuyen, P. Hung, L. Dung, M. Bach, and T. Tuan (2008), Seismic hazard assessment of Vietnam territory on the basis of deterministic approach, *Vietnam J. Geol. Series B*, 220–230.
Tsutsumi, H., and T. Sato (2009), Tectonic geomorphology of the southernmost Sagaing Fault and surface rupture associated with the May 1930 Pegu (Bago) earthquake, Myanmar, *Bull. Seismol. Soc. Am.*, *99*(4), 2155–2168.
Verma, R., M. Mukhopadhyay, and M. Ahluwalia (1976), Earthquake mechanisms and tectonic features of northern Burma, *Tectonophysics*, *32*(3), 387–399.
Vigny, C., A. Socquet, C. Rangin, N. Chamot-Rooke, M. Pubellier, M.-N. Bouin, G. Bertrand, and M. Becker (2003), Present-day crustal deformation around Sagaing fault, Myanmar, *J. Geophys. Res.*, *108*(B11), 2533, doi:10.1029/2002JB001999.
Wang, E., and B. Burchfiel (1997), Interpretation of Cenozoic tectonics in the right-lateral accommodation zone between the Ailao Shan shear zone and the eastern Himalayan syntaxis, *Int. Geol. Rev.*, *39*(3), 191–219.
Wang, E., B. C. Burchfiel, L. H. Royden, L. Chen, J. Chen, W. Li, and Z. Chen (1998), Late Cenozoic Xianshuihe-Xiaojiang, Red River, and Dali fault systems of southwestern Sichuan and central Yunnan, China, *Geol. Soc. London Spec. Publ.*, *327*, 1–108, doi:10.1130/0-8137-2327-2.1.
Wang, H., Z. Qiang, Z. Yuan, Y. Wang, H. Zhang, X. Zhao, and Y. Gu (1991), The distribution of seismic intensities and surface rupture in the Lancang-Gengma (Yunnan Province, China) earthquakes of November 6, 1988, *Acta Seismol. Sin.*, *3*, 008.
Wang, J.-N., Y.-L. Wang, X.-W. An, and X.-D. Yang (2006), Analysis of latest activity on NE-segment of West Branch of Nantinghe Fault, *J. Seismolog. Res.*, *29*(3), 264–268, doi:10.3969/j.issn.1000-0666.2006.03.010.
Wang, Y.-Z., E.-N. Wang, Z.-K. Shen, M. Wang, W.-J. Gan, X.-J. Qiao, G.-J. Meng, T.-M. Li, W. Tao, and Y.-L. Yang (2008), GPS-constrained inversion of present-day slip rates along major faults of the Sichuan-Yunnan region, China, *Sci. China, Ser. D Earth Sci.*, *51*(9), 1267–1283.
Wang, Y., Y.-N. Lin, M. Simons, and S. Thura Tun (2013a), Shallow rupture of the 2011 Tarlay earthquake (M_w 6.8), Eastern Myanmar, *Bull. Seismol. Soc. Am.*, in press.
Wang, Y., et al. (2013b), Permanent upper plate deformation in western Myanmar during the great 1762 earthquake: Implications for neotectonic behavior of the northern Sunda megathrust, *J. Geophys. Res. Solid Earth*, *118*, 1277–1303, doi:10.1002/jgrb.50121.
Wang, Y., K. Sieh, T. Aung, S. Min, S. N. Khaing, and S. T. Tun (2011), Earthquakes and slip rate of the southern Sagaing fault: insights from an offset ancient fort wall, lower Burma (Myanmar), *Geophys. J. Int.*, *185*(1), 49–64, doi:10.1111/j.1365-246X.2010.04918.x.
Wang, Y., K. E. Sieh, S. Min, S. Khaing, and S. Tun (2009), Smoking gun of the May-1912 Burma earthquake? Neotectonics of the Kyaukkyan fault system, Eastern Burma (Myanmar), Abstract #T33B-1912 paper presented at 2009 Fall Meeting, AGU, San Francisco, Calif.
Wells, D. L., and K. J. Coppersmith (1994), New empirical relationships among magnitude, rupture length, rupture width, rupture area, and surface displacement, *Bull. Seismol. Soc. Am.*, *84*(4), 974–1002.
Wesnousky, S. G. (1988), Seismological and structural evolution of strike-slip faults.
Wesnousky, S. G. (2006), Predicting the endpoints of earthquake ruptures, *Nature*, *444*(7117), 358–360.
Win Swe (1970), Rift-features at the Sagaing-Tagaung ridge, *Proc. 5th Burma Research Congress*, *Rangoon*.
Win Swe (2006), Earthquake hazard potentials in Myanmar: A science to public welfare outlook, in *Symp. Tectonics, Seismotectonics, and Earthquake Hazard Mitigation and Management of Myanmar*, Yangon.
Win Swe, C. Thacpaw, N. Thaung Thaung, and K. Nyunt (1972), Geology of part of the Chindwin basin of the central belt, Burma *Rep.*, 34 pp, Department of Geology, Arts and Science University, Mandalay.
Xie, Y. S., and M. B. Tsai (Eds.) (1983), *Compilation of Historical Materials of Chinese Earthquakes*, pp. 4912, Science Press, Beijing, China.
Yeats, R. S., K. E. Sieh, and C. R. Allen (1997), *The Geology of Earthquakes*, Oxford Univ. Press, Bejing, China.
Yu, W.-X., T.-J. Cai, and X.-Y. Hou (1991), Deformation zone of M = 7.6 Lancang earthquake, seismology and geology, *Seismolog. Geol.*, *13*(4), 343–352.
Zhu, Y., P. Li, and J. Ren (1994), Activity of Nandinghe fault zone and its Paleoearthquake events, *Earthquake Res. China*, *10*(4), 347–356.